



UNIVERSITÀ DI SIENA 1240

Dipartimento di Biotecnologie Mediche

**Dottorato in Biotecnologie Mediche**

XXXV° Ciclo

Coordinatore: Prof. L. Leoncini

**Bidirectional relationship between  
SARS-CoV-2 and Diabetes Mellitus**

Settore scientifico disciplinare: MED/13

*Candidata*

Daniela Fignani

Unisi

*Firma digitale del/della candidato/a*

*Supervisore*

Prof. Francesco Dotta

Unisi

*Co-supervisore*

Prof. Guido Sebastiani

Unisi

Anno accademico di conseguimento del titolo di Dottore di ricerca

2021/2022

Università degli Studi di Siena  
Dottorato in Biotecnologie Mediche  
XXXV° Ciclo

*Data dell'esame finale*

13/02/2023

*Commissione giudicatrice*

MARCO OGGIONI – Professore Ordinario – Dipartimento di Farmacia e Biotecnologie – Università di Bologna

RICCARDO MANGANELLI – Professore Ordinario – Dipartimento di Medicina Molecolare – Università di Padova

LUIGI GENERALI - Professore Associato – Dipartimento Chirurgico, Medico, Odontoiatrico e di Scienze Morfologiche - Università di Modena e Reggio Emilia

LUCIA PALLECCHI - Professore Associato - Dipartimento di Biotecnologie Mediche - Università di Siena

FRANCESCO DOTTA – Professore Ordinario – Dipartimento di Medicina, Chirurgia e Neuroscienze – Università di Siena

SIMONE GRANDINI - Professore Ordinario - Dipartimento di Biotecnologie Mediche -Università di Siena

GIANNI POZZI - Professore Ordinario - Dipartimento di Biotecnologie Mediche -Università di Siena

IANNELLI FRANCESCO - Professore Ordinario - Dipartimento di Biotecnologie Mediche -Università di Siena

MARCO FERRARI - Professore Ordinario - Dipartimento di Biotecnologie Mediche - Università di Siena

*Supplenti*

JEAN DENIS DOCQUIER - Professore Associato - Dipartimento di Biotecnologie Mediche - Università di Siena

MAURIZIO ZAZZI - Professore Ordinario - Dipartimento di Biotecnologie Mediche -Università di Siena

## Table of content

<b>1. Abstract</b>	<b>5</b>
<b>2. Introduction</b>	<b>6</b>
2.1 <i>Pancreatic islets: Architecture and Function</i>	6
2.2 <i>Diabetes Mellitus</i>	12
2.2.1 Type 1 diabetes	14
2.2.2 T1D genetic risk factors	15
2.2.3 T1D environmental risk factors	16
2.2.4 Autoimmune mechanisms in T1D	17
2.2.5 Type 2 diabetes	18
2.2.6 T2D genetic risk factors	22
2.2.7 T2D environmental risk factors	23
2.3 <i>SARS-CoV-2</i>	24
2.3.1 Pathogenesis of SARS-CoV-2 infection	24
2.3.2 Angiotensin-Converting Enzyme 2 (ACE2)	26
2.3.3 A novel ACE2 isoform	31
2.3.4 Physiological role of ACE2 in pancreatic islets	33
2.3.5 SARS-CoV-2, COVID-19 and Diabetes Mellitus: a bidirectional causal relationship?	34
<b>3. Aims of the Thesis</b>	<b>40</b>
<b>4. Material and Methods</b>	<b>41</b>
4.1 <i>Human Multiorgan and Autoptic Donors</i>	41
4.2 <i>Human pancreatic islets isolation</i>	45
4.3 <i>Cell culture</i>	46
4.4 <i>Laser capture microdissection (LCM)</i>	46
4.5 <i>RNA extraction from LCM isolated human pancreatic islets</i>	47
4.6 <i>RNA extraction from cells and tissues</i>	47
4.7 <i>RT-Real Time PCR analysis</i>	48
4.8 <i>ACE2 Immunohistochemistry analysis of human pancreatic sections</i>	49
4.9 <i>Immunofluorescence staining for ACE2-Insulin-Glucagon and ACE2-CD31</i>	50

4.10	<i>Insulin, Glucagon and SARS-CoV-2 Nucleocapsid Immunofluorescence staining</i> .....	51
4.11	<i>Cultured cells immunofluorescence</i> .....	52
4.12	<i>Image analysis</i> .....	53
4.13	<i>Micro-confocal High-content Screening analysis</i> .....	54
4.14	<i>RNA sequencing processing and analysis</i> .....	55
4.15	<i>Western blot analysis</i> .....	56
4.16	<i>ACE2 targeted Mass Spectrometric (MS)-Shotgun proteomics analysis</i> .....	56
4.17	<i>ACE2 promoter transcription factors (TF) binding motifs analysis</i> .....	57
4.18	<i>Data and Code Availability</i> .....	58
4.19	<i>Statistical analysis</i> .....	58
<b>5.</b>	<b>Results</b> -----	<b>58</b>
5.1	<i>ACE2 expression pattern in human pancreas</i> .....	58
5.2	<i>In human pancreatic islets ACE2 is preferentially expressed in <math>\beta</math>-cells</i> .....	69
5.3	<i>A short ACE2 isoform is prevalently expressed in the human <math>\beta</math>-cell line EndoC-<math>\beta</math>H1</i> .....	77
5.4	<i>Total ACE2 mRNA is expressed in human pancreatic islets and in the human beta-cell line EndoC-<math>\beta</math>H1</i> .....	81
5.5	<i>ACE2 expression is increased in EndoC-<math>\beta</math>H1 cells and in human pancreatic islets by pro-inflammatory cytokines</i> .....	83
5.6	<i>Upregulation of ACE2 in T2D</i> .....	92
5.7	<i>Presence of SARS-CoV-2 nucleocapsid in pancreatic <math>\beta</math>-cells of COVID-19 donors</i> .....	99
<b>6.</b>	<b>Discussion and conclusions</b> -----	<b>103</b>
<b>7.</b>	<b>Bibliography</b> -----	<b>112</b>



# 1. Abstract

Several studies demonstrated that COVID-19 has a more severe outcome in patients with diabetes; in addition, in normoglycemic patients, the infection can alter glycometabolic control increasing the risk to develop Type 2 Diabetes (T2D) or dysglycaemia. Thus, a bidirectional relationship between COVID-19 and diabetes can be hypothesized but a detailed analysis aimed at evaluating ACE2 expression pattern distribution in human pancreas is still lacking.

Increasing evidence demonstrated that the expression of Angiotensin I-Converting Enzyme type 2 (ACE2) is a necessary step for SARS-CoV-2 infection permissiveness.

Here, we took advantage of INNODIA network EUnPOD biobank collection to thoroughly analyze ACE2, both at mRNA and protein level, in multiple human pancreatic tissues and using several methodologies. Using multiple reagents and antibodies, we showed that ACE2 is expressed in human pancreatic islets, where it is preferentially expressed in subsets of insulin producing  $\beta$ -cells. ACE2 is also highly expressed in pancreas microvasculature pericytes and moderately expressed in rare scattered ductal cells. Moreover, using RT-qPCR, RNA-seq and High-Content imaging screening analysis, we demonstrated that pro-inflammatory cytokines, increase ACE2 expression in the  $\beta$ -cell line EndoC- $\beta$ H1 and in primary human pancreatic islets.

Finally, we demonstrated that ACE2 expression is increased in pancreatic islets of T2D donors in comparison to non-diabetic controls alongside with a higher colocalization rate between ACE2 and insulin using both anti-ACE2 antibodies. Of note, a higher frequency of peri-islets macrophages was detected in T2D donors respect to non-diabetic.

Upregulation of ACE2 was demonstrated in pancreatic islet  $\beta$ -cells of T2D donors. Higher ACE2 expression in T2D islets might increase their susceptibility to SARS-CoV-2 infection during COVID-19 disease in T2D patients, thus exacerbating glycometabolic outcomes and worsening the severity of the disease.

Taken together, our data indicate a potential link between SARS-CoV-2 and diabetes.

## 2. Introduction

### 2.1 Pancreatic islets: Architecture and Function

The pancreas can be defined as the central engine for controlling energy consumption and metabolism. It is a voluminous elongated gland located in the abdominal-pelvic cavity, between the posterior wall of the abdomen, duodenum and spleen. From the anatomical point of view, the pancreas is divided into three portions: head, body and tail. The head is located in the concavity formed by the duodenum, the body represents the intermediate segment and the tail which represents the thinned tract with which this organ ends. It is a mixed gland consisting of an exocrine (80-85%) and an endocrine (2%) portion. The exocrine portion is characterized by pancreatic acinar cells that synthesize and secrete digestive enzymes (proteases, amylases, lipases, nucleases) in an inactive form, to pour them directly into the duodenum under the influence of physiological stimuli; on the other hand, the endocrine component, is responsible for the secretion of hormones that are secreted and released into the bloodstream with the function of controlling the metabolism of sugars, fats and proteins. The endocrine compartment is organized in structures known as islets of Langerhans, whose cells are specialized in the secretion of specific hormones responsible for maintaining homeostatic blood glucose levels. The islets of Langerhans are a heterogenous mixture of endocrine cells scattered through the pancreas, including insulin-secreting  $\beta$ -cells, glucagon-secreting  $\alpha$ -cells, somatostatin-secreting  $\delta$ -cells, pancreatic polypeptide-secreting PP-cells and ghrelin-secreting  $\epsilon$ -cells, that function as mini-organs. In addition to the metabolic function, pancreatic islets are highly innervated and vascularized, providing numerous signals that can modulate and support cellular differentiation, survival and proliferation (1). The architecture and distribution of pancreatic islets is species-specific. The murine pancreatic islets are characterized of a central core of  $\beta$ -cells and  $\alpha$  and  $\delta$  cells located in the periphery of the islet, differentiating themselves from the human pancreatic islets in which the  $\alpha$ -  $\beta$ - and  $\delta$ - cells are heterogeneously distributed throughout the islet. There are also differences in the number of cells which characterize the islets of Langerhans between human and mouse: in human,  $\beta$ -cells represent the 50-70%, while in mice they are 60-80% of the total islet cells;  $\alpha$ -cells in human represent the 20-40%, while in mice are 10-20%;  $\delta$ -cells and PP-cells are the least frequent cell types and are less than 10% in human and less than 5% in mice. The  $\epsilon$ -cells, on the other hand, are less than 1% (**Figure 1**).

Studies on human islets suggest that these differences, probably, reach adult architecture about two years after birth (in fact, the replication rate of  $\beta$ -cells is greater during the first two years of age and then decreases in adolescence); on the other hand, in mice, the number of islets increases in the first 3-4 weeks of life and then remains stable over time (2,3). Comparative studies on pancreatic islets of different species have revealed surprising plasticity in the architecture of the islets and their composition. Physiological and pathological changes have been shown to lead to differences in the architecture, function and gene expression of islets, rather than species differences (4). In a study, it has been performed a three-dimensional islet distribution map and it has been estimated that in the healthy human pancreas there are on average 3.2 million islets, with a mean islet diameter of 102.92  $\mu\text{m}$  and a mean islet volume of 0.00068  $\text{mm}^3$  or 0.00069  $\mu\text{L}$ . Moreover, the majority of islets had a surface area between 1000 and 10000  $\mu\text{m}^2$ , while a minor fraction of more than 100000  $\mu\text{m}^2$ . By comparing the 2D distribution of islets in the pancreatic section area, it was observed that islets are grouped in the head of the pancreas and are gradually dispersed throughout the pancreas up to the tail region. Islet density gradually increases from the head to the tail region of the pancreas. The smaller islets stretched to clusters around blood vessels (5). The pancreatic islet shape confers a unique cellular arrangement. Recent data suggest that many changes in islet structure and function were associated with diabetes and were attributable to hyperglycaemia alone. In fact, these changes reversed when blood glucose is normalized. Thus, the uniqueness of this heterogeneous conformation has a deep functional implication (6,7).

The endocrine cells scattered through the pancreas have different functions and communicate with each other to guarantee glucose homeostasis.

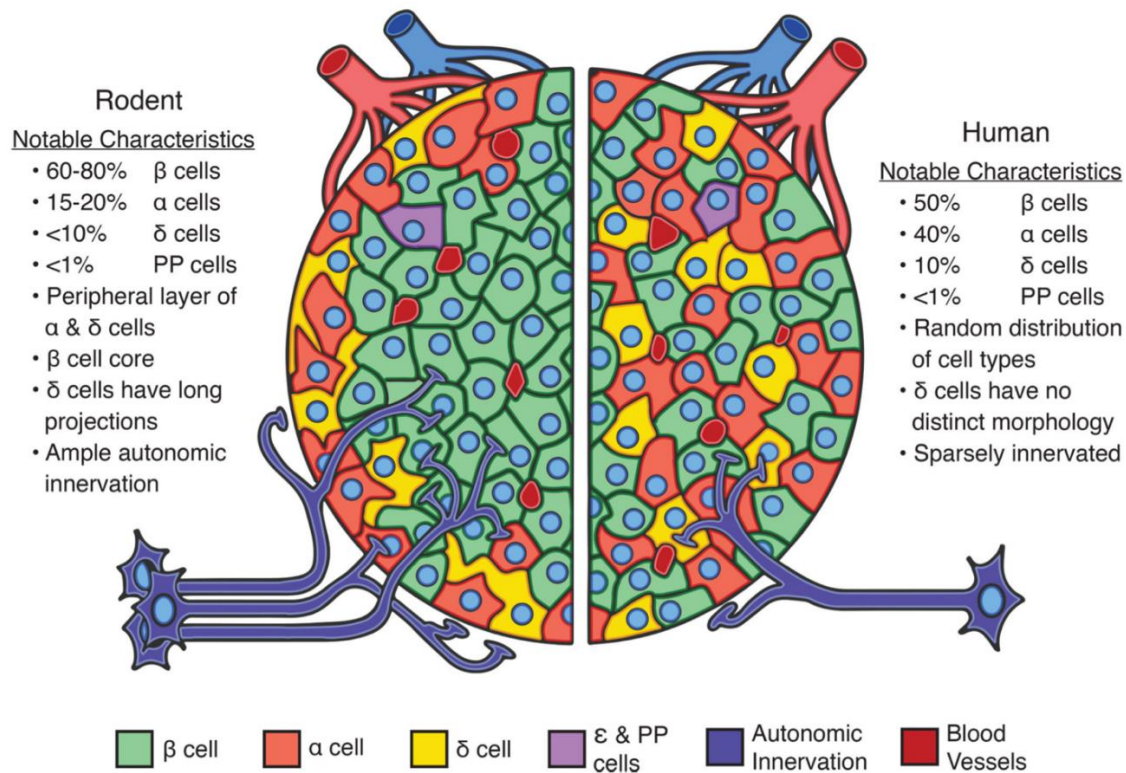


**Figure 1. Comparative architecture of pancreatic islets of mice and humans.** The architecture of the pancreatic islets of mice and humans differ greatly, but they also share many features in common. These shared characteristics make mouse islets useful experimental models for studying many aspects of human islet biology. The different types of endocrine cells in mice (left) and human islets (right) are similar between beta cells ( $\beta$ ; green), which make up most of the cell mass of the islet, and alpha cells ( $\alpha$ ; magenta) and delta ( $\delta$ ; yellow). The pancreatic polypeptide and epsilon cells (PP and  $\epsilon$ ; purple) are more spread out. Human pancreatic islets are characterized by highly structured cells that can have different sizes and conformations. Murine pancreatic islets are more uniform, with  $\alpha$  and  $\delta$  cells on the periphery of the islet surrounding a nucleus of  $\beta$  cells. The islets of both species are vascularized (dark red) and innervated (light blue) for rapid detection of changing energy needs, although murine islets are more densely innervated than human ones (8).

**$\alpha$ -cells** produce the glucagon in fasting conditions and its main function is to increase the amount of glucose in the blood by stimulating glycogenolysis and gluconeogenesis. In the pathophysiology of T2D, the glucagon has an important function; in fact, Unger and colleagues have demonstrated, in the bi-hormonal hypothesis, that both hypoinsulinaemia and hyperglucagonaemia can cause hyperglycaemia in T2D (9,10). Glucagon-like peptide 1 (GLP-1) and Gastric Inhibitor Polypeptide (GIP) are involved in the regulation of glucagon secretion; indeed, the somatostatin produced by  $\delta$ -cells, negatively regulate

glucagon secretion. It has been proposed that GLP-1 indirectly inhibits glucagon secretion through somatostatin secretion, regardless of  $\beta$  cell secretory products (11). Several studies have highlighted the ability of  $\alpha$ -cells to transdifferentiate into  $\beta$ -cells, in particular, it has been recently demonstrated that the administration of gamma aminobutyric acid (GABA) induced the trans-differentiation of  $\alpha$ -cells into  $\beta$ -cells maintaining a functional population of  $\alpha$  cells, suggesting that this treatment is important to guarantee the total proportion of islet cell type (12).

**$\beta$ -cells** are the most important and studied cells of the pancreatic islets. Insulin is the hormone released by  $\beta$ -cells in response to high glucose concentration, resulting into a decrease of blood sugar, increased synthesis of glycogen in the liver and muscle, increased usage of glucose by cells and inhibited the production of new glucose.

Insulin is a peptide consisting of two amino acid chains (A and B) held together by two disulphide bonds (A7-B7, A20-B19). Chain A is made up of 21 amino acids, while chain B is made up of 30 amino acids. In humans, the gene responsible for insulin synthesis is located in the short arm of chromosome 11. The insulin gene encodes a precursor protein of 110-amino acid known as preproinsulin that contains a hydrophobic N-terminal signal precursor that interacts with cytosolic ribonucleoprotein signal recognition particles (SRP) (13). The preproinsulin translocate through the rough endoplasmic reticulum (rER) membrane into the lumen where the signal peptide is cleaved by peptidases becoming proinsulin. In the ER proinsulin undergoes folding and maturation, then is transported from ER to the Golgi and trans-Golgi network apparatus where PC1/3 and PC2 (protein convertase 1-2-3) and CPE (carboxypeptidase) cleaved proinsulin to produce Insulin and C-peptide stored in secretory granules (**Figure 2**) (14,15). Recently, this canonical proinsulin processing pathway has been revisited more thoroughly. Recent evidence shows that in human  $\beta$ -cells the endoproteolytic cleavage of proinsulin was performed preferentially by PC1 and PC3 enzyme but PC2 activity was not detected. Moreover, it has been demonstrated that the inhibition of PC2 rendered  $\beta$ -cells able to secrete mature insulin while the suppression of PC1/3 enzyme inhibited proinsulin processing. In healthy human  $\beta$ -cells, PC2 immunoreactivity was not detected but its expression increased in  $\beta$ -cells of type 2 diabetic individuals, suggesting that the defect of PC2 expression in diabetic condition may contribute to the alteration of proinsulin processing and disease (16). This aspect represents mostly a debate and in the light of the latest published works, it is increasingly reported that  $\beta$  cell is characterized by a remarkable plasticity and ability to

adapt to physiological and pathological conditions. Marchetti et al., showed the presence of GLP-1-like peptide and PC1/PC3 immunoreactivity in subsets of  $\alpha$ -cells but not in  $\beta$ -cells. Moreover, the release of GLP-1 as well as the expression of PC1/PC3 genes were increased in type 2 diabetic respect to control islets, suggesting a strong dynamism of pancreatic islets cells following  $\beta$  cell dysfunction (17). The function of insulin is to keep plasma glucose levels within physiological limits (80-100 mg/dl); in fact, its secretion is controlled by the concentration of glucose in the blood. The increase of concentration of plasma glucose, leads to the entry of glucose into the  $\beta$ -cells thanks to the presence of the insulin-dependent transporter GLUT-2. An increase in cytosolic glucose causes an increase in the concentration of ATP, produced by the mitochondrial catabolism of sugar, which causes the closure of the ATP-dependent potassium channels, with depolarization of the membrane and opening of the voltage-dependent calcium channels. The intracellular increase in the calcium ion ( $Ca^{2+}$ ), which acts as a messenger, induces the fusion of the insulin-containing vesicles with the plasma membrane. Insulin is thus released from the granules in which it is contained. The target organs of insulin are mainly skeletal muscle, adipose tissue and liver expressing insulin receptor (INSR) located on the plasma membrane of their cells. In these organs it promotes glucose uptake, glycogen synthesis, stimulates exocytosis and activation of glucose transporters; it also favours the uptake of amino acids by increasing protein synthesis (18).

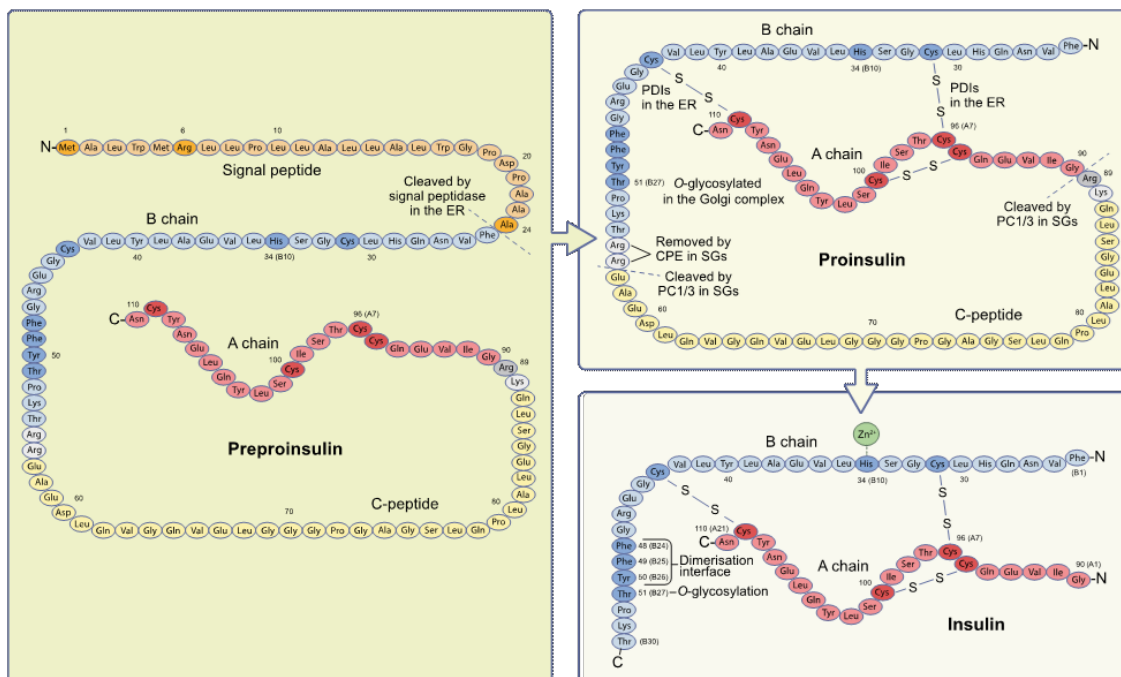


**Figure 2. Preproinsulin, proinsulin and insulin protein structure.** Preproinsulin (on the left) is composed by a N-terminal signal peptide, a B chain, the C-peptide and an A chain. After the cleavage of the signal peptide, the proinsulin is made up of a B chain and an A chain linked by the C-peptide. The mature insulin has a B chain of 30 amino acids and an A chain of 21 amino acids, held together by two disulfide bonds (19).

A recent work has found that  $\beta$ -cells, considered as a homogeneous cell population, differentiate between them in four main antigenically distinct subtypes and defined as  $\beta 1$ ,  $\beta 2$ ,  $\beta 3$ ,  $\beta 4$ . These cells are distinguished by differential expression of particular cellular markers: ST8SIA1 (Human Alpha-N-acetyl neuraminidase alpha-2, 8-sialyltransferase) and CD9 (cluster 9 differentiation) and are characterized by different gene expression profiles and glucose-stimulated insulin secretion. In T2D, the distribution of these  $\beta$ -cells is altered (20). These results open the way to new knowledge regarding the architecture of the pancreatic islets and the specific function of the cells they compose.

**$\delta$ -cells** secrete the somatostatin, which acts under conditions as a negative regulator of insulin, glucagon and pancreatic polypeptide (21). In a study, it has been demonstrated that  $\delta$ -cells can transdifferentiate in  $\beta$ -cells following acute depletion of  $\beta$  cell mass (22). It has been reported that the gene Hhex is essential for the maintenance of  $\delta$ -cells fate. In fact, the loss of Hhex gene led to a failure of paracrine regulation of insulin secretion contributing to T2D (23).

**PP-cell or F-cells** produce the pancreatic polypeptide, concentrated in particular in the head of pancreas. The regulation of the secretion of pancreatic polypeptide is done by vagal and enteric nervous input. This post-prandial hormone under low glucose, inhibit the release of glucagon. It is considered the satiety hormone (24,25).

However, it is worth noting that pancreatic islets are composed not only by endocrine cells but also by endothelial cells, cell of mesenchymal origin and nerves (26).

**Endothelial cells (ECs)** are flattened cells that form the walls of the capillaries, arterioles and venules that constitute the so-called microvasculature. In the endocrine pancreas these cells are highly fenestrated, with fenestrations around 95-100 nm, closed by a permeable diaphragm, that forms capillaries of 4-5  $\mu\text{m}$  of diameter with double basement membrane. Depending on the islet size, each islet is vascularized by 1-5 arterioles and in general, cells have a specific orientation, for example,  $\beta$ -cells apical pole is oriented towards a capillary

to facilitates the release of insulin into the microvasculature (27). ECs contribute to the glucose homeostasis through the transport of oxygen to the islets and the release of hormones in the circulation, furthermore, ECs are crucial for the insulin secretion,  $\beta$ -cell function and proliferation (28).

Mesenchymal cells are less than the 10% of the whole organ but they have a high heterogenicity. Mesenchymal cells play crucial role in the development of the pancreas, indeed mesenchymal cells secrete some factors such as fibroblast growth factor (FGF) and retinoic acid (RA), whose interaction with epithelial cells, induces cell proliferation (29). Also, pericytes have a mesenchymal origin; they are cell with a prominent body and elongated processes which encircle endothelial cells in capillary and microvasculature and control the vessels contractility. Pericytes are crucial for the angiogenesis that is activated after injury of the pancreas; indeed, through the collaboration with the endothelial cells, they can stabilize the vascular network; furthermore, pericytes respond to several signals to regulate the blood-flow to the islet (30).

The vasculature is surrounded by nerve fibers, composed by Schwann cells, that are responsible for a close nerve islet-cell interactions (31). Both sympathetic and parasympathetic nerves innervate pancreas, regulating the insulin secretion with the activation of parasympathetic fibers and glucagon with both parasympathetic and sympathetic nerves (32).

The communication of the cells that characterize the pancreatic islet is extremely fragile, and the alteration of the mechanisms regulated by them can lead to pathological conditions known as Diabetes Mellitus.

## **2.2 Diabetes Mellitus**

Diabetes mellitus (DM) is a heterogeneous group of chronic and progressive diseases mainly characterized by hyperglycaemia. Hyperglycaemia is caused by defects in insulin secretion, action or both, induced by the loss of  $\beta$  cell mass and/or by impaired  $\beta$ -cells function. Such alterations of  $\beta$ -cells can be due to both genetic and environmental factors, or to a combination of both (33). The most common symptoms of DM are polyuria, polydipsia, and weight loss, sometimes combined with polyphagia, and blurred vision. The chronic hyperglycaemia occurring in DM is associated with tissue damages, dysfunctions,



and failure of several organs, including retina, kidneys, nerves, heart, and blood vessels. Untreated diabetes determines a strong hyperglycaemia, which can result in acute consequences such as ketoacidosis, coma and nonketotic hyperosmolar syndrome (34). Recent data from the International Diabetes Federation (IDS) indicated that an estimated 537 million adults aged 20–79 years worldwide had DM in 2021 and the number is expected to increase to 783 million in 2045, with the prevalence raising from 10.5% to 12.2% (35,36). Given the high prevalence of diabetes among adults and its worldwide medical relevance, an early diagnosis is essential to determine therapeutic approaches. Although hyperglycaemia largely precedes the first clinical symptoms of diabetes, causing functional changes in several organs and tissues, during the asymptomatic period, it is possible to detect abnormalities in carbohydrate metabolism by measurement of fasting plasma glucose. According to the WHO, a level of fasting plasma glucose concentration  $> 7$  mmol/l allows to diagnose diabetes, while levels between 6.1 mmol/l and 7 mmol/l are considered as impaired fasting glucose, as prediabetes condition.

Different processes are involved in the onset and progression of diabetes:  $\beta$  cell loss, insulin resistance, dysregulation of carbohydrates, fat and protein metabolism and inflammation (37). Depending on the pathogenic mechanisms that lead to the development of this disease, diabetes can be classified in different forms. The most prevalent form of diabetes is type 2 diabetes (T2D), that occurs in  $\sim 90$ -95% of diabetic cases; whereas type 1 diabetes (T1D), occurs in 5-10% of diabetic population. Less common forms of diabetes include the gestational diabetes mellitus (that is usually diagnosed in the second or third trimester of pregnancy), the monogenic diabetes syndrome, the diseases of the exocrine pancreas and drug- or chemical-induced diabetes (such as the forms of diabetes that emerge in patients under glucocorticoid or anti-HIV/AIDS therapies, or patients subjected to organ transplantation) (38,39).

Type 2 diabetes is usually referred to as “non-insulin dependent diabetes” or “adult-onset diabetes” and is characterized by peripheral insulin resistance and reduced insulin secretion by  $\beta$ -cells. Albeit the aetiology of T2D is not completely known, there are several evidence demonstrating the crucial role played by both genetic and environmental factors. In fact, T2D patients have been shown to be often obese, overweight or with a high percentage of body fat in the abdominal region, suggesting that weight gain represents one of the main risk factors of T2D, exacerbated by the lack of physical activity and age (40). Importantly, a study conducted by GoT2D and T2D-GENES consortia and published in Nature in 2016,

performing whole genome sequencing of 2.657 Europeans with and without T2D, identified 126 genetic variants in 4 different loci are associated with T2D (41).

### 2.2.1 Type 1 diabetes

Type 1 Diabetes (T1D) is a cell-mediated autoimmune disease. The autoimmune reaction that causes T1D is mainly driven by activated autoreactive T cells, within the islets of Langerhans, triggering the destruction of the insulin-producing  $\beta$ -cells. The loss of  $\beta$  cell mass due to these autoreactive mechanisms leads to insulin deficiency and consequent hyperglycaemia. In order to compensate for the lack of endogenous insulin, T1D patients are usually provided with exogenous insulin (42).

In T1D, physiological alterations precede the onset of symptomatic type 1 diabetes. **Figure 3** summarizes the natural history of T1D from the exposure of genetically susceptible individuals to a putative environmental trigger until the appearance of the clinical symptoms. According to Insel and colleagues (43), T1D natural history is subdivided into three different consecutive stages from the precipitating events to the clinical manifestation. In the first stage,  $\beta$  cell mass and function is preserved and insulin is normally secreted, but patients already exhibit immunological dysregulation and develop autoantibodies against multiple  $\beta$  cell antigens [e.g., antibodies against Insulin (IAA), Insulin-associated Antigen 2 (IA2A), Glutamic Acid Decarboxylase (GAD65A), and Zinc Transporter (ZnT8A) (44,45)]. The second stage is characterized by asymptomatic  $\beta$  cell autoimmunity with consequent dysglycaemia; at this presymptomatic stage it is also possible to identify a reduction of C-peptide response. The third and last stage is characterized by the manifestation of the clinical symptoms of type 1 diabetes, such as insulin deficiency and hyperglycaemia (46).

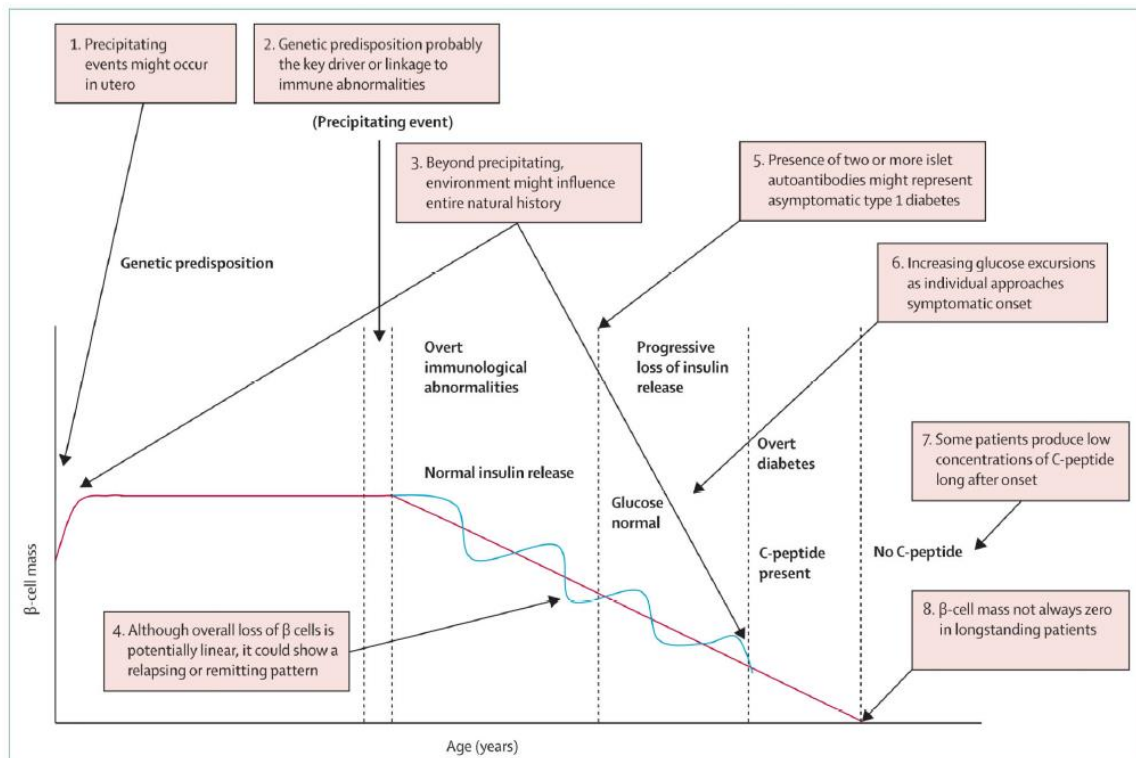


**Figure 3. Natural history of type 1 diabetes.** Schematic representation of the natural history of type 1 diabetes characterized by 3 stages: (i) immunological abnormalities, (ii) progressive loss of insulin secretion and (iii) T1D clinical symptoms manifestation (42).

### 2.2.2 T1D genetic risk factors

Genetic factors play an important role in conferring risk for T1D since the heritability of the disease has been estimated around 80% and more than 50 genetic loci has been associated with the onset of T1D. Among the numerous polymorphic loci that could increase genetic predisposition to T1D, the human leukocyte antigen (HLA) complex has been estimated to account for 30-50% of the genetic risk of type 1 diabetes (47). The HLA complex region is located on chromosome 6 and encodes for the three classes of the major histocompatibility complex (MHC) (48). Importantly, MHC class II (which is associated with a higher risk of T1D onset) is mainly expressed by antigen presenting cells (APC) which trigger the activation of the naïve CD4<sup>+</sup> lymphocytes, stimulating B cells to produce antibodies (49,50). T1D typically generates autoimmune responses which is caused by the alterations on  $\beta$ -cells antigen presentation (51,52). Although some of the mutations in the HLA complex region confer protection from the disease (such as DRB1\*1501 and

DQA1\*0102-DQB1\*0602), other mutations present one of the highest risks of T1D onset (i.e., higher risk in HLA 2 D3/D4 heterozygous Caucasian patients, and in D3 and D4 homozygous patients). One explanation for the very high susceptibility of the DR3/DR4 heterozygous genotype is the presence of DQ molecules, that can be formed from polypeptide chains encoded in trans in this genotype, in addition to those encoded in cis on each of the two haplotypes. The putative DQ molecule formed by DQA1\*03:01 on the DR3 haplotype and DQB1\*02:01 on the DR4 haplotype is found in cis on some African haplotypes; however, DQA1\*05:01 on the DR3 haplotype and DQB1\*03:02 on the DR4 haplotype are not found encoded in cis on any haplotype and maybe highly diabetogenic (53–55). Other non-HLA genetic loci that increase the probability to develop T1D are the ones encoding for INS, PTPN22, CTLA4 and IL2RA. Instead, polymorphisms in T1D susceptibility genes, such as IL2, INS VNTR, CD25, IFIH1, IL18RAP, IL10 and PTPN22, have been shown to influence the disease progression. Interestingly, these genes are also associated with other autoimmune diseases and to immune system regulation (56,57). Studies investigating the association between genetic polymorphisms and risk of T1D onset and progression are essential, from a medical point of view, as they could allow early diagnosis of diabetes and tailoring of optimal personalized therapies (58,59).

### **2.2.3 T1D environmental risk factors**

Although genetic susceptibility represents a crucial risk factor for the onset and progression of type 1 diabetes, it is not sufficient to explain the aetiology of the disease, neither to get a better understanding of the causes leading to T1D clinical symptoms, therefore, also environmental factors should be investigated (60).

Currently, little is known about the mechanisms triggering autoimmunity in T1D patients. However, it has been suggested that dietary factors (especially during infancy), exposure to toxins, lack of vitamin D in the serum, and viral and bacterial infections may represent environmental risk factors for the development of this disease. Among these factors, infections by Enteroviruses are thought to be particularly important and, therefore, have been largely investigated. Indeed, it has been shown that both mice and humans at the onset of type 1 diabetes show traces of Coxsackie B Virus (CBV) RNA in their blood; furthermore, the  $\beta$ -cells of these subjects express high level of Viral Protein 1 (VP1) (CVB

capsid protein) and Coxsackie Adenovirus Receptor (61,62). Whereas the mechanisms that triggers the loss of function  $\beta$ -cell mass are still unclear, there are accumulating evidence which suggests that virus may either directly kill  $\beta$ -cells or they may attract autoreactive T cells to the pancreatic exocrine cells, inducing the inflammatory response. Different studies suggest that CBV-infected  $\beta$ -cells could potentially induce the inflammatory response, being initially phagocytised by macrophages, which acquire the ability to present Langerhans islets antigens, activating the autoimmune response and consequently leading to T1D onset. Interestingly, pancreatic exocrine cells of infected individuals upregulate the expression of viral markers and sensors (e.g., HLA-1, PKR, RIG-1, MDA5, MxA), leading to chemokine release and, consequently, attracting immune cells and enhancing insulinitis (i.e., the immunological process responsible for the  $\beta$ -cells destruction) (63–65).

#### **2.2.4 Autoimmune mechanisms in T1D**

Dysregulation at thymus level and negative selection of autoreactive T cells are among the primary causes of autoimmune diabetes. In fact, it should be noted that the development of T1D is significantly affected by immune system dysregulation, such as insulinitis. Insulinitis is an extremely complex process in which a large, dynamic population of islet-infiltrating cells takes part in the insulitic lesion. Some cell types, that infiltrate the islets, act as professional antigen-presenting cells (e.g., B cells, dendritic cells, and macrophages) and provide a combination of stimuli capable to activate autoreactive CD4<sup>+</sup> and CD8<sup>+</sup> T cells, which are the principal effectors of T1D pathogenesis (**Figure 4**) (66,67). Activated CD4<sup>+</sup> T cells generally operate as T-helper cells (TH) secreting pro-inflammatory cytokines such as interferon gamma (IFN- $\gamma$ ) and interleukin (IL)-2; these cells infiltrate the endocrine pancreas, where they interact with APCs via MHC-II and enhance the inflammatory process. In fact, the interaction between CD4<sup>+</sup> T cells and APCs results in cytokines production, that supports CD8<sup>+</sup> T-cell proliferation and strengthens TH pro-inflammatory activity via a positive feedback loop. Furthermore, CD4<sup>+</sup> T cells have also been shown to exert a direct cytotoxic activity in advanced disease stages (68).

Cytotoxic T lymphocytes (CTLs) recognize islet antigens. After infiltration, the T-Cell Receptor (TCR) of the autoreactive CTL binds to its corresponding MHC on  $\beta$ -cells, creating an “immunologic synapse” (**Figure 4B**) (69). The formation and stabilization of multiple immunological synapses trigger CTLs to release IFN- $\gamma$ , perforin, and granzyme

B, finally destroying the  $\beta$  cell. As already mentioned, the diagnosis of T1D is confirmed by the presence of specific autoantibodies for the islet and  $\beta$ -cells antigens, such as IAA, GAD65, IA-2A, and ZnT8A, which have been demonstrated to be reliable markers of the islet autoimmunity that precede clinical onset of T1D (70).

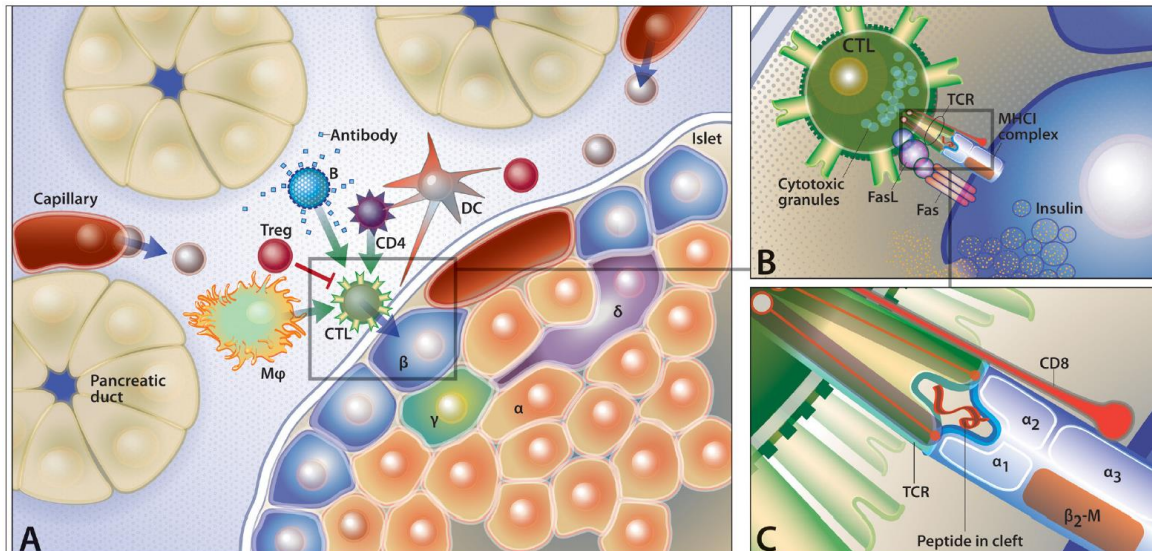


**Figure 4. Immune cells interactions in T1D.** **A.** The pancreatic islets contain insulin-producing  $\beta$  cells, which are the targets of autoreactive T cells. Antigen-presenting cells (macrophages, dendritic cells, and  $\beta$  cells) stimulate CD4<sup>+</sup> and CD8<sup>+</sup> T cells, which infiltrate the islets and generate an inflammatory microenvironment in which  $\beta$ -cells are destroyed. **B.** T-cell receptors (TCRs) of Cytotoxic T lymphocytes (CTL) bind to MHC-I complexes on the surface of  $\beta$ -cells, creating an immunological synapse, which triggers the release of cytotoxic granules and increased expression of Fas ligand, inducing apoptosis of target cells. **C.** The antigen that drives the proliferation and cytotoxic function of CTL through TCR signaling is a combination of a particular peptide and proper MHC-I molecule (69).

### 2.2.5 Type 2 diabetes

Type 2 Diabetes (T2D) is the most common form of diabetes, which accounts for 90% to 95% of all diabetic patients (71). T2D is a metabolic disease characterized by a combination of genetic and environmental factors that result in decreased insulin function at sites of insulin action and a reduced ability of pancreatic  $\beta$ -cells to enhance insulin synthesis and secretion in response to increased blood glucose levels (**Figure 5**) (72).

Pathophysiological changes are characterized by  $\beta$ -cell dysfunction, insulin resistance and chronic inflammation, which progressively hinders the control of blood glucose levels and the development of microvascular (retinopathy, neuropathy) or macrovascular (atherosclerosis) complications. Obesity and physical inactivity together with genetic predisposition, may lead to insulin resistance causing beta cell stress and the progressive loss of glucose-induced insulin secretion. The development of T2D has been subdivided into five stages, each of which is characterized by major changes in mass, phenotype and  $\beta$ -cell function (73):

1. Compensation characterized by the increase in insulin secretion to try to restore the normal glucose level despite the insulin resistance resulted from obesity, sedentary lifestyle and genetic predisposition. This increased secretion of insulin is determined by a rise in  $\beta$ -cell mass;
2. Stable adaptation happens when it is not anymore possible to maintain physiological blood glucose level and  $\beta$ -cells have to adapt to face the increased blood glucose level that cause glucotoxicity;
3. Unstable early decompensation develops when the blood glucose level rapidly rises, and  $\beta$ -cell are not anymore able to compensate with the production and the secretion of insulin the glucotoxicity;
4. Stable and constant decompensation with changes in  $\beta$ -cell mass, function and differentiation;
5. Severe decompensation in which the loss of  $\beta$ -cells is so severe that people, to survive, need insulin.

In the first stage of this process  $\beta$ -cells mass increases due to replication and neogenesis thus inducing a hyperinsulinemia condition. However, due to the presence of genetic predisposition a  $\beta$ -cell dysfunction and apoptosis may occur leading to impaired glucose tolerance and then to overt T2D. The chronic insulin demand and the decrease of insulin production may cause the depletion of  $\beta$ -cell insulin granules storage, leading to impaired insulin secretion and inadequate insulin production which seems to be a consequence of the ER dysfunction.

The stimulating factors involved in  $\beta$ -cells compensatory processes, include an increased supply of nutrients in particular glucose and free fatty acids (FFA), insulin, growth factors and a greater sensitivity to incretins such as GLP-1 which promotes  $\beta$ -cell proliferation and neogenesis to prevent apoptosis (74). Insulin and insulin growth factors 1 and 2 (IGF-1 and IGF-2) bind to insulin receptor (IR), causing the activation of IRS1-IRS2, which can activate the PI3K/Akt/mTOR pathway. The signaling of IRS-2 through the phosphorylation of PKB (protein-kinase B) and the inactivation of the transcription factor FOXO1, increases the expression levels of the PDX1 gene, an important factor involved cell proliferation and  $\beta$ -cell function and survival. In addition, the activation of PKB determines the protection from apoptosis through phosphorylation and the inhibition of pro-apoptotic proteins such as BAD (75).

High blood concentrations of pro-inflammatory cytokines, such as C-reactive protein, interleukin-6 (IL-6) and tumour necrosis factor (TNF), are associated with an increased risk of T2D, while a high concentration of adiponectin, that is characterized by an anti-inflammatory effect, is associated with a reduced risk (76). Furthermore, IL-6 is a cytokine with a double effect: Linneman and colleagues observed that pre-treatment with IL-6 renders  $\beta$ -cells resistant to apoptosis induced by proinflammatory cytokines, and inhibition of autophagy with chloroquine prevents the ability of IL-6 to protect from apoptosis. Importantly, they found that IL-6 can activate STAT3 and the autophagy enzyme GABARAPL1 in human islets. They also see evidence of decreased IL-6 pathway signaling in islets from donors with T2D. Based on their results, authors proposed direct stimulation of autophagy as a novel mechanism for IL-6-mediated protection of  $\beta$ -cells from stress-induced apoptosis (77). Guo and colleagues, firstly analysed the expression of islet-enriched transcription factors in murine Min6  $\beta$  cell line following oxidative stress induced by  $H_2O_2$ , demonstrating that MAFA, MAFB, PDX1, and NKX6.1 were selectively inactivated. They further observed that MAFA and NKX6.1, essential factors for  $\beta$  cell development and function, are sequentially and selectively lost upon induction of hyperglycaemia in db/db mice. Importantly, MAFA, MAFB, PDX1, and NKX6.1 levels were also severely compromised in islets from human T2D donors. Following the development of peripheral insulin resistance, pancreatic  $\beta$ -cells try to restore a condition of normoglycemia through an adaptive compensatory process (78). In order to meet the requirement of insulin,  $\beta$ -cells adapt both their mass and function to release sufficient insulin to maintain blood glucose homeostasis. In fact, in subjects which present a



combination of genetic predisposition and injurious environmental risk factors, the process of  $\beta$  cell compensation could fail, resulting in a progressive decline in  $\beta$  cell function leading to a  $\beta$  cell dysfunction. Dysfunctional  $\beta$ -cells are no more capable to sustain the secretory demand of insulin. This is caused by the combination of a decrease in  $\beta$  cell mass and a chronic exposition to persisting hyperglycaemia stress. It was reported that hyperglycaemia is able to induce a glucotoxic effect on  $\beta$ -cells: in fact,  $\beta$ -cells exposed to high glucose concentration increase their expression of the pro-apoptotic receptor FAS on the cell surface. Prolonged condition of hyperglycaemia stimulus is able to induce a stress response in  $\beta$  cells, promoting their production of pro-inflammatory cytokines such as IL-1 $\beta$ . IL-1 $\beta$  is able to promote a Fas-triggered apoptosis in  $\beta$  cells, through the activation of the transcription factor NF-kB. Apoptosis of  $\beta$  cells, that means a reduction of  $\beta$  cell mass of ~40% respect to healthy patients, leads to a gradual lack of global insulin secretion which exacerbate the progression of insulin deficiency promoting the development of T2D.

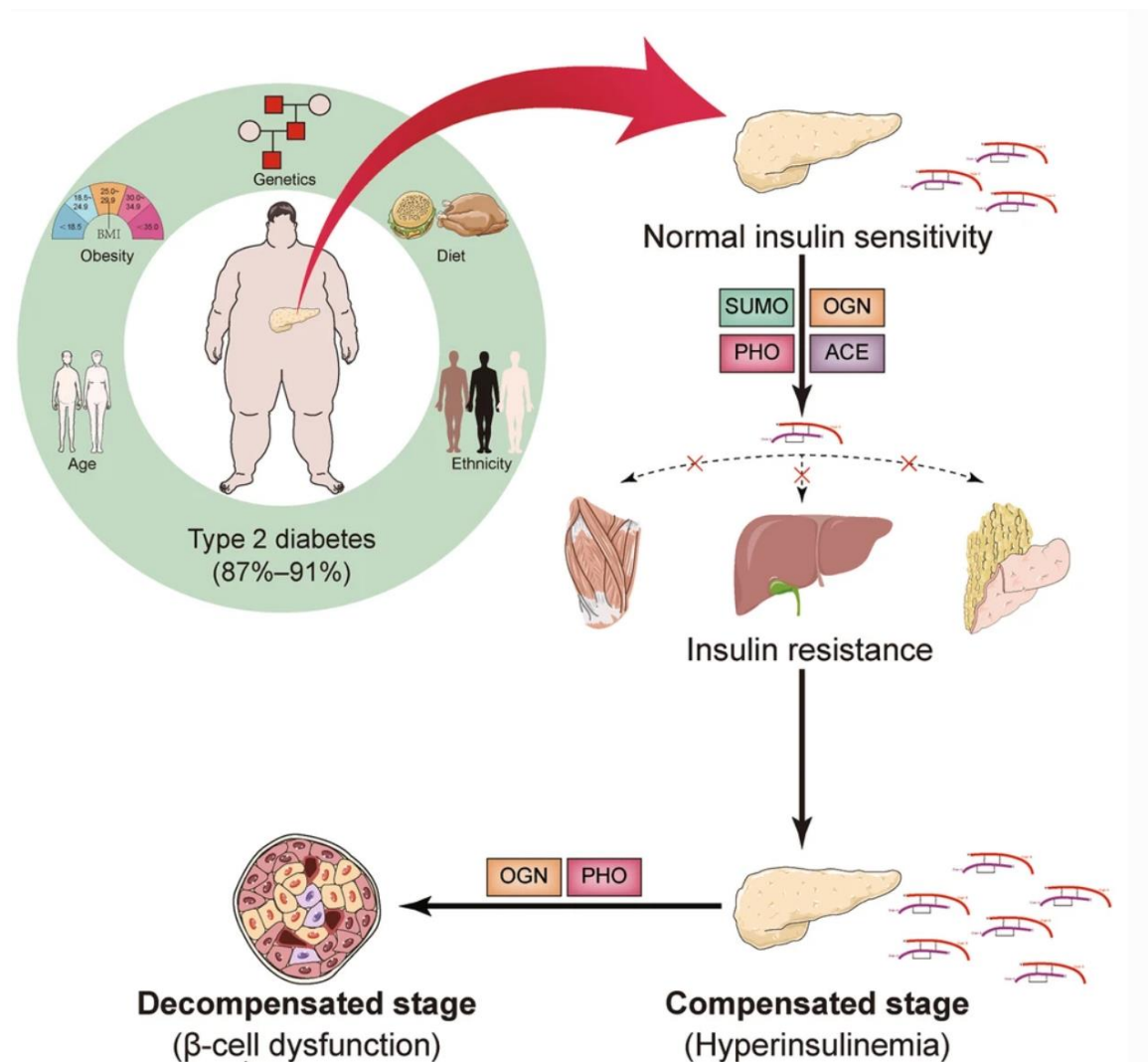


**Figure 5. Workflow of the development of T2D.** Multiple factors can favour the development of insulin resistance, inducing  $\beta$ -cells compensation in order to secrete more insulin, and leading to the initial hyperinsulinemia followed-up by  $\beta$ -cell dysfunction and T2D onset (72).

### 2.2.6 T2D genetic risk factors

T2D is a polygenic disease that results from the interaction between genetic and environmental factors. The genetic risk to develop T2D derived from combination between alterations in multiple genes scattered all across the genome (79). Evidence for a genetic component of T2D has come from in twins, first degree relatives of those with T2D and epidemiological studies have found to have an extremely high prevalence of T2D. Higher concordance rates are found among monozygotic twins (96%) than dizygotic twins; the 40% of first-degree relatives of T2D patients may develop diabetes, conversely the incident rate is only 6% in the general population (80).

Several single gene mutations have been identified as contributing of T2D. In fact, the mutations in hepatic nuclear factor (HNF) 1 or 4 are associated with severe impairment in insulin secretion and characterized a form of T2D called maturity onset diabetes of youth (MODY) and T2D patients with mutations in the insulin-receptor gene exhibit extreme insulin resistance 78,79. In a study, 152 single polymorphisms have been examined in 71 candidate genes associated to the disease and found several genes which can cause insulin resistance such as ABCC8 (sulphonyl urea receptor), KCNJ11 (KIR6.2), SLC2A2 (GLUT2), HNF4A (HNF4 $\alpha$ ), and INS; other genes are associated with insulin action (INSR, PIK3R1, SOS1) (**Figure 6**) (81).

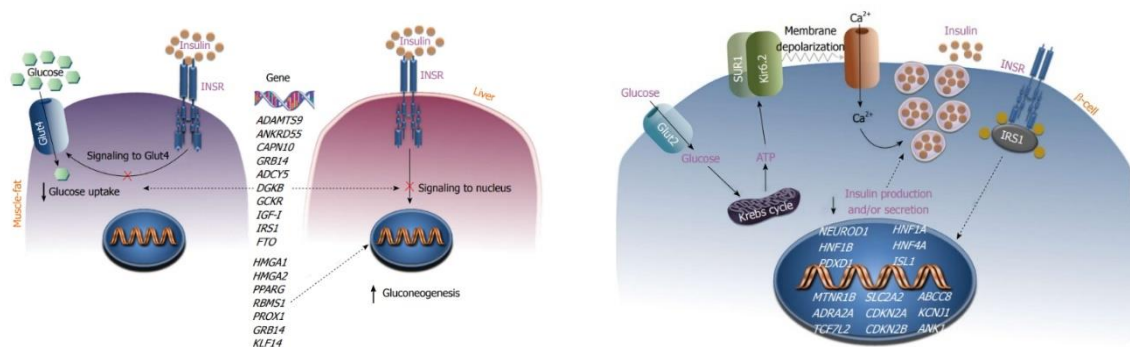


**Figure 6. Mechanism of insulin resistance.** The figure on the left shows the mechanisms by which gene variants can alter the action of insulin in the muscle, adipose and liver tissues of the target insulin. Peripheral insulin resistance in muscle and fat reduces cellular glucose uptake, while insulin resistance in the liver results in a failure to suppress glucose production and gluconeogenesis. Genes whose variations may affect the risk of developing insulin resistance and T2DM are indicated in black italics uppercase. The figure on the right shows a dysfunctional beta cell. Reduced insulin secretion is shown in beta cells with gene variants linked to T2DM. Genes associated with defects in beta cell mass and / or function are indicated in capital white italics (Adapted from (81)).

Genome-wide associated studies (GWAS) have identified approximately 75 susceptibility loci correlated to T2D. Examples of candidate genes are *KCNJ11* (potassium inwardly rectifying channel, subfamily J, member 11) that encodes for Kir6.2 ATP-sensitive potassium channel playing an important role in the regulation of insulin secretion (82), *TCF7L2* (transcription factor 7-like 2) which encodes for a member of Wnt signaling pathway active in the beta cell. The risk allele of the *TCF7L2* gene is located in intron 3, and it has been demonstrated that the upregulation of *TCF7L2* protein lead to impaired insulin secretion in beta cells, incretin effect and enhanced rate of hepatic glucose production (83); *IRS1* (insulin receptor substrate 1) has an effect on insulin action; *MTNR1B* (melatonin-receptor gene), *PPARG2* (peroxisome proliferator-activated receptor gamma 2), *IGF2BP2* (insulin-like growth factor two binding protein 2), *CDKN2A* (cyclin-dependent kinase inhibitor 2A), *HHEX* (haematopoietically expressed homeobox) and *FTO* (fat mass and obesity associated) gene (84).

### **2.2.7 T2D environmental risk factors**

There are several non-genetic factors directly or indirectly linked to Type 2 Diabetes, such as lifestyle, food and its components, persistent organic pollutants as well as the gut ecosystem that can lead obesity and oxidative stress. Lifestyle habits have a strong impact on a person's health and well-being (85). Some lifestyle habits like alcohol intake, smoking, exercise, sedentariness as well as stress, insomnia and the use of clinical drugs are closely related to certain diseases such as type 2 diabetes. For example, the stress has an effect on glucose metabolism through hypothalamic-pituitary-adrenal (HPA) axis and its constant activation can have negative effects on insulin activities causing insulin resistance (86). The diet is the most common environmental cause of T2D. It has been shown that a huge calorie

restriction can revert diabetes in T2D patients (87). Oxidative stress and inflammation are linked to T2D probably due to insufficient antioxidant defence. Several studies have demonstrated that low dietary intake of antioxidant such as beta-carotene, alfa-tocopherol and vitamin E can compromise the insulin action. In fact, diets rich of antioxidant, fruit and vegetables could prevent pancreatic beta cell dysfunction, reducing the risk of T2D (88).

The gut microbiota is vital to maintain individual health and it has been demonstrated to be associated with several metabolic disease including obesity and T2D. Several studies have shown that patients with T2D are characterized by increased abundance of Lactobacillus and lower abundance of butyrate-producing microbes, suggesting a strong correlation between Proteobacteria and Gram-negative Bacteroidetes and T2D (89). A meta-analysis study on coffee consumption, has demonstrated that both caffeinated coffee and decaffeinated coffee are associated with reduced diabetes risk, with a 25-30% lower risk for drinking three or more cups per day (90). Furthermore, there is a strong correlation between cigarette smoke and increased risk of T2D compared to non-smokers (91). Other environmental factors related to T2D are stress, depression or anxiety, all factors that increase the risk to develop T2D (92).

## **2.3 SARS-CoV-2**

### **2.3.1 Pathogenesis of SARS-CoV-2 infection**

On January 9, 2020, a new coronavirus leading to a respiratory disease called Covid-19, was isolated in Wuhan-China. On March 11, 2020, it was declared responsible for a pandemic outbreak by the World Health Organization (WHO). Coronaviruses are enveloped RNA viruses, classified in seven different coronaviruses that cause respiratory and intestinal infections in animals and humans (93).

SARS-CoV-2 is a single stranded positive-sense RNA virus with 16 non-structural proteins and 4 main structural protein including spike, membrane, envelope and nucleocapsid proteins (**Figure 7**).

At present, WHO has reported Covid-19 infection in 171 Countries and has confirmed more than 500 million of cases of COVID-19, caused by the SARS-CoV-2.

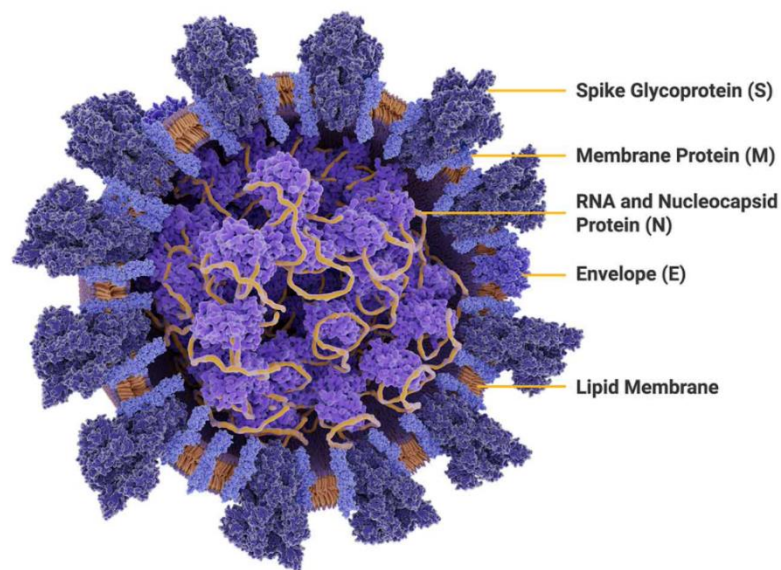


**Figure 7. Structure of SARS-CoV-2.** The structural protein of the SARS-CoV-2 are the spike glycoprotein, the membrane protein, the nucleocapsid protein and the envelope (From Promega).

SARS-CoV-2 can infect host tissue due to a 5 stages process: attachment, viral entry, viral replication and protein synthesis, maturation and release. The attachment is mediated by the spike protein (S), subdivided in three domains: a large outer domain, a single channel transmembrane anchor and a short intracellular domain. This glycoprotein is cleaved in two subunits, the S1 and the S2 by a transmembrane protease serine2 (TMPRSS2), that make the cleavage in the region between the amino acids 620 and 900. The S1 subunit bind the host receptor ACE2 (**Figure 8**) (94), instead the S2 subunit is involved in membrane fusion and together allow the fusion of the viral membrane with the host cell, inducing the genome release into the cytoplasm (95).

Once in the cytoplasm, the viral genome uncoats to set the viral RNA free and the host cell machinery is used to translate two polyproteins that are then processed to obtain the 16 non-structural proteins. During this step there is also the transcription and translation of an RNA-dependent RNA polymerase to synthesize a negative strand of RNA as a template; this template is necessary for the production of the positive strand RNA and the structural proteins, which are assembled to produce virions that are released in vesicles after the apoptosis/necrosis of the host cells, thus activating the host inflammatory response. The

inflammatory response allows the release of pro-inflammatory cytokines and the production of T cells and macrophages, which can lead to the cytokine storm, inducing the acute respiratory distress syndrome (ARDS) and organs damage (96–98).

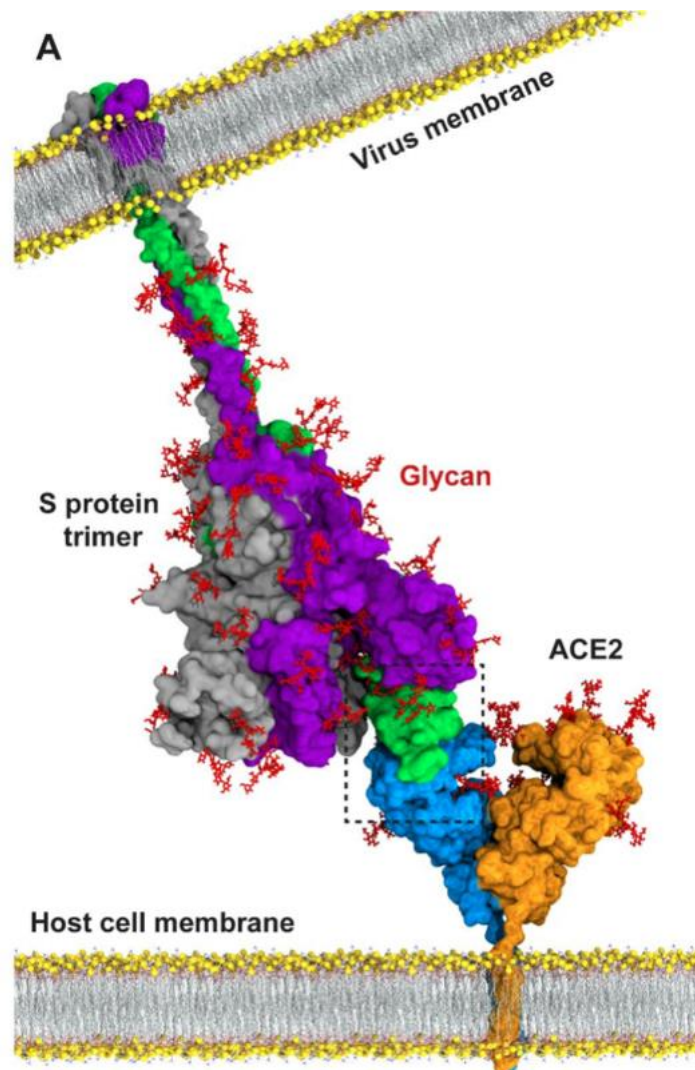


**Figure 8. ACE2 receptor SARS-CoV-2 interaction.** Spike protein is a homotrimer which binds the homodimer ACE2 receptor expressed on host cell membrane (Adapted from (94)).

### 2.3.2 Angiotensin-Converting Enzyme 2 (ACE2)

Angiotensin-Converting Enzyme 2 (ACE2) gene maps to chromosome X and is composed of 20 introns and 19 exons; this gene encodes a transmembrane glycoprotein of 805 amino acids with different domains, that are the N-terminal signal peptide, the ectodomain, the transmembrane domain and the C-terminal cytoplasmic domain (**Figure 9**) (99).

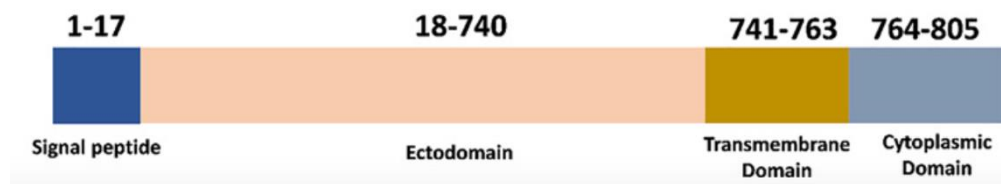


**Figure 9. ACE2 domains.** ACE2 has a N-terminal signal peptide (1-17 aa), an ectodomain (18-740 aa), a transmembrane domain (741-763 aa) and a C-terminal cytoplasmic domain (764-805 aa) (99).

ACE2 is a carboxypeptidase negatively regulating the renin-angiotensin-system (RAS) through the cleavage of the Angiotensin II, whose receptors are ATR1 and ATR2, into Angiotensin(1-7) which binds Mas and inducing vasodilatation, but it can also control the amino acids uptake in small intestine, glucose metabolism and pancreatic  $\beta$ -cell function (100).

Transcriptomic profiling of ACE2 performed by three different consortia in multiple human tissues, showed high level of Ace2 in the intestinal tract, kidney, testis, gallbladder, heart, thyroid gland, adipose tissue and pancreas while other organs showed lower expression of Ace2 (**Figure 10**) (101,102).

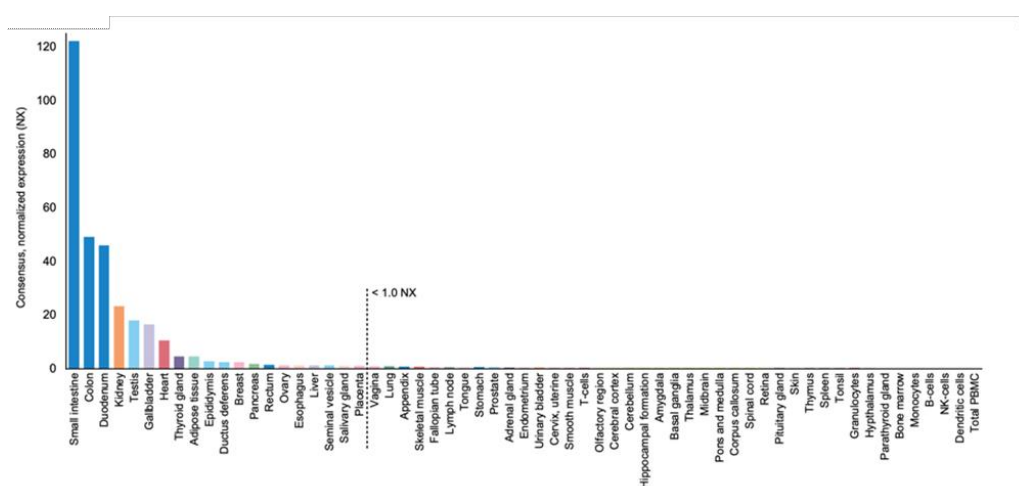


**Figure 10. Ace2 expression in human tissues based on transcriptomic analysis.** Ace2 is mainly expressed in the intestinal tract, but has a good expression also in kidney, testis, gallbladder, heart,



thyroid gland, adipose tissue, breast, pancreas, ovary and liver. The expression level of Ace2 in lung are under the cut-off (Adapted from (101)).

Together with the transcriptomic profiling of ACE2 in tissues, the Human Cell Atlas Consortium has analyzed the expression of Ace2 in single cellular type, which highlighted the enrichment of alveolar cell type 2 (AT2), bronchus and nasal mucosa with the highest expression observed in ciliated cells and goblet cells (103,104). This expression, although at low levels, explains the ability of coronaviruses to primarily infect the respiratory tract. It has been proposed that the initial host immune response to SARS-CoV-2 may trigger an interferon-driven upregulation of ACE2, leading to an increase in the number of cells in respiratory epithelia susceptible for SARS-CoV-2 infection, which could potentially explain the possibility of SARS-CoV-2 to enter via ACE2 receptors in the respiratory tract despite low ACE2 expression under normal conditions (105–107). To fully understand the role of ACE2 it is imperative to evaluate also its protein expression profiles across multiple tissues and cells. Hilmet and colleagues previously evaluated ACE2 protein expression by immunohistochemistry using two different antibodies in 44 different human tissues and organs. The immunoreactivity was manually quantified in 159 different cell types showing that the results are in line with the scRNA-seq, indeed ACE2 is abundant in intestinal tract and distinct expressed in kidney, gallbladder and testis. Other organs with lower mRNA expression level than the organs mentioned above, such as thyroid gland, seminal vesicle and pancreas, showed positivity in smaller subsets of cells. The protein profiling was also performed by Western Blot and mass spectrometry that showed high protein level in kidney, intestinal tract, pancreas, placenta and heart (**Figure 11**) (101).



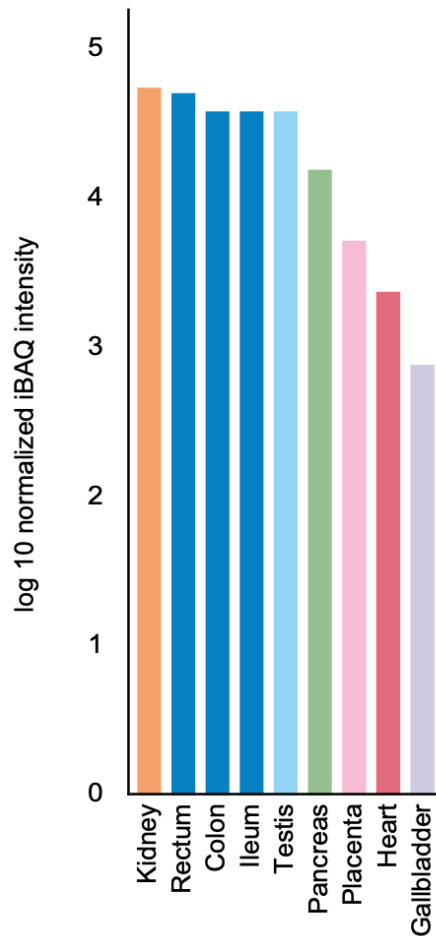


**Figure 11. ACE2 protein abundance in different tissue.** ACE2 protein is highly expressed in kidney, intestinal tract, testis, pancreas, placenta and heart (101).

Given the ability of the SARS-CoV-2 to cause severe vascular injury, it was suggested that the virus can directly enter into ECs, using the ACE2 receptor. However, the analysis of RNA sequencing based on ENCODE data from arterial, venous and microvascular beds area showed very low or no basal ACE2 expression in ECs compared with epithelial cells. Surprisingly, ACE2 transcript reads were detected in pericytes, suggesting that this type of cells can be infected by the SARS-CoV-2 and giving indirect effect on endothelial cells (108).

Meta-analysis of scRNAseq, confirmed that *Ace2* is mainly expressed in murine brain pericytes and (Vascular Smooth Muscle Cells) VSMCs, while the ACE2 protein expression, assessed by immunofluorescence, showed that the ACE2 positive cells are in the peri-endothelial region and in those cells showing a pericytes-like morphology (He *et*

*al.*, 2020). In addition, scRNA-seq showed that *Ace2* is expressed in pericytes residing also in other organs, such as heart (109).

To confirm these data in the human context, a dataset representing the developing human prefrontal cortex was used to highlight that ACE2 positive cells express at least one pericyte markers. Similarly, the analysis of scRNAseq data from healthy human heart identified a cluster of cells with high ACE2 expression alongside with pericytes markers; in contrast, no evidence of ACE2 expression human heart endothelial cells were found (110). In line with these findings, Coate and colleagues demonstrated that ACE2 has a perivascular expression and found that it is mainly colocalized with the pericytes markers PDGFR $\beta$  and NG2 (**Figure 12**) (111).

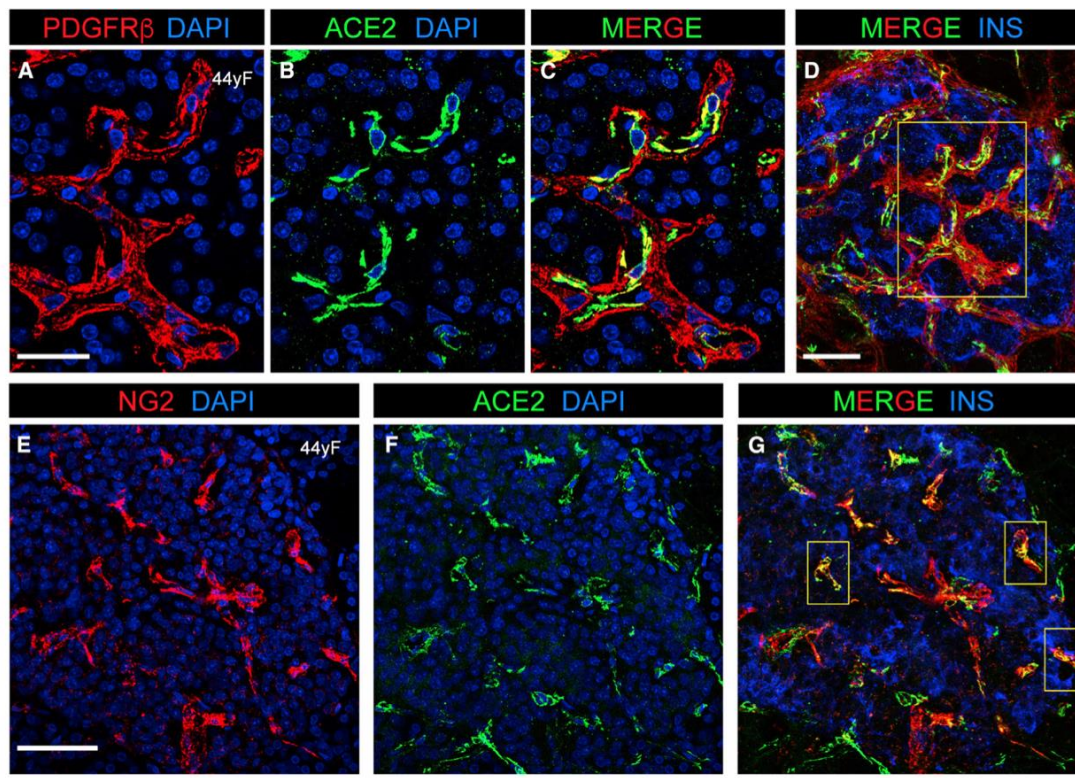


**Figure 12. Expression of ACE2 in pericytes.** ACE2 in microvasculature is expressed in pericytes cells as demonstrated by the colocalization between ACE2 and pericytes markers (111).

### 2.3.3 A novel ACE2 isoform

Given the importance of the respiratory tract in SARS-CoV-2 infection, Blume and colleagues studied the expression of ACE2 in airways epithelia, identifying a new isoform of ACE2, called short ACE2 (s-ACE2), that resulted tightly regulated by IFNs treatment and infection with rhinovirus, but not by SARS-CoV-2. This short ACE2, composed by 11 exons, starts with a new unannotated first exon, called exon 9a and exons 10-19 of the long ACE2 transcript (**Figure 13**) (112), is mainly expressed in airways and indeed, in nasal epithelium the level of short ACE2 are higher than the level of long ACE2.

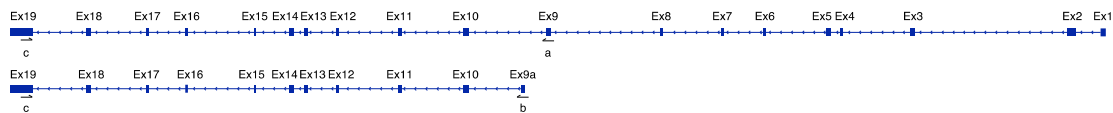


**Figure 13. Long ACE2 and short ACE2 exons.** The long ACE2 is composed by 19 exons, while the short isoform contains 10 exons that derived from the original transcript and a 11 exon that is not present in the long ACE2 (112).

It is important to note that the regulation of the short isoform depends on promoter elements localized upstream of the transcriptional start site of the short isoform and this regulation is independent from the regulation of the long ACE2 expression. It has been confirmed also that this short isoform is able to generate a protein product of around 52 kDa, whom expression is typical of nasal and bronchial epithelia; such isoform is lacking the Spike protein binding domain implicating that the SARS-CoV-2 cannot bind this receptor to directly infect airways epithelial cells (**Figure 14**) (112).

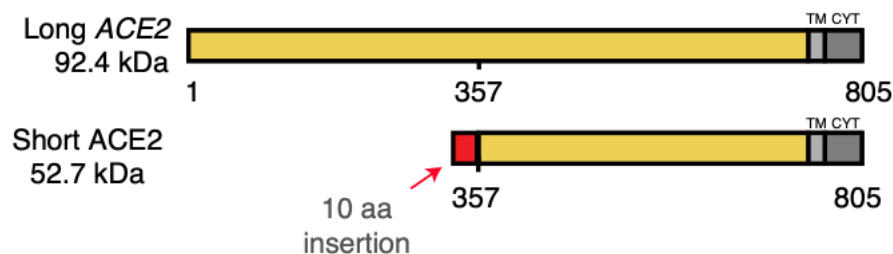


**Figure 14. Short and long ACE2 protein product.** The short ACE2 isoform lacks the binding domain for SARS-CoV-2 (112).

Furthermore, the expression of short ACE2 can be modulated by IFNs and by viral infections, more than long ACE2 and this, given the structure of the short ACE2, excludes the possibility that IFNs can enhance the SARS-CoV-2 infection through an upregulation of ACE2 expression. However, its regulation by IFNs suggests that short ACE2 may play an important role in the innate antiviral defense mechanism in the airways.

Another research group confirmed the existence of the short isoform of ACE2, called delta ACE2 or dACE2, which can be induced by IFNs and viruses including SARS-CoV-2. This study demonstrated how the long ACE2 isoform can start from two different exons and the delta ACE2 start from an exon localized on the intron 9 (**Figure 15**) (113). The novel isoform encodes a protein of 459 amino acids, which compared to the long ACE product, loss 339 amino acids of the N-terminal domain and 17 amino acids of the signal peptide. The loss of the N-terminal domain avoids the recognition by the SARS-CoV-2 of this isoform of ACE2, so even if the expression of dACE2 increases in presence of SARS-CoV-2 infection, the virus cannot use this receptor to infect cells.

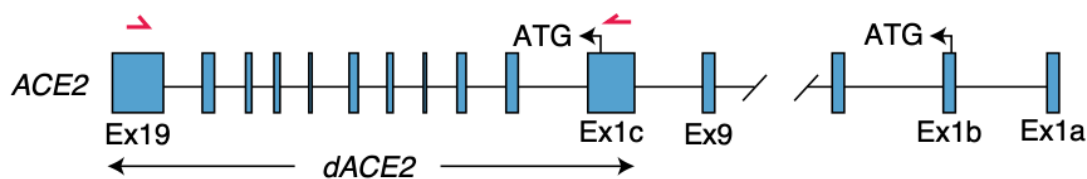


**Figure 15. Long ACE2 and dACE2 exons.** The long ACE2 transcription can start from two different exons, which are the Ex1a and Ex1b, while the transcription of the dACE2 starts from the Ex1c, localized on intron 9 (113).

Similarly to what previously reported by Blume and colleagues, this study showed that the expression of the short ACE2 isoform is under the control of its own promoter elements that are activated in the presence of IFN and/or viral infections, known to be potent inducer of the IFNs response. It has been also demonstrated that dACE2 expression is upregulated in SARS-CoV-2 infection, but given the apparent impossibility of the virus to bind the dACE2, the role of the isoform in the COVID-19 is yet to investigated (113), thus remaining unclear.

### 2.3.4 Physiological role of ACE2 in pancreatic islets

It is important to note that ACE2 plays important roles in the regulation of pancreatic islet function and in glucose homeostasis. In pancreatic islets, ACE2 directly controls the levels of Angiotensin(1-7) thanks to its enzymatic ability to cleave the Angiotensin-II into Angiotensin(1-7), thus reducing the production of Reactive Oxygen Species (ROS). Of note, an important enemy for pancreatic islet function is the oxidative stress and the ROS synthesis which are increased by the binding of the Ang II to its receptors; in this case, ACE2 attenuates the oxidative stress due to the cleavage of Angiotensin-II into Angiotensin(1-7) (**Figure 16**) (114).

In addition, Angiotensin(1-7) can affect  $\beta$ -cells activity by increasing the production of cAMP and GAD67/GABA and, consequently, insulin synthesis, secretion and proliferation.

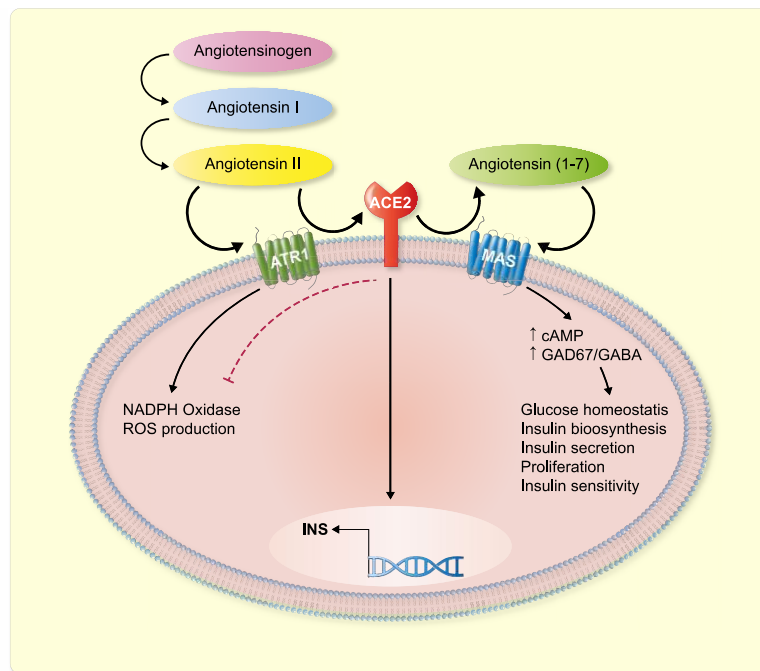


**Figure 16. Function of ACE2 in pancreatic  $\beta$ -cells.** ACE2 affects the activity of  $\beta$ -cells, mediating different activities. ACE2 is directly involved in the degradation of Ang II through its cleavage into downstream products. This can inhibit the activation of NADPH oxidase and the ROS production mediated by Ang-II. On the other hand, ACE2 can favor glucose homeostasis, through insulin biosynthesis and insulin secretion and/or proliferation of  $\beta$ -cells through the formation of Ang(1-7) and its subsequent binding to the MAS receptor (115).

The glucose homeostasis is maintained by the modulation of the ACE2/Ang(1-7)/MAS pathway, controlling the GAD67/GABA signaling in pancreatic islets; indeed, in ACE2 KO mice, GAD67 and GABA expression decreased significantly causing the development of obesity and T2D (116).

The cleavage of AngII in Ang(1-7) regulates the islet microcirculation and affects islet survival and function; indeed Ang(1-7), after the binding with MAS receptor, determines vasodilation by improving intra-islet vessel density, increases insulin content in islet and the first phase of the insulin secretion in  $\beta$ -cells. Moreover Ang(1-7) prevents palmitate-induced apoptosis in  $\beta$ -cells, reduces the iNOS activity in islets and increases calcium flux during release of insulin. Additionally, ACE2 is involved in the regulation of mitochondrial metabolism and in the maintenance of the mitochondrial homeostasis. Moreover, it has been observed that the overexpression of ACE2 in INS-1 cells reduced detrimental effects due to the presence of ROS, and increased insulin secretion (117,118).

Of note, ACE2 KO mice showed decreased first-phase insulin secretion compared to WT mice, leading to the development of impaired glucose homeostasis (100).

Another research group confirmed that ACE2-deficient mice became progressively glucose intolerant, highlighting the important role of ACE2 in insulin secretion. Furthermore, ACE2 deficiency deteriorated islet function through a mechanism that primarily involves the microvasculature (119). Overall, these studies show that ACE2 function in pancreatic islets and in  $\beta$ -cells is likely to have a protective effect on survival and function.

### **2.3.5 SARS-CoV-2, COVID-19 and Diabetes Mellitus: a bidirectional causal relationship?**

The presence of ACE2 in SARS-COV-2 target cells is an indispensable requirement for a productive infection (120–122). Considering that ACE2 is expressed in the human pancreas, including insulin-producing  $\beta$ -cells, this prompted out to an important question: can SARS-CoV-2 infect pancreatic islets, thus causing their functional impairment?

Although ACE2 expression in islets and  $\beta$ -cells is now well documented in a series of studies, initial investigations reported conflicting results quickly turning it into a matter of debate. According to some studies ACE2 was expressed in exocrine pancreas, but there

was no evidence of ACE2 in endocrine components (111,123). In contrast, other studies have clearly identified ACE2 in pancreatic islet  $\beta$ -cells (124–127).

Elucidating SARS-CoV-2 tropism in pancreatic islet is fundamental, due to the evidence that COVID-19 seems to have a more severe outcome in patients with diabetes (128) and, more importantly, that SARS-CoV-2 can induce or trigger new-onset diabetes (129,130).

Since the first cases of COVID-19 infection, it has been observed that patients with diabetes have a poor prognosis due to multiple factors such as age, sex, ethnicity, comorbidities such as hypertension and cardiovascular disease, obesity, and a pro-inflammatory and pro-coagulative state (**Figure 17**) (131).

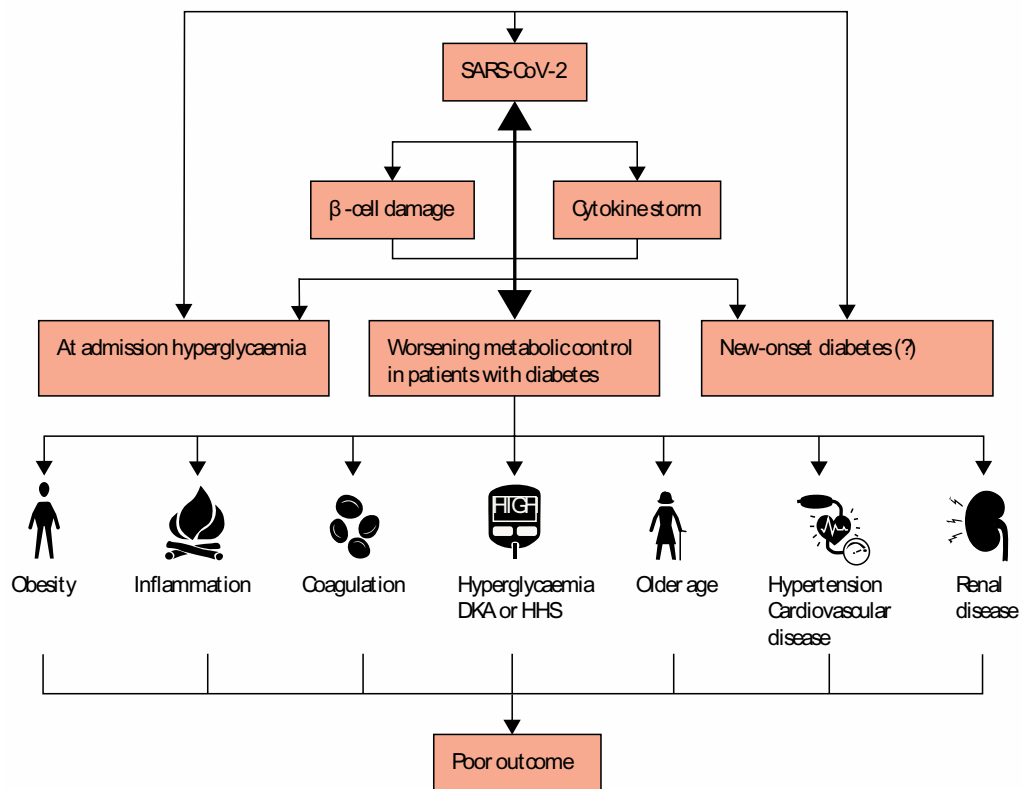


**Figure 17. Biunivocal relationship between COVID-19 and diabetes.** A poor prognosis is usually observed in elderly patients and worldwide age-specific case-fatality rate occurred very high among patients with one or more underlying chronic diseases including cardiocirculatory, renal, pulmonary, central nervous system and mental illness, diabetes mellitus and malignancies (131).



In Wuhan during the first month of the pandemic, among 1561 patient with COVID-19, 9.8% of them had diabetes and these patients required admission to intensity care unit (ICU). In a retrospective study, a subgroup of 24 patients with diabetes had higher mortality (16,5% rate), compared to none of the 26 patients without diabetes (0% rate) (132). Data from nine hospitals demonstrated that the 58% of patient who required hospitalization due to COVID-19 had T2D (133). A retrospective study, considering more than 7000 patients with COVID-19 and including 952 patients with pre-existing T2D have demonstrated that patients with pre-existing T2D have higher mortality rate, greater requirement of medications and more prevalence of multiorgan damage than non-diabetic patients (Zhu *et al.*, 2020). Two different studies showed that patient with diabetes, after the SARS-CoV-2 infection have an higher probability to ICU admission (134,135); other studies highlighted the higher mortality of patients with T2D than patients without diabetes (128,132,134–139). Yang and colleagues, in a study population of 4648 people (140), showed that those with diabetes have an higher probability to develop severe disease than people without diabetes (**Figure 18**).

	Article type	Study population	Prevalence of diabetes	Outcome	Risk
Zhang et al <sup>3</sup>	Retrospective	258	24%	Mortality	3.64 (1.08–12.21)*
Kumar et al <sup>4</sup>	Meta-analysis	16 003	9.8%	Severe disease	2.75 (2.09–3.62)*
Kumar et al <sup>4</sup>	Meta-analysis	16 003	9.8%	Mortality	1.90 (1.37–2.64)*
Guan et al <sup>10</sup>	Retrospective	1590	NA	Composite†	1.59 (1.03–2.45)‡
Li et al <sup>11</sup>	Meta-analysis	1525	9.7%	ICU admission§	2.21 (0.88–5.57)¶
Fadini et al <sup>12</sup>	Meta-analysis	1687	NA	Severe disease	2.26 (0.98–4.82)
Fadini et al <sup>12</sup>	Meta-analysis	355	35.5%	Mortality	1.75
Petrilli et al <sup>13</sup>	Retrospective	5279	22.6%	Hospital admission	2.24 (1.84–2.73)*
Roncon et al <sup>14</sup>	Meta-analysis	1382	NA	ICU admission	2.79 (1.85–4.22)*
Roncon et al <sup>14</sup>	Meta-analysis	471	NA	Mortality	3.21 (1.82–5.64)*
Zhou et al <sup>15</sup>	Retrospective	191	19%	Mortality	2.85 (1.35–6.05)*
Zhu et al <sup>16</sup>	Retrospective	7337	13%	Mortality	1.49 (1.13–1.96)‡
Yan et al <sup>17</sup>	Retrospective	193	25%	Mortality	1.53 (1.02–2.3)‡
Sardu et al <sup>18</sup>	Retrospective	59	44%	Survival	0.172 (0.051–0.576)‡
Yang et al <sup>19</sup>	Meta-analysis	4648	NA	Severe disease	2.07 (0.88–4.82)*
Barron et al <sup>20</sup>	Cohort study	61 414 470	0.4% type 1 diabetes	Mortality	3.50 (3.15–3.89)*
Barron et al <sup>20</sup>	Cohort study	61 414 470	4.7% type 2 diabetes	Mortality	2.03 (1.97–2.09)*

ICU=intensive care unit. NA=not given. \*Odds ratio (95% CI). †ICU admission, or invasive ventilation, or death. ‡Hazard ratio (95% CI). §Calculated for 1056 patients (in three of six studies). ¶Risk ratio (95% CI). ||Rate ratio (95% CI not given).



**Figure 18. COVID-19 outcomes according to pre-existing diabetes.** Several studies showed higher mortality in patient with diabetes, other studies highlighted the development of severe disease in diabetic patients compared with non-diabetic ones and some studies showed an higher probability of ICU admission in those patients with diabetes (131).

Different studies have also demonstrated that COVID-19 infection can cause hyperglycaemia, more than what previously observed for other viral infections such as SARS-CoV-1 and hepatitis C (141); in particular, it was observed that in case of SARS-CoV-2 infection, some patients can develop impaired glucose homeostasis alongside with altered insulin secretion and  $\beta$ -cell function. Among American veterans without diabetes, a SARS-CoV-2 infection was associated with higher risk of diabetes. In details, a retrospective cohort study conducted on more than 2 million of veterans showed how, following the SARS-CoV-2 infection, 0,5 % of veterans developed diabetes in the following 120 days and the 0,6% in 193 days. Moreover among the subgroup of individuals who were hospitalized, the rate of diabetes development in 120 days were 2,8% and 3,2% in 193 days (142).

Montefusco and colleagues, studied a group of 551 patient with COVID-19, with 151 patients affected by T2D at hospital admission. During their in-hospital stay, hyperglycaemia was measured not only in diabetic patient but also in the 46% of patient that did not have diabetes at the admission. Among patients without diabetes who showed new onset hyperglycaemia, 35% of them continued to have hyperglycaemia and 2% developed T2D, while the remaining percentage (63%) showed a complete remission. Of note, mean hemoglobin A1c (HbA1c) were similar between patients with new-onset hyperglycaemia and normoglycaemic patients confirming the new-onset of hyperglycaemia putatively corresponding to COVID-19 infections. These patients have been evaluated also for the alteration in glycemic control, not detectable by fasting glycaemia, performing the professional continuous glucose monitoring (CGM). The CGM analysis showed that in normoglycemic patient with COVID-19, there was a significantly longer duration of glycaemia above 140 mg/dl and this alteration persists in some patients, also after recovery. Furthermore, mean fasting insulin, proinsulin, C-peptide levels, homeostasis model assessment of  $\beta$ -cell dysfunction (HOMA-B) and homeostasis model assessment of insulin resistance (HOMA-IR), but not insulin-to-proinsulin ratio, were significantly higher in patients with COVID-19 as compared to healthy controls (143).

COVID-19 may induce a severe inflammatory state resembling that which is observed in T2D; in the long term, these effects may lead to  $\beta$ -cell exhaustion and worsening of diabetes caused by islet hyperstimulation and glucose toxicity. Of note, some cytokines, such as IL-1 $\beta$ , IL-4, IL-6, IL-7, IL-8, IL-10, IL-13, G-CSF, MIP-1 $\beta$  and TNF are upregulated in the sera of patients with COVID-19 compared to healthy controls and some of these cytokines, such as IL-1  $\beta$ , IL-2, IL-4, IL-7, IL-8, IL-10, IL-13, IL-17, G-CSF and IFN- $\gamma$  were also increased in the serum of patients who recovered from COVID-19 (143). Notably, these cytokines are able to increase the apoptosis rate of human pancreatic islets cells (144). In addition, in patients who recovered from COVID-19 and who experienced new-onset hyperglycaemia, a reduction of IL-6 was observed, thus conferring a putative role to IL-6 in the induction of metabolic alterations observed during COVID-19 (143).

A cohort study performed on more than 600 patients with COVID-19 confirmed that SARS-CoV-2 infection increases the risk to develop new-onset hyperglycaemia and T2D in comparison to patients with influenza, suggesting that the higher risk to develop T2D is not caused by a general morbidity after a viral illness, but is caused directly by a SARS-CoV-2 mediated mechanism (145).

The ability of the SARS-CoV-2 to directly infect human pancreatic islet is controversial, and as previously written different studies have shown different results. However, *in vitro* studies confirmed that SARS-CoV-2 infection cause a decrease in insulin content and GSIS, but also an increase in  $\beta$ -cell apoptosis (124). In another study, Birabaharan and colleagues showed that SARS-CoV-2 can directly infect pancreatic cells using the ACE2 receptor which is expressed at higher level in pancreas than in lungs (146).

As early as in 2020 Yang et. al used human pluripotent stem cells (hPSCs) to generate human cells, tissues and organoids that allows us to model the SARS-CoV-2 infection *in vitro* differentiated pancreatic islets; using this model they showed the presence of ACE2 on  $\alpha$  cells and  $\beta$ -cells, but not in  $\delta$  cells and in acinar, ductal and mesenchymal cells. ACE2 on  $\alpha$  and  $\beta$ -cells is needed by the virus to entry into the cells (147).

Steenblock and colleagues showed that the SARS-CoV-2 infects human pancreas due to the detection of the SARS-CoV-2-N capsid protein in exocrine and endocrine components. In addition, by using RNA in situ hybridization, viral RNA has been detected in insulin producing  $\beta$ -cells and not in exocrine components (126) .

Similarly, Muller and colleagues highlighted the ability of SARS-CoV-2 to infect both endocrine and exocrine pancreatic cells using ACE2 receptor to entry and to replicate into these cells. Of particular interest, endocrine cells, following the infection of the SARS-CoV-2, can go through a functional change, causing dilatation and vacuolization of the endoplasmic reticulum and Golgi apparatus complex, a suggestion of the ER stress, related with low glucose-dependent insulin response. Pathway analysis of the genes enriched in SARS-CoV-2-infected human islets highlighted canonical biological pathways associated with virus infection, including cellular stress response, eukaryotic translation initiation factor 2 (eIF2) signaling pathway, as well as interferon and JAK-STAT signaling. To determine, instead, the activity of the  $\beta$ -cells that have been infected by SARS-CoV-2 the level of insulin were evaluated, showing lower level of insulin in cell infected by virus than in control cells, but higher level of  $\alpha$  and ductal cells markers such as GCG, PRSS1 and PRSS2, suggesting that  $\beta$ -cells were transdifferentiated (125,127).

However, it should be noted that other studies postulated different mechanisms of action of SARS-CoV-2 *in vitro* pancreatic islets. *In vitro* studies performed by van der Heide and colleagues confirmed that SARS-CoV-2 targets pancreatic islets, mainly  $\beta$ -cells, but also  $\alpha$ -cells, causing a productive infection and a downregulation of multiple proteins associated with  $\beta$ -cells survival and diabetes development. Of note, it was shown that the virus is not able to cause cytopathic effects on pancreatic cells, but it causes a small, but significant reduction of insulin secretion in infected  $\beta$ -cells. The inflammatory response was evaluated using the tissue culture supernatant and showed an elevated levels of chemokines CXCL10 and CXCL11 and their inducer IFN $\gamma$  (148).

### **3. Aims of the Thesis**

The presence of ACE2 in SARS-COV-2 target cells is an indispensable requirement for a productive infection and several reports indicate a wide, although variable, distribution of ACE2 expression. After three years of SARS-CoV-2 pandemic, it is now generally accepted that diabetic individuals have a more severe COVID-19 course.

Conversely, COVID-19 patients have different metabolic changes and some of them develop diabetes mellitus. Thus, there is a bidirectional relationship between COVID-19 and diabetes.

Based on these information, the aims of this thesis are:

- i)* To evaluate ACE2 expression pattern in exocrine and endocrine pancreas.
- ii)* To detect a putative differential expression of ACE2 in human pancreatic tissue sections obtained from a large cohort of T2D multiorgan donors in comparison to non-diabetic ones;
- iii)* To evaluate putative relationship between ACE2 expression and inflammation.
- iv)* To confirm the SARS-CoV-2 infection in human pancreatic  $\beta$ -cells.

## 4. Material and Methods

### 4.1 Human Multiorgan and Autaptic Donors

Human pancreatic sections analysed in this study for ACE2 evaluation in non-diabetic condition were obtained from pancreata of brain-dead adult non-diabetic multiorgan donors within the European Network for Pancreatic Organ Donors with Diabetes (EUnPOD), a project launched in the context of the INNODIA consortium ([www.innodia.eu](http://www.innodia.eu)). Whole pancreata were processed following standardized procedures at University of Pisa. Formalin fixed paraffin embedded (FFPE) pancreatic tissue sections and frozen OCT pancreatic tissue sections were obtained from n=7 adult non-diabetic multiorgan donors, and from n=1 longstanding T1D donor pancreas (**Table 1**). In INNODIA EUnPOD network, pancreata not suitable for organ transplantation were obtained with informed written consent by organ donors' next-of-kin and processed with the approval of the local ethics committee of the Pisa University.

Case/ Sample ID	Gender	Age (Years)	BMI (Kg/m <sup>2</sup> )	AutoAb (ELISA)	HiRes HLA	Cause of Death	Tissue type	HI Purity (Dithizone Stain- %)	HI Purity (insulin ICC-%)	Used for
141117	M	49	25.8	GADA neg, IA- 2A neg, ZnT8A neg	HLA:A*03,68 ; B*35,47; C*04,06; DRB1*03,08; DQB1*02,04	Cardiovascul ar disease	FFPE and fresh-frozen pancreatic tissue	--	--	IHC/LCM
181117	M	39	23.6	GADA neg, IA- 2A neg ZnT8A neg	HLA:A*03,33 ; B*14, B*14 SD B65; C*08; DRB1*01, DQB1*05	Trauma	FFPE and fresh-frozen pancreatic tissue	--	--	IHC/LCM
110118	F	46	32.5	GADA neg IA-2A neg, ZnT8A neg	HLA:A*24; B*15,18; C*7; DRB1*04,11; DQB1*3	Cardiovascul ar disease	FFPE and fresh-frozen pancreatic tissue	--	--	IHC/LCM
300318	F	56	24.5	GADA neg, IA- 2A neg, ZnT8A neg	HLA:A*2; B*07,50; C*06,07; DRB1*03,15; DQB1*02,06	Trauma	FFPE and fresh-frozen pancreatic tissue	--	--	IHC
210518	M	44	24.5	GADA neg, IA- 2A neg, ZnT8A neg	HLA:A*24,34 ; B*15,55; C*03,07; DRB1*11,13; DQB1*3	Cardiovascul ar disease	FFPE and fresh-frozen pancreatic tissue	--	--	IHC
161118	F	39	22.3	GADA neg, IA- 2A neg, ZnT8A neg	HLA:A LR*03,68; B*07,51; C*07,14; DRB1*01,15; DQB1*05,06	Cardiovascul ar disease	FFPE and fresh-frozen pancreatic tissue	--	--	IHC/LCM
110119	M	22	27.2	GADA neg, IA- 2A neg, ZnT8A neg	HLA:A*01,02 ; B*08,18; C*07,07; DRB1*03,11; DQB1*02,03	Trauma	FFPE and fresh-frozen pancreatic tissue	--	--	IHC/LCM
Islet prep 1	F	23	22.5	n/a	n/a	Cardiac arrest	Enzymatic- isolated pancreatic islets	--	46	RNA-seq
Islet prep 2	M	31	27.8	n/a	n/a	Cerebral haemorrhage	Enzymatic- isolated pancreatic islets	--	66	RNA-seq
Islet prep 3	M	77	24.5	n/a	n/a	Cerebral haemorrhage	Enzymatic- isolated pancreatic islets	--	59	RNA-seq
Islet prep 4	F	64	29.4	n/a	n/a	Cerebral haemorrhage	Enzymatic- isolated pancreatic islets	--	47	RNA-seq
Islet prep 5	F	58	21.3	n/a	n/a	Cerebral haemorrhage	Enzymatic- isolated pancreatic islets	--	67	RNA-seq
Islet prep 6	M	67	25.7	n/a	n/a	Trauma	Enzymatic- isolated pancreatic islets	--	48	RNA-seq
Islet prep 7	F	87	23.8	n/a	n/a	Cerebral haemorrhage	Enzymatic- isolated pancreatic islets	--	60	RNA-seq
Islet prep 8	F	67	24.6	n/a	n/a	Cerebral haemorrhage	Enzymatic- isolated pancreatic islets	--	44	RNA-seq

Islet prep 9	F	83	37.1	n/a	n/a	CVD	Enzymatic- isolated pancreatic islets	--	51	RNA-seq
Islet prep 10	F	84	24.5	n/a	n/a	CVD	Enzymatic- isolated pancreatic islets	--	58	RNA-seq
Islet prep 11	F	40	22.5	n/a	n/a	Stroke	Enzymatic- isolated pancreatic islets	--	59	RNA-seq
Hi#2	M	52	34.2	n/a	n/a	n/a	Enzymatic- isolated pancreatic islets	≥70%		qRT-PCR ACE2 mRNA
Hi#3	M	50	27.4	n/a	n/a	n/a	Enzymatic- isolated pancreatic islets	≥70%		qRT-PCR ACE2 mRNA
Hi#4	M	55	28	n/a	n/a	n/a	Enzymatic- isolated pancreatic islets	≥70%		qRT-PCR ACE2 mRNA
Hi#8	M	38	23.1	n/a	n/a	Cardiovascul ar disease	Enzymatic- isolated pancreatic islets	90%		qRT-PCR ACE2 mRNA

**Table 1.** Characteristics of non-diabetic multiorgan donors. Main descriptive characteristics are reported alongside with tissue type obtained. Human islets (HI) purity values (only for pancreatic islets enzymatic isolation) and type of analysis performed, are reported as well.

Human pancreatic sections analysed in this study for ACE2 evaluation in diabetic vs non-diabetic condition and for CD68 analysis were obtained from pancreata of brain-dead adult non-diabetic and T2D multiorgan donors, COVID-19 negative. Pancreata not suitable for organ transplantation were obtained with informed written consent by organ donors' next-of-kin and processed following standardized procedures by University of Pisa (Pisa, Italy). Multiple formalin-fixed paraffin embedded (FFPE) tissue sections were obtained from n=20 non-diabetic controls (CTR) [9F, 11M; age:  $70.6 \pm 7.0$  years (mean  $\pm$  S.D.); BMI:  $26.2 \pm 4.1$  Kg/m<sup>2</sup>) and from n=20 T2D pancreata (6F, 14M; age:  $71.7 \pm 7.6$  years (mean  $\pm$  S.D.); BMI:  $27.1 \pm 2.7$  Kg/m<sup>2</sup> (mean  $\pm$  S.D.)) whose clinical characteristics are described in **Table 2**.

	Pancreas ID	Gender (M/F)	Age (y)	BMI (Kg/m <sup>2</sup> )	Abdominal circumference (cm)	Years from diagnosis of diabetes	ICU stay (days)	Cold Ischemia Time (hours)	Mean glycemia (mg/dl)
1	ND_HP 05/11/13	F	63	23,3	90	/	1	15	152
2	ND_HP 06/11/20	F	62	23,53	87	/	3	15	163
3	ND_HP 09/12/20	M	65	27,8	116	/	12	14	252
4	ND_HP 10/06/13	F	69	20,8	80	/	3	13	138

5	ND_HP 12/11/13	M	74	24,83	100	/	2	13	161
6	ND_HP 13/02/14	M	78	23,15	94	/	1	14	115
7	ND_HP 13/06/20	M	71	34,6	130	/	9	12	130
8	ND_HP 14/05/13	F	76	19,53	90	/	2	17	66
9	ND_HP 16/09/20	M	81	27,68	107	/	2	18	110
10	ND_HP 16/12/20	F	75	34,89	145	/	5	16	181
11	ND_HP 19/02/20	F	59	27,68	126	/	2	17	134
12	ND_HP 22/02/14	F	64	29,38	115	/	2	20	159
13	ND_HP 22/05/13_B	F	64	23,4	108	/	1	n/a	159
14	ND_HP 24/02/20	M	74	32,98	120	/	1	36	146
15	ND_HP 25/03/13	M	69	25	87	/	6	17	148
16	ND_HP 27/06/20	M	79	27,8	132	/	21	13	160
17	ND_HP 28/05/13	M	69	25,05	85	/	1	12	111
18	ND_HP 28/09/20_A	M	83	25,7	89	/	1	13	127
19	ND_HP 29/02/20	F	75	23,44	63	/	1	16	155
20	ND_HP 08/10/13	M	62	24,69	110	/	1	14	126
21	T2D_HP 07/12/10	F	73	22,2	90	9	1	11	155
22	T2D_HP 13/05/10	M	79	27,3	105	5	2	15	200
23	T2D_HP 06/07/10	M	69	25,9	88	11	2	15	334
24	T2D_HP 06/11/10	M	78	25,9	103	25	2	13	203
25	T2D_HP 07/02/11_B	M	68	27,8	105	6	9	11	234
26	T2D_HP 08/09/11	F	53	33,1	117	7	2	12	138
27	T2D_HP 10/01/20	F	72	25,39	90	n/a	2	n/a	130
28	T2D_HP 10/03/17	M	79	27,18	110	n/a	2	n/a	210
29	T2D_HP 10/12/08_A	F	75	29,4	105	2	1	13	153
30	T2D_HP 14/07/11	M	62	33,1	118	5	n/a	12	171
31	T2D_HP 15/02/09	M	77	26,1	97	30	3	12	n/a
32	T2D_HP 16/05/10	M	59	29,4	80	4	1	12	181
33	T2D_HP 16/12/11	M	75	26,1	110	n/a	1	15	374
34	T2D_HP 17/10/11	M	61	24,6	92	10	2	14	177
35	T2D_HP 19/09/10	F	79	29,2	110	6	n/a	29	269
36	T2D_HP 20/06/11	M	76	26	95	14	2	n/a	165
37	T2D_HP 21/09/11	M	78	24,5	90	9	4	48	303
38	T2D_HP 23/01/11	F	73	27,3	108	30	1	11	214
39	T2D_HP 26/10/10	M	69	27,7	97	5	5	13	151
40	T2D_HP 31/03/11	M	79	24,7	106	8	1	12	211

**Table 2:** Available main clinical characteristics for each nondiabetic and type 2 diabetic donors included in the study. Gender, Age (years), BMI (kg/m<sup>2</sup>), Abdominal circumference (cm) and disease duration (years) are reported.

Human pancreatic FFPE tissue sections analysed in this study for SARS-CoV-2 NP presence were obtained from autopsy-derived tissues from n=13 non-diabetic without COVID-19 and n=16 non-diabetic with SARS-CoV-2 infection multiorgan donors collected by Université Libre de Bruxelles (ULB) (**Table 3**).



Control subjects ID		COVID+ Patients ID	
1	16A00019	14	20A00031
2	16A00024	15	20A00038
3	16A00065	16	20A00039
4	16A00067	17	20A00042
5	16A00073	18	20 A00044
6	16A00075	19	20A00045
7	16A00086	20	20A00047
8	16A00101	21	20A00048
9	16A00107	22	20A00049
10	16A00119	23	20A00053
11	16A00135	24	20A00055
12	16A00151	25	20A00056
13	16A00157	26	20A00061
		27	20A00068
		28	20A00072
		29	20A00074

**Table 3:** ID of control subjects and COVID-19+ patients analyzed after autopsy. ID of control subjects and COVID+ patient from whom derived FFPE pancreatic section.

## 4.2 Human pancreatic islets isolation

Human pancreatic islets were obtained from n=4 non-diabetic multi-organ donors (Table 1). Briefly, purified islets were prepared by intraductal collagenase solution injection and density gradient purification, as previously described. At the end of the isolation procedure, fresh human pancreatic islets preparations were resuspended in CMRL culture medium (cat. 11-530-037, ThermoFisher Scientific, Waltham, MA, USA) supplemented with L-Glutamine 1% (cat. G7513-100ML), Antibiotic/Antimicotic 1% (A5955-100ML, Sigma Aldrich, St. Louis, MO, USA), FBS 10% and cultured at 28°C in a 5% CO<sup>2</sup> incubator.

### 4.3 Cell culture

EndoC- $\beta$ H1 human  $\beta$ -cell line (27,28) was obtained by UniverCell-Biosolutions (Toulouse-France) and used for all experiments between passages 78-88. EndoC- $\beta$ H1 were cultured at 37 °C with 5% CO<sup>2</sup> in coated flask (coating medium composition: DMEM high-glucose cat. 51441C, Penicillin/Streptomycin 1% cat. P0781, ECM 1% cat. E1270 and Fibronectin from bovine plasma 0.2% cat. F1141 - all from Sigma Aldrich, St. Louis, MO, USA) and maintained in culture in low-glucose DMEM (cat. D6046) supplemented with 2% BSA fraction V (cat. 10775835001),  $\beta$ -Mercaptoethanol 50  $\mu$ M (cat. M7522), L-Glutamine 1% (cat. G7513), Penicillin/Streptomycin 1% (cat. P0781), Nicotinamide 10 mM (cat. N0636), Transferrin 5.5  $\mu$ g/mL (cat. T8158) and Sodium selenite 6.7 ng/mL (cat. S5261) (all from Sigma Aldrich, St. Louis, MO, USA).

HeLa cells (ATCC CCL-2), passages 33-34, were cultured at 37 °C with 5% CO<sup>2</sup> in a 100 mm petri plate and maintained in culture in high glucose DMEM (cat. 51441C) supplemented with L-Glutamine 1% (cat. G7513), Antibiotic/Antimycotic 1% (A5955-100ML, Sigma Aldrich, St. Louis, MO, USA) and FBS 10%.

In order to evaluate ACE2 expression in human  $\beta$ -cells under diabetogenic stress conditions, EndoC- $\beta$ H1 cell line was subjected to palmitate-induced lipotoxic and inflammatory stress. Briefly, EndoC- $\beta$ H1 cells were plated at a density of  $2,5 \times 10^5$ /well in 24-well plates or  $5 \times 10^4$ /well in 96-well plates. After 48 h, palmitate and inflammatory stimuli were performed as previously described (29,30). In details, palmitate and inflammatory stresses have been induced respectively by 2 mM of Sodium Palmitate (cat. P9767-5G - Sigma Aldrich, St. Louis, MO, USA) or 0,5% EtOH (as control treatment) for 24 h, or cytokines mix IL-1 $\beta$  (50 U/mL) (cat. #201-LB-005 - R&D System, Minneapolis, MN, USA), TNF $\alpha$  (1000 U/mL) (cat. T7539 - Sigma Aldrich, St. Louis, MO, USA) and IFN $\gamma$  (1000 U/mL) (cat. 11040596001- Roche, Basilea, Switzerland) for 24 h.

### 4.4 Laser capture microdissection (LCM)

Pancreatic human tissue samples (n=5) from EUnPOD multiorgan donors (**Table 1**) were frozen in Tissue-Tek OCT compound and then 7- $\mu$ m thick sections were cut from frozen OCT blocks. Sections were fixed in 70% ethanol for 30 s, dehydrated in 100% ethanol for 1 min, in 100% ethanol for 1 min, in xylene for 5 min and finally air-dried for 5 min. Laser

capture microdissection (LCM) was performed using an Arcturus XT Laser-Capture Microdissection system (Arcturus Engineering, Mountain View, CA, USA) by melting thermoplastic films mounted on transparent LCM caps (cat. LCM0214 - ThermoFisher Scientific, Waltham, MA, USA) on specific islet areas. Human pancreatic islets were subsequently visualized through islet autofluorescence for LCM procedure. Thermoplastic films containing microdissected cells were incubated with 10  $\mu$ l of extraction buffer (cat. kit0204 - ThermoFisher Scientific, Waltham, MA, USA) for 30 min at 42 °C and kept at -80°C until RNA extraction. Each microdissection was performed within 30 min from the staining procedure. Overall n=50 microdissected pancreatic islets from each case were analysed.

#### **4.5 RNA extraction from LCM isolated human pancreatic islets**

Total RNA was extracted from each LCM sample using PicoPure RNA isolation kit Arcturus (cat. kit0204 - ThermoFisher Scientific, Waltham, MA, USA) following manufacturer's procedure. Briefly, the cellular extracts were mixed with 12.5  $\mu$ l of EtOH (100%) and transferred to the purification column filter membrane. DNase treatment was performed using RNase-Free DNase Set (cat. 79254 - Qiagen, Hilden, Germany). Total RNA was eluted in 11  $\mu$ l of DNase/RNase-Free Water and LCM captures deriving from human sample were pooled and subjected to a subsequent concentration through Savant SpeedVac SC100 centrifugal evaporator. Agilent 2100 Bioanalyzer technology with RNA Pico chips (cat. 5067-1513 Agilent Technologies, Santa Clara, CA, USA) was performed for each RNA sample, in order to analyse RNA integrity (RIN) and concentration.

#### **4.6 RNA extraction from cells and tissues**

For gene expression evaluation, total RNA was extracted from approximately  $3.0 \times 10^5$  EndoC- $\beta$ H1 or from fresh lung tissue (0.5x0.5x0.5cm), obtained from a lung tumour surgery donor by dissecting a not affected portion of the tissue (obtained with informed written consent of the patient and approved by the local Ethics Committee at the University of Siena). Direct-zol RNA Miniprep Kit (cat. R202-Zymo Research, Irvine, CA, US) was adopted following manufacturer's instructions. Briefly, the pelleted cells were resuspended in QIAzol (cat. 79306, Qiagen), mixed with equal volume of Ethanol 100% and transferred

to Zymo-Spin™ IICR Column. DNase digestion was performed using RNase-Free DNase Set (cat. 79254). RNA was eluted in 30 µl of DNase/RNase-Free Water. Fresh lung tissue was maintained in PBS1X on ice immediately after surgery, until ready for the RNA extraction. Homogenization of the tissue was performed using 600 µl of QIAzol and Lysing Matrix latex beads (MP Biomedicals, cat. 6913-100) in FastPrep-24 automated homogenizer (1min, full speed). The homogenate was diluted with vol/vol Ethanol 100% and then transferred in Zymo-Spin™ IICR Column. RNA extraction was performed following manufacturer's instructions.

#### **4.7 RT-Real Time PCR analysis**

Total RNA extracted from EndoC-βH1 and collagenase-isolated human pancreatic islets samples was quantified using Qubit 3000 Fluorometer (ThermoFisher Scientific, Waltham, MA, USA), while those extracted from LCM-islets were quantified using 2100 Bioanalyzer-RNA 6000 Pico Kit (cat. 50671513, Agilent Technologies, Santa Clara, CA, USA) as well as RNA integrity (RIN). Samples with RIN<5.0 were excluded. Reverse transcriptase reaction was performed using SuperScript™ VILO™ cDNA Synthesis Kit (cat. 11754050-ThermoFisher Scientific, Waltham, MA, USA).

cDNA deriving from LCM human pancreatic islets was then amplified using TaqMan PreAmp Master Mix (cat. 4488593, ThermoFisher Scientific, Waltham, MA, USA) following manufacturer's instructions. Real-Time PCR analysis was performed using TaqMan gene expression assays using primers (see Resources Table) and SensiFast Probe Lo-ROX Kit (cat.# BIO-84020, Bioline) following manufacturer's recommendation. Data were collected and analysed through Expression Suite software 1.0.1 (ThermoFisher Scientific, Waltham, MA, USA) using 2-ΔCt or 2-ΔΔCt method. ViiA7 Real-Time PCR thermocycler instrument (ThermoFisher Scientific, Waltham, MA, USA) was used to perform Real-Time PCR reactions.

## 4.8 ACE2 Immunohistochemistry analysis of human pancreatic sections

In order to evaluate the staining pattern of ACE2 in human pancreatic tissues, we analyzed FFPE sections (7- $\mu$ m thickness), prepared by using a microtome (cat. RM2125 RTS - Leica Microsystems, Wetzlar, Germany) and baked overnight at 37°C, from two different portions of pancreatic tissue for each multiorgan donor (listed in **Table 1**).

After deparaffinization and rehydration through decreasing alcohol series (Xylene-I 20min, Xylene-II 20min, EtOH 100% 5min, EtOH 95% 5min, EtOH 80% 5min, EtOH 75% 5min) pancreatic sections were incubated with 1X Phosphate-Buffered Saline with Ca<sup>2+</sup> and Mg<sup>2+</sup> (PBS 1X) supplemented with 3% H<sub>2</sub>O<sub>2</sub> (cat. H1009 - Sigma Aldrich, St. Louis, MO, USA) for 30min, to block endogenous peroxidases. Heat-induced antigen retrieval was performed using 10 mM citrate buffer pH 6.0 in microwave (600W) for 10 minutes, maintaining boiling conditions. Sections were incubated with PBS 1 $\times$  supplemented with 5% rabbit serum (cat. SCBD33ISV - Sigma Aldrich, St. Louis, MO, USA) to reduce non-specific reactions. Then, sections were incubated overnight at +4°C with primary antibody monoclonal mouse anti-Human ACE2 (cat. MAB933, R&D System, Minneapolis, MN, USA) diluted 1:33 (15  $\mu$ g/ml) in PBS 1 $\times$  supplemented with 5% rabbit serum. The next day, sections were incubated with secondary antibody polyclonal rabbit anti-mouse HRP-conjugate (cat. P0260, Dako, Agilent Technologies, Santa Clara, CA, USA) diluted 1:100 in PBS 1 $\times$  for 1h at room temperature (RT). Subsequently, the sections were incubated with one drop of 3,3' Diaminobenzidine (DAB) chromogen solution (cat. RE7270-K, Novolink MAX DAB, Leica Microsystems, Wetzlar, Germany) for 5 minutes, to trigger the chromatic reaction. Stained sections were then counterstained with hematoxylin (cat. MHS31, Sigma Aldrich, St. Louis, MO, USA) for 4 minutes, for better visualization of the tissue morphology. After the dehydration through increasing alcohol series, the pancreatic sections were mounted with Eukitt mounting medium (cat. S9-25-37, Bio Optica, Milan, Italy) and covered with a coverslip allowing them to dry. In order to further evaluate ACE2 expression in pancreas sections, the same ACE2 IHC protocol was applied to other 2 primary antibodies anti-Human ACE2: monoclonal rabbit anti-Human ACE2 (cat. Ab108252, Abcam, Cambridge, UK) diluted 1:100 in PBS 1 $\times$  supplemented with 5% goat serum; and polyclonal rabbit anti-Human ACE2 (cat. Ab15348, Abcam, Cambridge, UK) diluted 1:2000 in PBS 1 $\times$  supplemented with 5% goat serum. The secondary antibody in

both cases was polyclonal goat anti-rabbit HRP-conjugate (cat. 111-036-003, Jackson ImmunoResearch, Philadelphia, PA, USA), diluted 1:1000 in PBS 1× for 1h at room temperature (RT).

All the 3 primary antibodies anti-Human ACE2, with respective secondary antibodies, were also used to perform a positive control staining in FFPE human lung sections (7- $\mu$ m thickness), in order to double check the specificity of the primary antibodies.

To confirm the staining specificity, 1  $\mu$ g of polyclonal rabbit anti-human ACE2 (cat. ab15348 - Abcam, Cambridge, UK) was tested with or without 10  $\mu$ g of the immunizing human ACE2 peptide (cat. 15325 – Abcam, Cambridge, UK).

In-situ CD68 expression was evaluated using immunohistochemical staining using mouse monoclonal anti-Human CD68 (cat. M0876 - Agilent Technologies, Santa Clara, CA, USA) and insulin (cat. IR002 - Agilent Technologies, Santa Clara, CA, USA).

#### **4.9 Immunofluorescence staining for ACE2-Insulin-Glucagon and ACE2-CD31**

FFPE pancreatic sections (see above) were analysed by triple immunofluorescence in order to simultaneously evaluate the expression pattern of ACE2, insulin and glucagon. Briefly, after deparaffinization and rehydration through decreasing alcohol series (see above), pancreatic sections were subjected to heat induced antigen retrieval using 10 mM citrate buffer pH 6.0 in microwave (600W) for 10 minutes. Sections were incubated with PBS 1X supplemented with 3% Bovine Serum Albumin (BSA, cat. A1470-25G, Sigma Aldrich, St. Louis, MO, USA) to reduce non-specific reactions. Then, sections were incubated with primary antibody monoclonal mouse anti-human ACE2 (cat. MAB933, R&D System, Minneapolis, MS, USA) diluted 1:33 in PBS 1X supplemented with 3% BSA, overnight at +4°C, followed by polyclonal Rabbit anti-human Glucagon (cat. A0565, Agilent Technologies, Santa Clara, CA, USA) diluted 1:500 in PBS 1X supplemented with 3% BSA, and prediluted polyclonal Guinea Pig anti-human Insulin (cat. IR002 - Agilent Technologies, Santa Clara, CA, USA) as second and third primary antibodies for 1h at room temperature (RT). Subsequently, sections were incubated with goat anti-guinea pig Alexa-Fluor 555 conjugate (cat. A21435, Molecular Probe, ThermoFisher Scientific, Waltham, MA, USA) diluted 1:500 in PBS 1X, goat anti-rabbit Alexa-Fluor 647 conjugate

(cat. A21245, Molecular Probe, ThermoFisher Scientific, Waltham, MA, USA) diluted 1:500 in PBS 1X and goat anti-mouse 488 conjugate (cat. A11029 - Molecular Probe, ThermoFisher Scientific, Waltham, MA, USA) diluted 1:500 in PBS 1X, as secondary antibodies for 1h. Sections were counterstained with 4',6-Diamidino-2-phenylindole dihydrochloride (DAPI, cat. D8517, Sigma-Aldrich) diluted 1:3000 in PBS 1X, and then mounted with Vectashield antifade medium (cat. H-1000, Vector Laboratories, Burlingame, CA, USA) and analysed immediately or stored at +4°C until ready for confocal image analysis.

For ACE2-CD31 double immunofluorescence staining, FFPE pancreas sections were incubated overnight at +4°C with primary antibody monoclonal mouse anti-human ACE2 (cat. MAB933, R&D System, Minneapolis, MS, USA) diluted 1:33 in PBS 1X supplemented with 3% BSA and with polyclonal rabbit anti-CD31 (cat. Ab28364, Abcam, Cambridge, UK) diluted 1:50 in the same blocking buffer. Subsequently, sections were incubated with goat-anti rabbit Alexa-Fluor 594 conjugate (cat. A11037, Molecular Probe, ThermoFisher Scientific, Waltham, MA, USA) diluted 1:500 in PBS 1X, and goat anti-mouse 488 conjugate (cat. A11029 - Molecular Probe, ThermoFisher Scientific, Waltham, MA, USA) diluted 1:500 in PBS 1X, as secondary antibodies for 1h. Sections were counterstained with DAPI and then mounted as described above.

#### **4.10 Insulin, Glucagon and SARS-CoV-2 Nucleocapsid Immunofluorescence staining**

FFPE tissue sections obtained from pancreata of non-diabetic multiorgan donors positive for SARS-CoV-2 infection (**Table 3**) were analyzed using quadruple immunofluorescence for insulin (INS), glucagon (GCG), SARS-CoV-2 nucleocapsid and nuclei counterstain (DAPI). After deparaffinization and rehydration through decreasing alcohol series (Xylene-I 20 min, Xylene-II 20 min, EtOH 100% 5 min, EtOH 95% 5 min, EtOH 80% 5 min, EtOH 75% 5 min, H<sub>2</sub>O<sub>2</sub> 10 min) pancreatic sections were subjected to heat-induced antigen retrieval using Tris-EDTA buffer [10 mmol/l Tris (cat. T1503-500g, Sigma Aldrich, St. Louis, MO, USA), 1 mmol/l EDTA (cat. E4884-100g, Sigma Aldrich, St. Louis, MO, USA) 0.05% vol./vol. Tween-20 (cat. 170-6531 – Bio-Rad, Hercules, California, USA), pH 9.0] for 20 min at 100°C. After three washes in TBS1X [50 mM Tris-Cl (cat. T3252-100g Sigma

Aldrich, St. Louis, MO, USA), pH 7.6; 150 mM NaCl (cat. S7653 - Sigma Aldrich, St. Louis, MO, USA)] the sections were incubated with TBS1X supplemented with 3% Bovine Serum Albumin (BSA) (cat. A1470-25G - Sigma Aldrich, St. Louis, MO, USA) for 30 minutes at room temperature (RT) to avoid non-specific reactions. Then, sections were incubated with primary antibody polyclonal rabbit anti-nucleocapsid (cat. GTX135361, GeneTex, Irvine, CA, USA) diluted 1:1000 (final concentration: 1 µg /ml) in TBS1X supplemented with 3% BSA overnight at +4°C. After 3 washes in TBS1X the sections were incubated for 1h at RT with ready to use polyclonal guinea pig anti-human insulin (cat. IR002 - Agilent Technologies, Santa Clara, CA, USA) further diluted 1:5 and monoclonal mouse anti-human glucagon (cat. MAB1249 - R&D System, Minneapolis, MN, USA) diluted 1:300 (final concentration: 0,16 µg/ml) in TBS1X supplemented with 3% BSA. Then, the sections were incubated 1 h with related secondary antibodies, all diluted 1:500 (4 µg/ml) in TBS1X: goat anti-guinea pig Alexa-Fluor 555 conjugate (cat. A21435 - Molecular Probes, ThermoFisher Scientific, Waltham, MA, USA); goat anti-mouse Alexa-Fluor 647 conjugate (cat. A21236 - Molecular Probes, ThermoFisher Scientific, Waltham, MA, USA) and goat anti-rabbit 488 conjugate (cat. A11034 – Molecular Probes, ThermoFisher Scientific, Waltham, MA, USA). Sections were counterstained for 5 minutes with 4',6-Diamidino-2-phenylindole dihydrochloride (DAPI, cat. D8517, Sigma-Aldrich) diluted 1:3000 in TBS1X and then mounted with Dako Fluorescence Mounting Medium (cat. S3023 – Agilent Technologies, Santa Clara, CA, USA). The sections were stored overnight at +4°C until image analysis.

#### **4.11 Cultured cells immunofluorescence**

Cultured EndoC-βH1 cells were immunostained for ACE2 and insulin as follows. Cytokines-treated or untreated cells were fixed in 4% PFA for 10 min, washed for 10 min in 0.1 mol/L glycine, permeabilized in 0,25% Triton-X-100 for 5 min and blocked in 3% BSA+0.05% Triton-X100 in PBS without Ca<sup>2+</sup> and Mg<sup>2+</sup> for 30 min. EndoC-βH1 cells were incubated with prediluted antibody polyclonal Guinea Pig anti-Human Insulin (cat. IR002 - Agilent Technologies, Santa Clara, CA, USA) for 1h at RT. Then, the cells were washed with PBS without Ca<sup>2+</sup> and Mg<sup>2+</sup> and incubated with monoclonal mouse anti-Human ACE2 (cat. MAB933, R&D System, Minneapolis, MS, USA) diluted 1:33 in BSA 1% in PBS without Ca<sup>2+</sup> and Mg<sup>2+</sup> or with monoclonal rabbit anti-Human ACE2 (cat.



ab108252, Abcam, Cambridge, UK) diluted 1:100 in BSA 1% in PBS without Ca<sup>2+</sup> and Mg<sup>2+</sup>, or with polyclonal rabbit anti-Human ACE2 (cat. ab15348, Abcam, Cambridge, UK) diluted 1:2000 in BSA 1% in PBS without Ca<sup>2+</sup> and Mg<sup>2+</sup>, and then incubated with primary or with negative isotype control mouse IgG2a (cat. X0943 - Agilent Technologies, Santa Clara, CA, USA) or negative isotype control rabbit IgG (cat. Ab199376, Abcam, Cambridge, UK) for 60 min. Next, EndoC- $\beta$ H1 cells were rinsed with PBS without Ca<sup>2+</sup> and Mg<sup>2+</sup> and incubated with goat anti-mouse-488 1:500 in 1% BSA in PBS without Ca<sup>2+</sup> and Mg<sup>2+</sup>, or with goat anti-rabbit-488 diluted 1:500 in 1% BSA in PBS without Ca<sup>2+</sup> and Mg<sup>2+</sup> for 30 min and with goat-anti rabbit Alexa-Fluor 594 conjugate (cat. A11037, Molecular Probe, ThermoFisher Scientific, Waltham, MA, USA). Finally, the cells were incubated with 4',6-Diamidino-2-phenylindole dihydrochloride (DAPI, cat. D8517, Sigma Aldrich, St. Louis, MO, USA) diluted 1:3000 in PBS 1X and then mounted with Vectashield antifade medium (cat. H-1000 - Vector Laboratories, Burlingame, CA, USA) and analysed immediately or stored at +4°C until ready for confocal image analysis.

HeLa cells were immunostained for ACE2 as follows. The cells were first fixed in 4% PFA for 10 min, washed for 10 min in 0.1 mol/L glycine, permeabilized in 0,25% Triton-X-100 for 5 min and blocked in 3% BSA+0.05% Triton-X-100 in PBS without Ca<sup>2+</sup> and Mg<sup>2+</sup> for 30 min. The cells were subsequently washed with PBS without Ca<sup>2+</sup> and Mg<sup>2+</sup> and then incubated with monoclonal mouse anti-Human ACE2 (cat. MAB933, R&D System, Minneapolis, MS, USA) diluted 1:33 in BSA 1% in PBS without Ca<sup>2+</sup> and Mg<sup>2+</sup> or with negative isotype control mouse IgG2a (cat. X0943 - Agilent Technologies, Santa Clara, CA, USA). Then, HeLa cells were rinsed with PBS without Ca<sup>2+</sup> and Mg<sup>2+</sup> and were incubated with goat anti-mouse-488 1:500 in 1% BSA in PBS1X without Ca<sup>2+</sup> and Mg<sup>2+</sup>, or with goat anti-rabbit-488 diluted 1:500 in 1% BSA in PBS1X without Ca<sup>2+</sup> and Mg<sup>2+</sup>. Cells were counterstained with DAPI and then mounted as described above.

#### **4.12 Image analysis**

Images were acquired using Leica TCS SP5 confocal laser scanning microscope system (Leica Microsystems, Wetzlar, Germany). Images were acquired as a single stack focal plane or in z-stack mode capturing multiple focal planes (n=40) for each identified islet or selected representative islets. Sections were scanned and images acquired at 40 $\times$  or 63 $\times$  magnification. The same confocal microscope setting parameters were applied to all stained

sections before image acquisition in order to uniformly collect detected signal related to each channel.

Colocalization analysis between ACE2 and insulin and between ACE2 and glucagon were performed using LasAF software (Leica Microsystems, Wetzlar, Germany). The region of interest (ROI) was drawn to calculate the colocalization rate (which indicates the extent of colocalization between two different channels and reported as a percentage) as a ratio between the colocalization area and the image foreground. Evaluation of the signal intensity of ACE2 expression in human pancreatic islets of EUnPOD donors was performed using the LasAf software ([www.leica-microsystem.com](http://www.leica-microsystem.com)). This software calculates the ratio between intensity sum ROI (which indicates the sum ROI of the grey-scale value of pixels within a region of interest) of ACE2 channel and Area ROI ( $\mu\text{m}^2$ ) of human pancreatic islets. Both in colocalization and intensity measurement analysis, a specific threshold was assigned based on the fluorescence background. The same threshold was maintained for all the images in all the cases analysed.

#### **4.13 Micro-confocal High-content Screening analysis**

Cultured EndoC- $\beta$ H1 cells were immunostained for ACE2 and insulin as reported above. Cytokines-treated or untreated cells were fixed in 4% PFA for 10 min, washed for 10 min in 0.1 mol/L glycine, permeabilized in 0,25% Triton-X-100 for 5 min and blocked in 3% BSA+0.05% Triton-X100 in PBS without  $\text{Ca}^{2+}$  and  $\text{Mg}^{2+}$  for 30 min. EndoC- $\beta$ H1 cells were incubated with antibody polyclonal Guinea Pig anti-Human Insulin (cat. A21435 - Agilent Technologies, Santa Clara, CA, USA) diluted 1:1740 in BSA 1% in PBS without  $\text{Ca}^{2+}$  and  $\text{Mg}^{2+}$  and with monoclonal mouse anti-Human ACE2 (cat. MAB933, R&D System, Minneapolis, MS, USA) diluted 1:33 in BSA 1% in PBS without  $\text{Ca}^{2+}$  and  $\text{Mg}^{2+}$  for 1h at RT or with negative isotype control mouse IgG2a (cat. X0943 - Agilent Technologies, Santa Clara, CA, USA). Then, EndoC- $\beta$ H1 cells were washed with PBS without  $\text{Ca}^{2+}$  and  $\text{Mg}^{2+}$  and incubated with goat anti-mouse-488 (cat. A11029 - Molecular Probe, ThermoFisher Scientific, Waltham, MA, USA) and goat anti-guinea pig-555 (cat. A21435, Molecular Probe, ThermoFisher Scientific, Waltham, MA, USA) 1:500 in 1% BSA in PBS without  $\text{Ca}^{2+}$  and  $\text{Mg}^{2+}$ . EndoC- $\beta$ H1 cells were incubated with 4',6-Diamidino-2-phenylindole dihydrochloride (DAPI, cat. D8517, Sigma Aldrich, St. Louis, MO, USA) diluted 1:3000 in PBS 1X; then washed with PBS without  $\text{Ca}^{2+}$  and  $\text{Mg}^{2+}$  and

analysed immediately. Fluorescence images of EndoC- $\beta$ H1 cells were analysed using Opera Phoenix High Content Screening System (PerkinElmer, Waltham, MA, USA) acquiring multiple images using 63 $\times$  magnification; nine microscopic areas per well were automatically selected. Automated image analysis was performed using Harmony<sup>®</sup> High-Content Imaging (PerkinElmer, Waltham, MA, USA), and fluorescence intensity of treated or untreated cells were measured based on Alexa-555 (insulin) and Alexa-488 (ACE2) fluorochromes. Images were first segmented into nuclei and cytoplasm using the Find Nuclei building block on the DAPI channel and the Find Cytoplasm on the 488 (ACE2) channel. To detect ACE2 signals, Find spots building block was applied to the 488 fluorescence channel inside the cytoplasm area previously detected. The intensity rate was obtained from the average of the nine areas and values reported as Corrected Spot Intensity (which is the "Mean Spot Intensity" minus "Spot Background Intensity").

#### **4.14 RNA sequencing processing and analysis**

Total RNA of EndoC- $\beta$ H1 cells and of pancreatic human islets exposed or not to IFN $\alpha$  or to IL-1 $\beta$  + IFN $\gamma$  for the indicated time points was obtained and prepared for RNA sequencing as described. Bioanalyzer System 2100 (Agilent Technologies, Wokingham, UK) was used to evaluate samples quality by determining RNA integrity number (RIN) values. Only samples presenting RIN values > 9 were analyzed. The obtained libraries were submitted to a second quality control before sequencing on an Illumina HiSeq 2500. The Salmon software version 0.13.2 was used to re-analyse our original RNA-seq data by mapping the sequenced reads to the human reference transcriptome from GENCODE version 31 (GRCh38) using the quasi-alignment model. Gene expression is represented in Transcripts Per Million (TPM). Differentially expressed genes were identified with DESeq2 version 1.24.0. The estimated number of reads obtained from Salmon were used to run the DESeq2 pipeline. In summary, in this approach the DESeq2 normalizes samples based on per-sample sequencing depth and accounting for the presence of intra-sample variability. Next, data were fit into a negative binomial generalized linear model (GLM) and computed using the Wald statistic. Finally, obtained p-values were adjusted for multiple comparisons using the false discovery rate (FDR) by the Benjamini-Hochberg method. Genes were considered significantly modified with an FDR < 0.05.

#### **4.15 Western blot analysis**

Total proteins from EndoC- $\beta$ H1 cells were extracted using a lysis buffer (20 mM Tris-HCl pH 8.0, 137 mM NaCl, 1% (w/v) NP-40, 2mM EDTA) supplemented with 1X protease inhibitors (Roche). Total proteins were quantified using Bradford assay, and 50-100  $\mu$ g protein/lane were separated using SDS-PAGE Tris-Glycine gradient Bis-Acrylamide gel 4-20%. Proteins were then transferred to Nitrocellulose 0.2  $\mu$ m membrane using wet electrophoresis system. Upon transfer onto nitrocellulose, membranes were washed 3 times with TBST1X (Tris-HCl 25 mM, NaCl 150 mM, Tween 20 0,1%, pH 7.4) and then incubated 2h with 5% non-fat dry milk in TBST1X. To identify ACE2, three different antibodies were used: #Ab108252, #Ab15348 (Abcam) and #MAB933 (R&D system) were respectively diluted 1:1000, 1:500 and 1:250 in 5% non-fat dry milk in TBST1X and incubated o/n at +4°C and then with Goat anti-rabbit (#111-036-003, Jackson Laboratories) or Goat anti-Mouse (#115-036-003, Jackson Laboratories) diluted 1:5000 in 2% non-fat dry milk in TBST1X 1 h RT. After 3 washes with TBST1X and 1 wash in TBS1X, chemiluminescent signal was detected by using ECL solution (GE Healthcare, Little Chalfont, Buckinghamshire, UK-RPN2232). Chemiluminescent analysis of immunoblot results was performed by using LAS400 analyzer (GE Healthcare, Little Chalfont, Buckinghamshire, UK-RPN2232).

#### **4.16 ACE2 targeted Mass Spectrometric (MS)-Shotgun proteomics analysis**

To perform ACE2 targeted MS analysis, EndoC- $\beta$ H1 cells were lysed with RIPA buffer 1X and protein lysate concentration quantified through BCA assay. Then the protein lysate was mixed with 400  $\mu$ L of urea 8M in Tris-HCl 100mM pH 8,5 (UA), with the addition of 100 mM DTT. The mixture was charged on a filter 10 K Pall, incubated 30min RT and centrifuged 13,800xg 30min. The filter was washed twice with 400  $\mu$ L of UA and centrifuged 13,800xg 30min, then incubated with 100  $\mu$ L of 50 mM of iodoacetamide (IAC) solution in a thermo-mixer for 1min 150 RPM and without mixing for 20min, then centrifuged at 13,800xg for 20min. After these steps, the filter was washed twice with 400  $\mu$ L of UA and centrifuged at 13,800xg 30min, twice with 400  $\mu$ L of 50 mM ammonium bicarbonate (AMBIC), and then centrifuged twice, a first time at 13,800xg for a30min and

a second time at 13,800xg for 20min. Next, 40  $\mu$ L of 50 mM AMBIC were added to the filter together with trypsin (ratio trypsin/proteins 1:25) and incubated O/N 37°C. The sample was then transferred into a new collecting tube and centrifuged at 13,800xg for 10min. Subsequently, 100  $\mu$ L of 0.1% formic acid was added on the filter and centrifuged 13,800xg 10min. Finally, filter the was discarded and the solution was desalted with OASIS cartridges according to manufacturers' instructions. The retrieved peptides were concentrated through SpeedVac and the sample was resuspended in a solution of 3% acetonitrile, 96.9% H<sub>2</sub>O and 0.1% formic acid. The analyses were performed on a Q-Exactive Plus mass spectrometer (ThermoFisher Scientific), equipped with electrospray (ESI) ion source operating in positive ion mode. The instrument is coupled to an UHPLC Ultimate 3000 (ThermoFisher Scientific). The chromatographic analysis was performed on a column Acquity UPLC Waters CSH C18 130Å (1 mm X 100 mm, 1,7  $\mu$ m, Waters) using a linear gradient and the eluents were 0.1% formic acid in water (phase A) and 0.1% formic acid in acetonitrile (phase B). The flow rate was maintained at 100  $\mu$ L/min and column oven temperature at 50°C. The mass spectra were recorded in the mass to charge (m/z) range 200-2000 at resolution 35K at m/z 200. The mass spectra were acquired using a “data dependent scan”, able to acquire both the full mass spectra in high resolution and to “isolate and fragment” the ten ions with highest intensity present in the full mass spectrum. The raw data obtained were analyzed using the Biopharma Finder 2.1 software from ThermoFisher Scientific. The elaboration process consisted in the comparison between the peak list obtained “in silico” considering the expected aminoacidic sequence of human ACE2 protein (Uniprot ID: Q9BYF1), trypsin as digestion enzyme and eventual modifications (carbamidomethylation, oxidation, etc.).

#### **4.17 ACE2 promoter transcription factors (TF) binding motifs analysis**

ACE2 proximal promoter sequence was retrieved from Ensembl Genome browser database (<http://www.ensembl.org/index.html>) [Release 100 (April 2020)]. ACE2 gene (ENSG00000130234) was searched in Human genome GCRh38.p13 assembly. The sequence of interest was retrieved using “Export Data” function by selecting 1000 bp upstream 5' Flanking Sequence (GRCh38:X:15602149:15603148:-1) and downloaded in FASTA format. The analysis of TF binding motifs was performed using Transcription

factor Affinity Prediction (TRAP) Web Tool ([http://trap.molgen.mpg.de/cgi-bin/trap\\_receiver.cgi](http://trap.molgen.mpg.de/cgi-bin/trap_receiver.cgi)). In TRAP, ACE2 promoter sequence was analysed by using both TRANSFAC.2010.1 and JASPAR vertebrate databases and human promoters as background model.

#### **4.18 Data and Code Availability**

The NCBI GEO accession number for RNA sequencing data reported in this paper are: GSE133221, GSE108413, GSE137136.

#### **4.19 Statistical analysis**

Results were expressed as mean  $\pm$  SD. Statistical analyses were performed using Graph Pad Prism 8 software. Comparisons between two groups were carried out using Mann-Whitney U test (for non-parametric data) or Wilcoxon matched-pairs signed rank test. Differences were considered significant with p values less than 0.05.

## **5. Results**

### **5.1 ACE2 expression pattern in human pancreas**

In order to evaluate primary anti-ACE2-MAB933 specificity, we performed an immunofluorescence staining with isotype primary antibody (**Figure 19**). Moreover, a negative control with only secondary antibody incubation (no primary antibody control sample) was also included in order to exclude potential background artifacts generated by the secondary antibody or the enzymatic detection reaction (**Figure 20A**). A negative control with only secondary antibody incubation (no ACE2-MAB933 primary antibody control sample) was also included in order to exclude any background artifacts or fluorochrome overlaps (**Figure 20B, C**).

In order to check for the specificity of the staining performed we also made an ACE2 peptide competition reaction with Ab15348 antibody which confirmed the validity of the staining (**Figure 21**). Overall, these two antibodies offer a high degree of specificity.

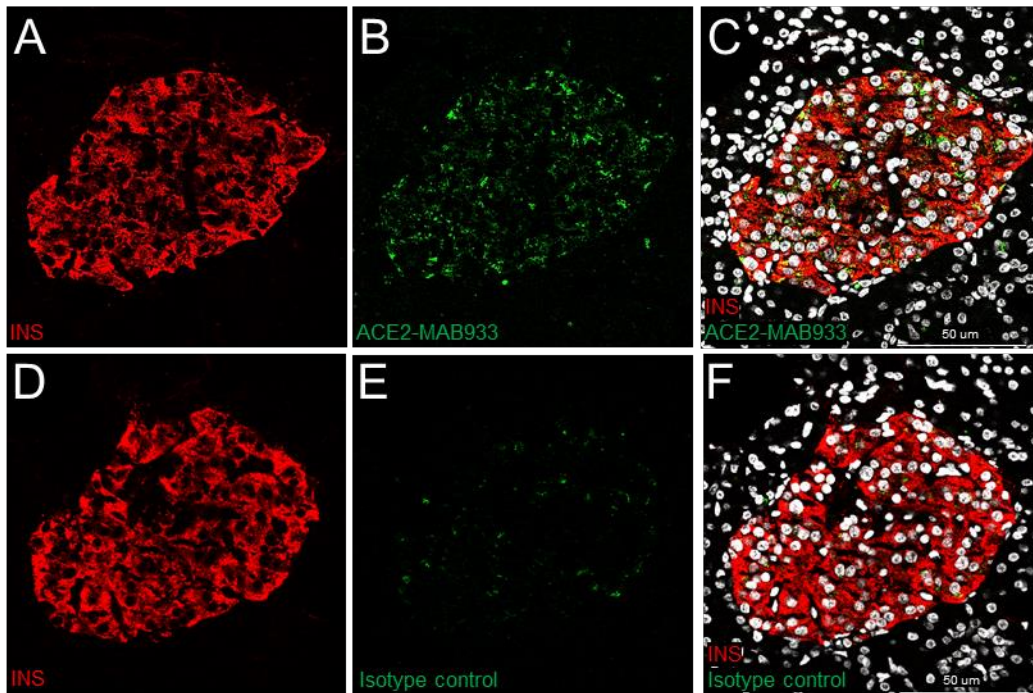


**Figure 20. Negative isotype control of the immunofluorescence analysis.** Representative confocal images of negative control of the immunofluorescence analysis of insulin/ACE2-MAB933 using isotype primary antibody. FFPE pancreatic section stained for insulin (INS, red, panel A) and ACE2-MAB933 (green, panel B) and merged signals showing colocalization between insulin and ACE2-MAB933 in yellow (panel C). Representative confocal images of FFPE pancreatic section stained for insulin (INS, red, panel D) and ACE2-MAB933 isotype control (panel E). Merged channels (panel F) showing no signal for ACE2 and no colocalization between insulin and ACE2. Scale bars in panel c and f is 50  $\mu\text{m}$ .

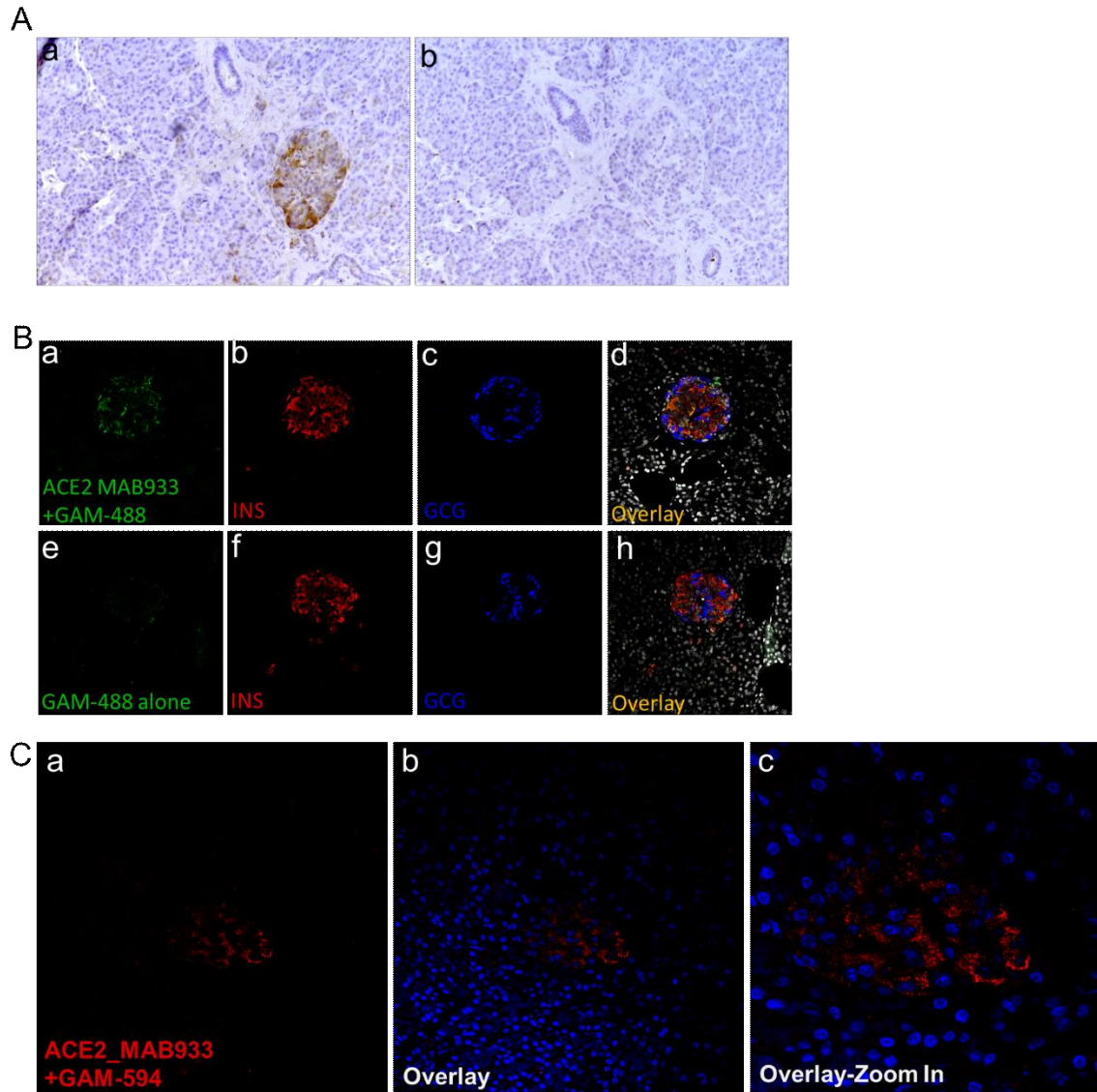


**Figure 20. ACE2-MAB933 negative control staining in human pancreas.** (A) Immunohistochemistry of a FFPE pancreatic section from an adult-non-diabetic multiorgan donor (id: 210518) using MAB933 anti-ACE2 antibody (panel-a) or secondary antibody-only (panel-b). (B) Triple Immunofluorescence of a FFPE pancreatic section from an adult-non-diabetic multiorgan donor (id: 210518) using MAB933 anti-ACE2 antibody (panel-a) or fluorescently-labeled Goat Anti Mouse (GAM) secondary antibody-only as negative control for ACE2 (panel-b). (C) ACE2 immunofluorescent staining in FFPE pancreatic section from an adult-non-diabetic multiorgan donor (id: 210518) using MAB933 anti-ACE2 antibody (panel-a) with another fluorescently labeled Goat Anti Mouse-594, in order to exclude background staining artifacts due to the previously adopted ACE2 fluorescent detection system.



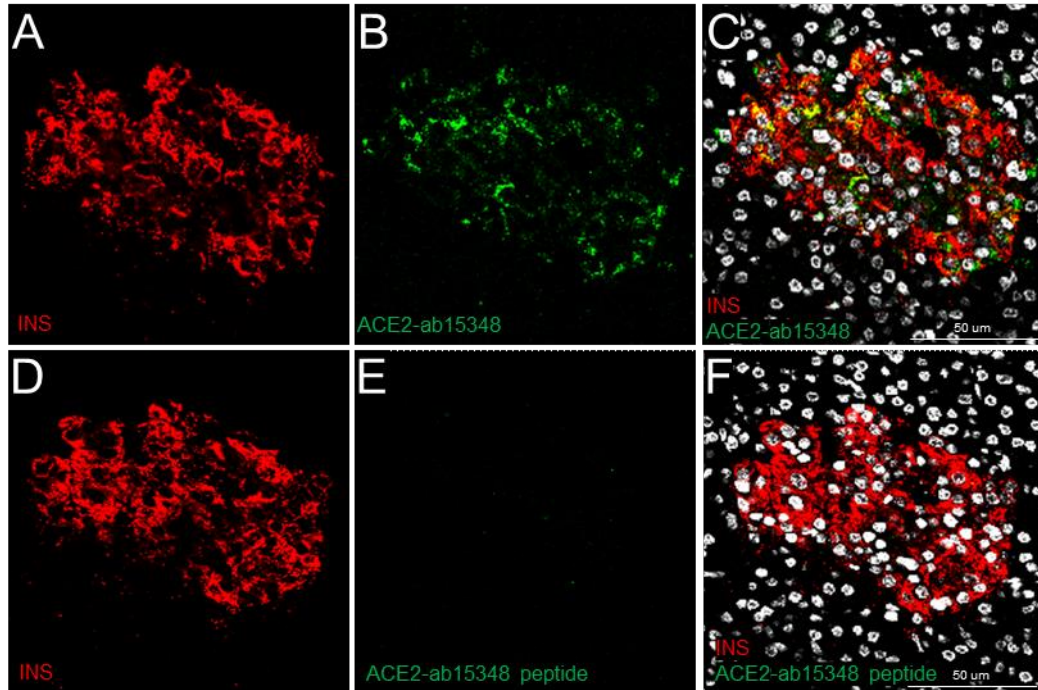


**Figure 21. ACE2-ab15348 negative control of the immunofluorescence analysis.** a) Representative confocal images of negative control of the immunofluorescence analysis of insulin/ACE2 using a peptide competition assay toward Ab anti-ACE2 ab15348 of FFPE pancreatic section stained for insulin (INS, red, panel A) and ACE2-ab15348 (green, panel B) and merged signals showing colocalization between insulin and ACE2-ab15348 in yellow (panel C). Representative confocal images of FFPE pancreatic section stained for insulin (INS, red, panel D) and ACE2 AB15348 pre-incubated with a specific ACE2 peptide (panel E) and showing no signal. Merged channels (panel F) showing no signal for ACE2 and no colocalization between insulin and ACE2. Scale bars in panel c and f is 50  $\mu\text{m}$ .

To determine the ACE2 protein expression pattern in human pancreatic tissue, we first performed a colorimetric immunohistochemistry analysis to detect ACE2 on formalin-fixed paraffin embedded (FFPE) pancreatic sections obtained from seven ( $n = 7$ ) adult non-diabetic multiorgan donors collected by the INNODIA EUnPOD biobank (**Table 1**). To specifically detect ACE2 protein in such context, we initially used a previously validated monoclonal anti-human ACE2 antibody (R&D MAB933) (7) which passed the validation criteria suggested by the International Working Group for Antibody Validation (IWGAV) (7,40).

For each pancreas, two sections derived from two different FFPE tissue blocks belonging to different parts of the organ (head, body, or tail) were analyzed. Based on pancreas morphometry and histological composition, we identified three main cell types positive for ACE2 (**Figures 22A–F**). In the exocrine pancreas there was a marked and intense staining in a subset of vascular components (endothelial cells or pericytes) found in inter-acini septa (**Figures 22A, B**). We also identified ACE2 positive cells in the pancreatic ducts even though only some scattered cells with a clear ACE2 signal were detected (**Figures 22C, D**). Of interest, we observed a peculiar ACE2 staining pattern in the endocrine pancreatic islets showing a diffuse ACE2 signal in a subset of cells within the islet parenchyma (**Figures 22E, F, Figure 23**). However, the observed ACE2 expression in the islets was lower than the expression observed in the microvasculature, the latter representing the main site for ACE2 expression in the pancreas. In all cases analyzed, including different blocks of the same case, a similar expression pattern of ACE2 was observed even though a certain degree of variability in terms of ACE2 staining intensity within the islets was noted (**Figure 23**).

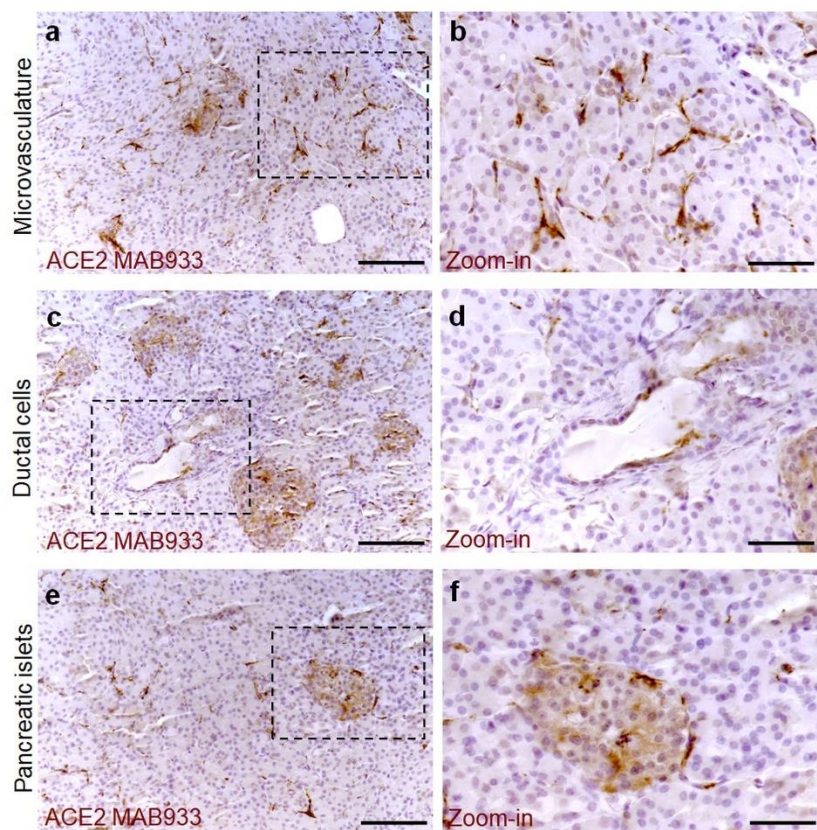


**Figure 22. ACE2 staining pattern in human pancreas.** Immunohistochemistry for ACE2 in human pancreatic tissue sections (case #110118) using ACE2-MAB933 antibody. ACE2 is



markedly expressed in microvasculature associated cells (A, B) in some rare ductal cells (C, D) and in a subset of endocrine cells within pancreatic islets (E, F). Scale bars in (A, C, E) 150  $\mu$ m. Scale bars in (B, D, F) 70  $\mu$ m. Zoom-in images are reported in (B, D, F).

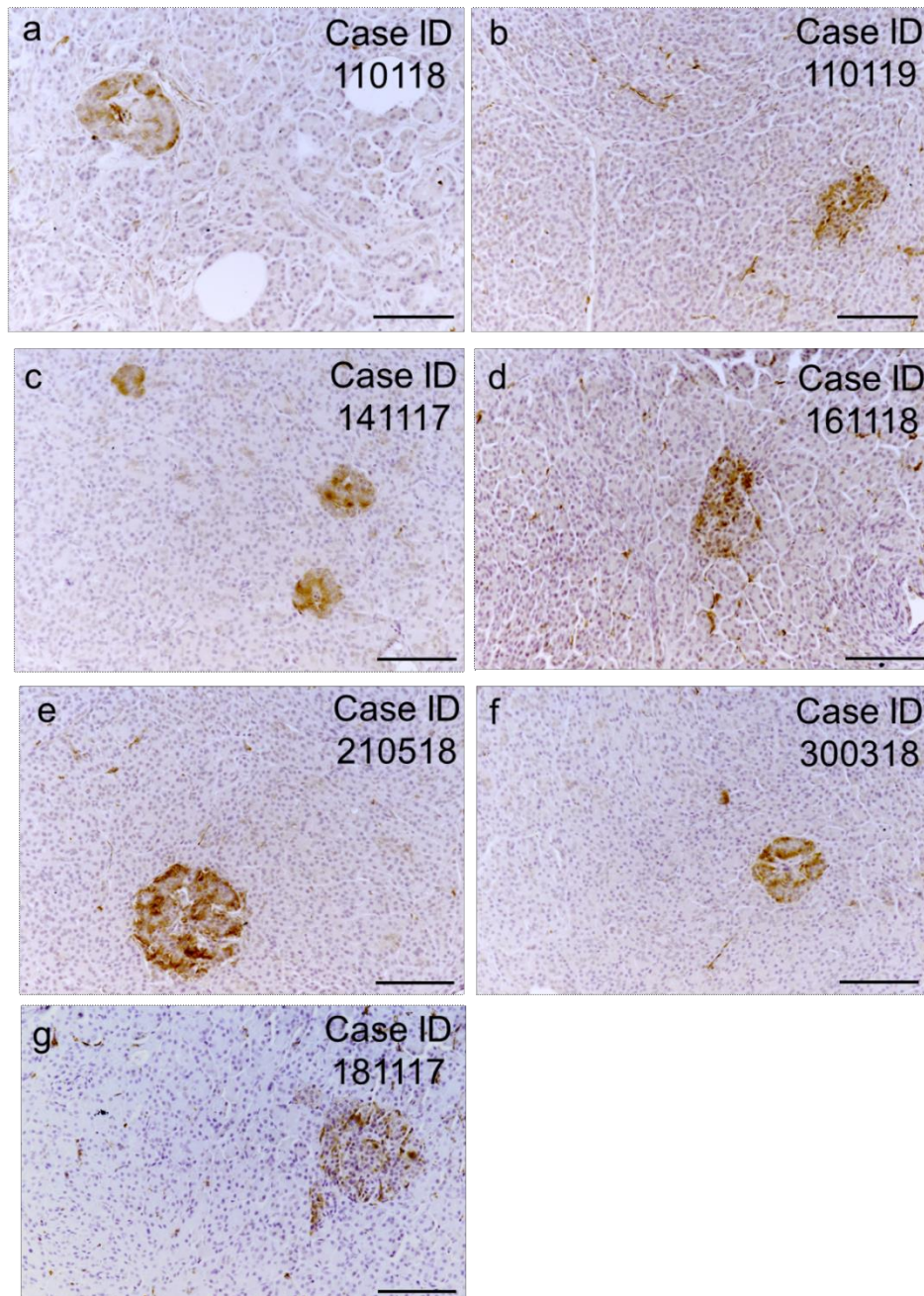


**Figure 23. Representative images of all cases showing expression of ACE2 (MAB933) in human pancreatic islets.** Representative images of ACE2 IHC staining in human pancreatic FFPE sections obtained from seven different non-diabetic multiorgan donors. Scale bar: 100  $\mu$ m.

The highest signal of ACE2 within the pancreas was observed in putative association with the microvasculature (**Figures 22A, B**). Of note, in such context, a lobular staining pattern of the microvasculature associated ACE2 was evident, as demonstrated by the presence of positive cells in certain lobules and low or null expression in other lobules of the same pancreas section (**Figure 24A**). ACE2 staining pattern in inter-acini septa suggested an overlap with cells associated with the microvasculature, most likely endothelial cells. In order to explore such possibility, we performed a double immunofluorescent staining on the pancreas FFPE sections for ACE2 and the endothelial cell specific marker CD31. The results showed that ACE2 signal is associated, but not superimposed, with the CD31-specific one, thus resembling the tight association of pericytes with endothelial cells and strongly suggesting the presence of ACE2 in microvasculature pericytes (**Figure 24B**).

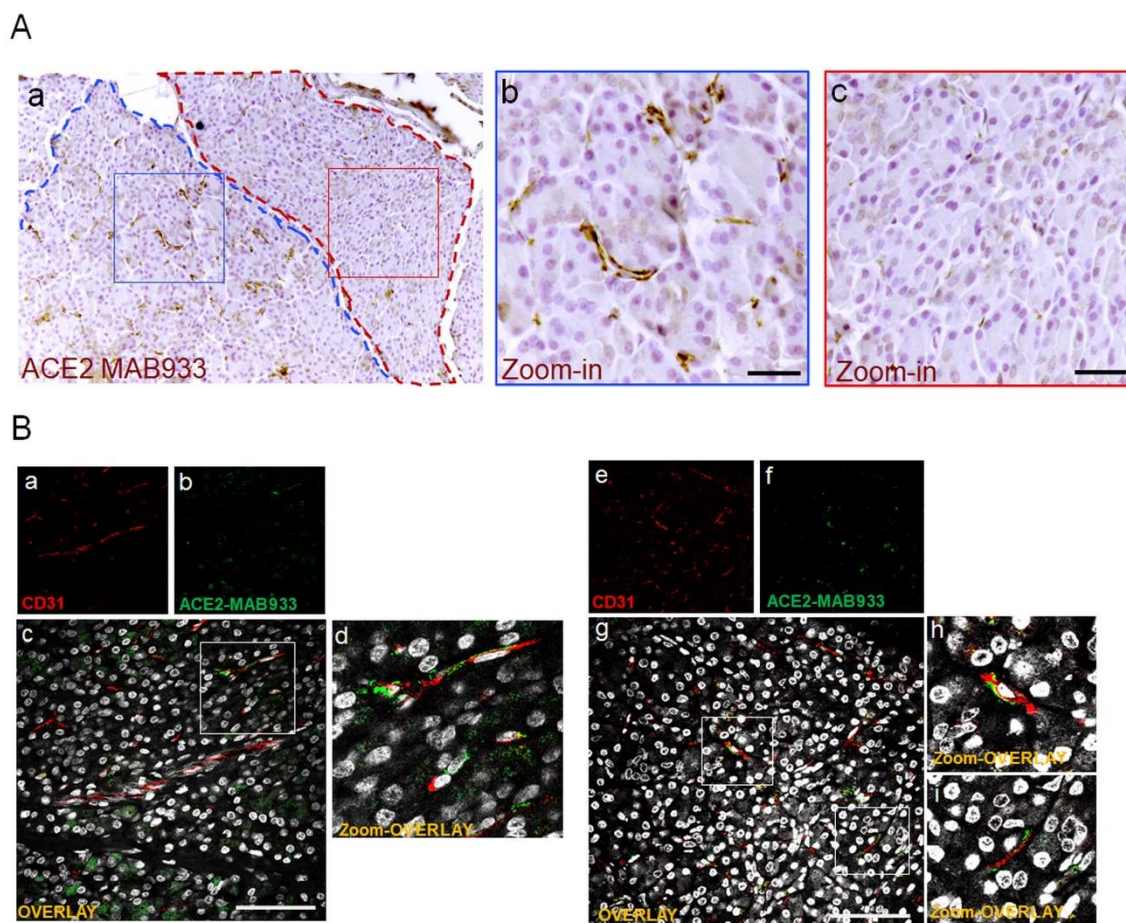


**Figure 24. In microvasculature, ACE2 is putatively expressed in pericytes.** (A) Representative image of human pancreatic Formalin-Fixed Paraffin Embedded (FFPE) section stained for ACE2 in case #301118. In panel-a, a representative image of a pancreatic section showing two adjacent lobules (blue and red dotted lines) with different staining for ACE2 in endothelial cells/pericytes. A specific segmentation of the two lobules with high (blue) (zoom-in, panel-b) and low or null

expression of ACE2-MAB933 (red) (zoom-in, panel-c) is shown, suggesting lobularity of ACE2 expression in exocrine endothelial cells/pericytes of human pancreas. Scale bar in panel-a: 100  $\mu$ m. Scale bar in panels-b and -c: 30  $\mu$ m. (B) Double immunofluorescence staining of ACE2 (green) and CD31 (red) in FFPE pancreas sections from Body01A of Case #110118 (panels-a to -d) and of Body01B of Case #141117 (panels-e to -i). Digital zoom-in overlay images are shown in panels-d, -h and -i. Scale bar in panels-d and -g: 100  $\mu$ m.

In order to confirm the ACE2 cellular distribution observed in the pancreas using MAB933 antibody, we tested two additional anti-ACE2 antibodies from Abcam: Ab15348 and Ab108252. According to the information obtained by R&D and Abcam, while MAB933 and Ab15348 are reported to recognize the C-terminus portion of ACE2 (18-740aa and 788-805aa, respectively), Ab108252 is specifically designed to react with a linear peptide located in the N-terminal ACE2 protein sequence (200–300aa). It has been recently reported that a 459 aa short-ACE2 isoform (357–805aa of ACE2 + 10aa at N-terminus) can be co-expressed alongside the full-length ACE2 protein (1–805aa) (**Figure 25A**) (24, 25); the short-ACE2 misses part of the N-terminal region targeted by Ab108252 antibody. We observed ACE2 islet-related signal using both MAB933 (**Figure 25B**) and Ab15348 (**Figure 25C**), but the Ab108252 antibody did not show any positivity within the islet parenchyma (**Figure 25D**), raising the possibility that the most prevalent ACE2 isoform within pancreatic islets is the short one. Of note, the three antibodies tested showed ACE2 positivity in the microvasculature, thus suggesting a putative differential distribution of the two ACE2-isoforms in the human pancreas.



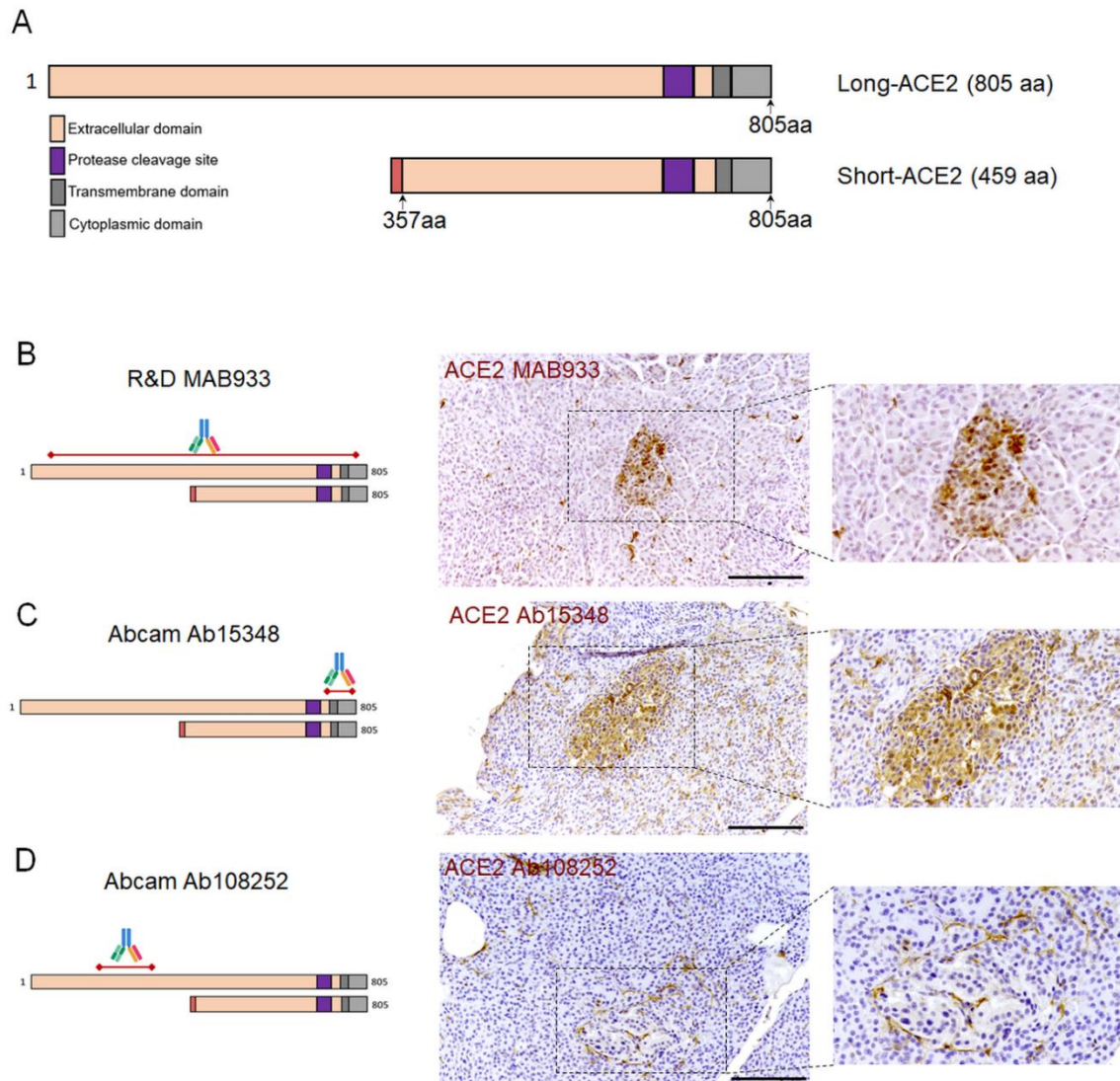


**Figure 25. ACE2 immunohistochemistry staining pattern in human pancreatic islets using MAB933, Ab15348, and Ab108252 antibodies.** (A) Aligned sequences and structures of recently described ACE2 isoforms, long-ACE2 (805aa, ~110 kDa) and short-ACE2 (459aa, ~50kDa). Main ACE2 protein domains are reported with different colours. (B) R&D MAB933, (C) Abcam Ab15348 and (D) Ab108252 antibody predicted target sequence within the two ACE2 isoforms, alongside with immunohistochemistry staining distribution in pancreatic islets. Scale bars in (B–D) are 100  $\mu$ m.

As a positive control for our immunohistochemistry method and ACE2 antibodies adopted, we evaluated FFPE lung tissue sections. As previously shown (7, 41, 42), we observed scattered positive cells (putatively AT2 pneumocytes) in the alveolar epithelium both using MAB933 and Ab15348 (**Figures 26, panels-a and -b**). In contrast, we did not observe any signal using Ab108252 (**Figure 26, panel-c**). Collectively, these results indicate that the same staining pattern were obtained by using two out of three antibodies that may recognize both ACE2 isoform (short-ACE2 and long-ACE2) thus confirming: (i) a high ACE2 expression in microvasculature pericytes; (ii) rare scattered ACE2 positive ductal cells; (iii) diffuse though weak ACE2 positive staining in a subset of cells within human pancreatic islets.

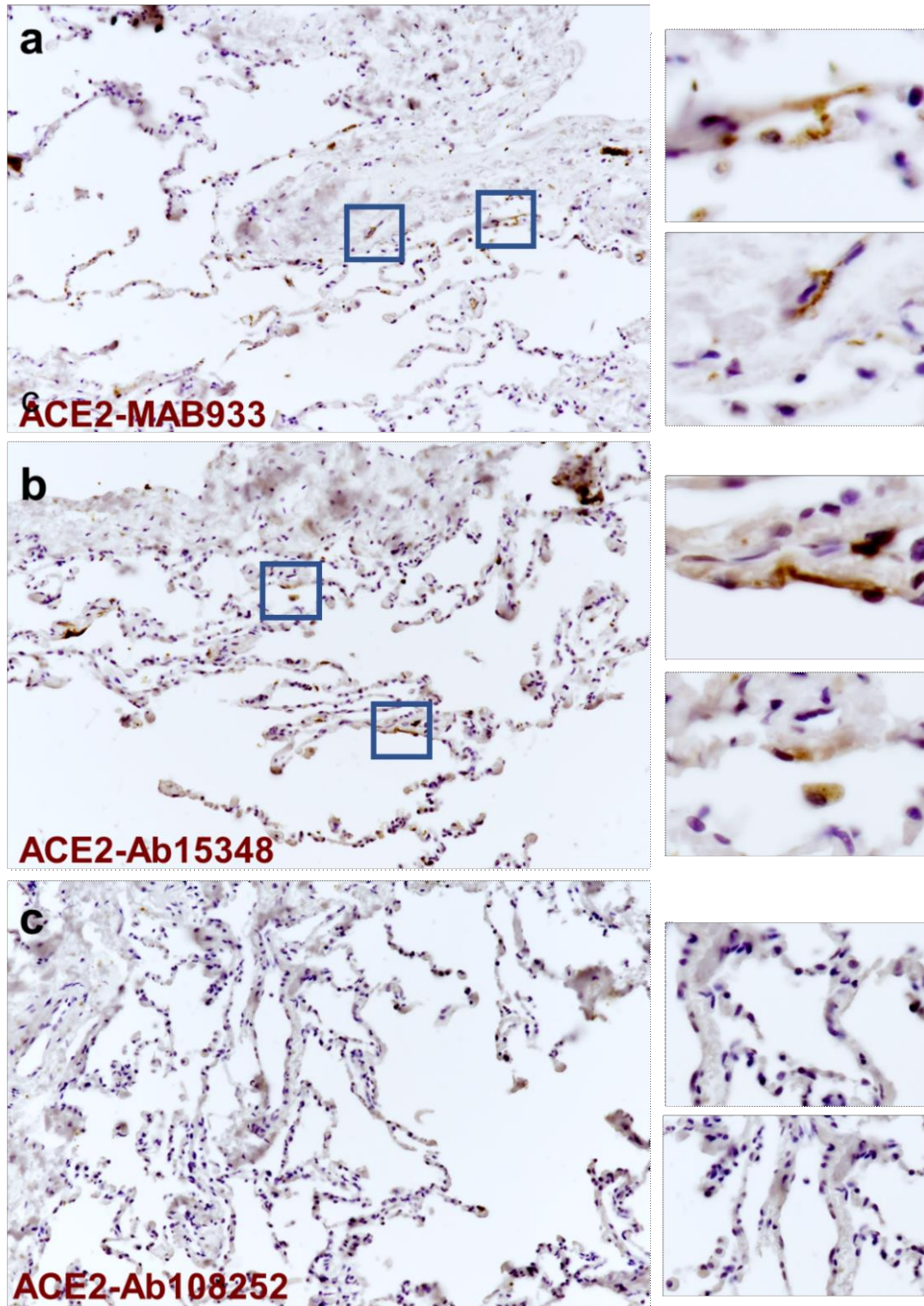


**Figure 26. ACE2 staining positive control.** Anti-ACE2 MAB933 (panel-a), Ab15348 (panel-b) and Ab108252 (panel-c) antibodies immunohistochemistry in FFPE lung tissue sections. Zoom-in insets are shown on the right, adjacent to each main related image.



## 5.2 In human pancreatic islets ACE2 is preferentially expressed in $\beta$ -cells

Using both MAB933 and Ab15348 we observed ACE2 signal in pancreatic islets which suggests that ACE2 is expressed in endocrine cells. Therefore, we sought to determine which pancreatic islet cell subset contributes to ACE2 signal in such context. To do so, we performed a triple immunofluorescence analysis on the same set of FFPE pancreatic sections of nondiabetic multiorgan donors, aimed at detecting glucagon-positive  $\alpha$ -cells, insulin-positive  $\beta$ -cells, and ACE2 signals (**Figure 27 and Figure 28**). Using MAB933, ACE2 preferentially overlapped with the insulin-positive  $\beta$ -cells (**Figure 27A, panels-a to -m**), being mostly colocalized with insulin and low/not detectable in  $\alpha$ -cells (**Figure 27A, panels-e, -f, -l, -m**). Such staining pattern was observed in all cases and was consistent between two different FFPE pancreas blocks of the same case (**Table 4**). As expected, ACE2-only positive cells within or around pancreatic islets were also observed (**Figure 27A, panel g**), potentially indicating the presence of ACE2-positive pericytes interspersed in the islet parenchyma or surrounding it. Intriguingly, in the  $\beta$ -cells a major fraction of ACE2 was observed in the cytoplasm and partially overlapped with insulin positive signal, while in a subsets of them only a minor fraction of the ACE2 signal was attributable to several spots located on plasma membrane (**Figure 27A; Figure 29A red arrow, and Figure 29B**). In microvasculature pericytes, the ACE2-positive signal was mainly observed in plasma membrane (**Figure 27A, panel-g; Figure 29A green arrow**) as previously described (43). There were also some ACE2-negative  $\beta$ -cells (**Figure 29A, white arrow**). Colocalization rate analysis between ACE2-insulin and ACE2- glucagon, performed on a total of 128 single pancreatic islets from seven different adult non-diabetic cases, confirmed the significant preferential expression of ACE2 in  $\beta$ -cells compared to  $\alpha$ -cells (colocalization rate: ACE2-INS  $57.6 \pm 19.3\%$  vs. ACE2-GCG  $6.8 \pm 5.4\%$   $p < 0.0001$ ) (**Figure 27B and Figure 30A**). The comparison of colocalization rates between ACE2-insulin and ACE2-glucagon among all cases analyzed, confirmed the consistent preferential expression of ACE2 in  $\beta$ -cells in comparison to  $\alpha$ -cells (**Figure 27B**). These results were confirmed when comparing different blocks of the same case (**Table 4**). There was however heterogeneity in terms of the ACE2-insulin colocalization rate among different islets (ACE2-INS colocalization rate range: 0.6–91.4%). Such heterogeneity was also highlighted by the presence of rare ACE2-negative pancreatic islets in the same pancreas section. Inter-islets heterogeneity was also clearly observed regarding ACE2 islet-

related signal intensity analysis (**Figure 27C**). Of note, some cases showed a lower ACE2-insulin mean colocalization rate and islet-ACE2 signal intensity compared to the other ones (**Figure 27D**), thus suggesting a high degree of heterogeneity among cases also in terms of islet-ACE2 expression. No significant correlation between ACE2-islets signal intensity and age, BMI or cold-ischemia time were observed in our donors cohort (**Figure 30B**).

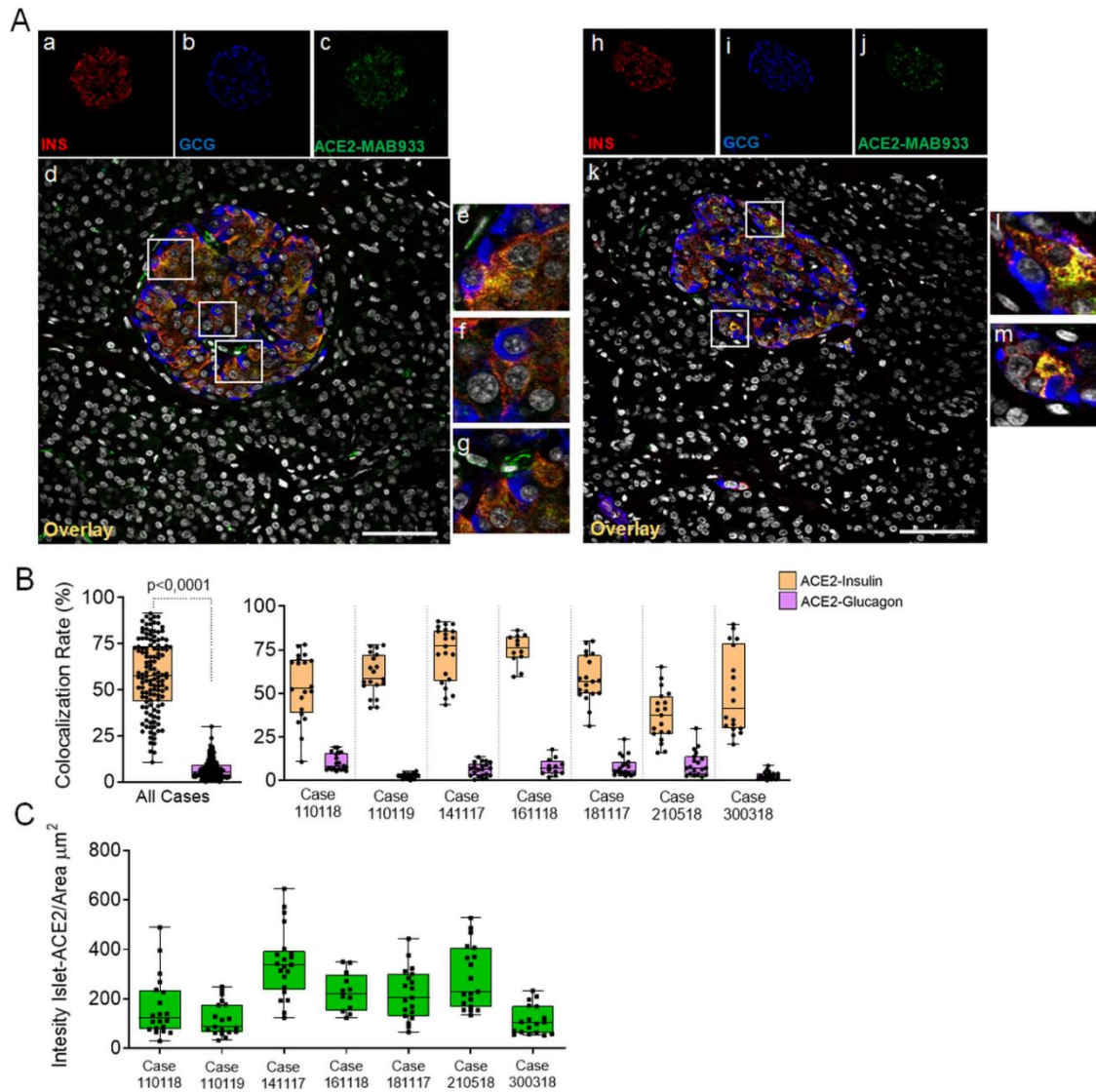


**Figure 27. In human pancreatic islets, ACE2 is preferentially expressed in insulin-producing  $\beta$ -cells.** Triple immunofluorescence staining and image analysis of FFPE human pancreatic section stained for insulin (red), glucagon (blue) and ACE2-MAB933 (green). (A) Representative islets of two different cases. Panels-a to -g: representative pancreatic islet of FFPE pancreas block Body01A of case #110118. Panels-h to -m: representative pancreatic islet of FFPE pancreas block Body01B of case #141117. Panels-e to -g: digital zoom in images of the pancreatic islet shown in panel-d.

Panels-l and -m: digital zoom in images of the pancreatic islet shown in panel-k. Scale bar in panels-d and -k: 100  $\mu\text{m}$ . (B) Colocalization rate analysis of overlapping ACE2-insulin and ACE2-glucagon in 128 single pancreatic islets of seven different cases. p-value was calculated using Wilcoxon matched-pairs signed rank test. On the right: colocalization rate analysis of ACE2-insulin and ACE2-glucagon in each of the seven cases analyzed. For each case, a total of 7–11 islets/section were analyzed. (C) Analysis of the intensity of ACE2 islet-related signals in the cases analyzed. Values are shown as fluorescence intensity of each islet reported as the sum of gray-scale values for each pixel normalized for the islets area (ROI,  $\text{mm}^2$ ).

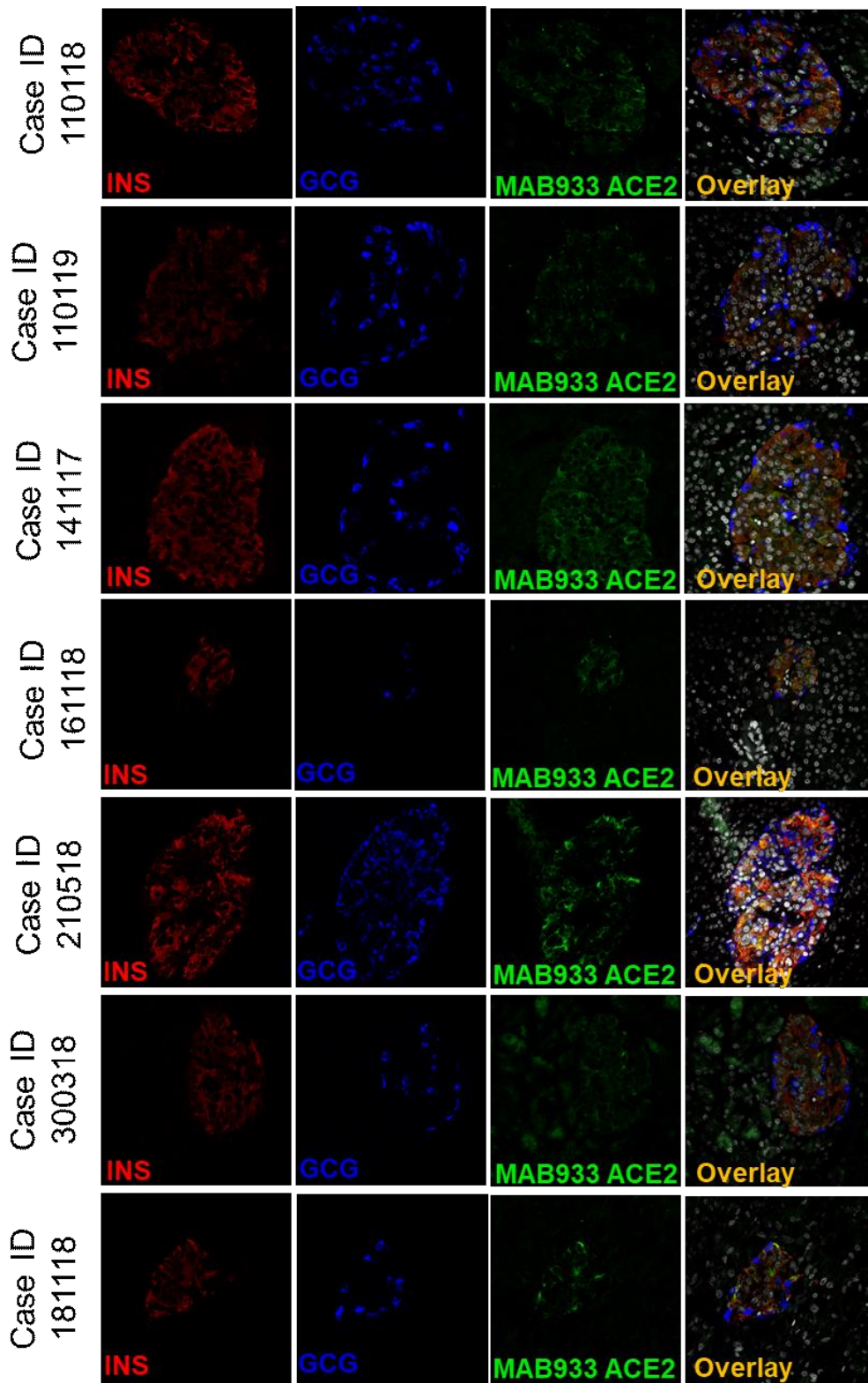


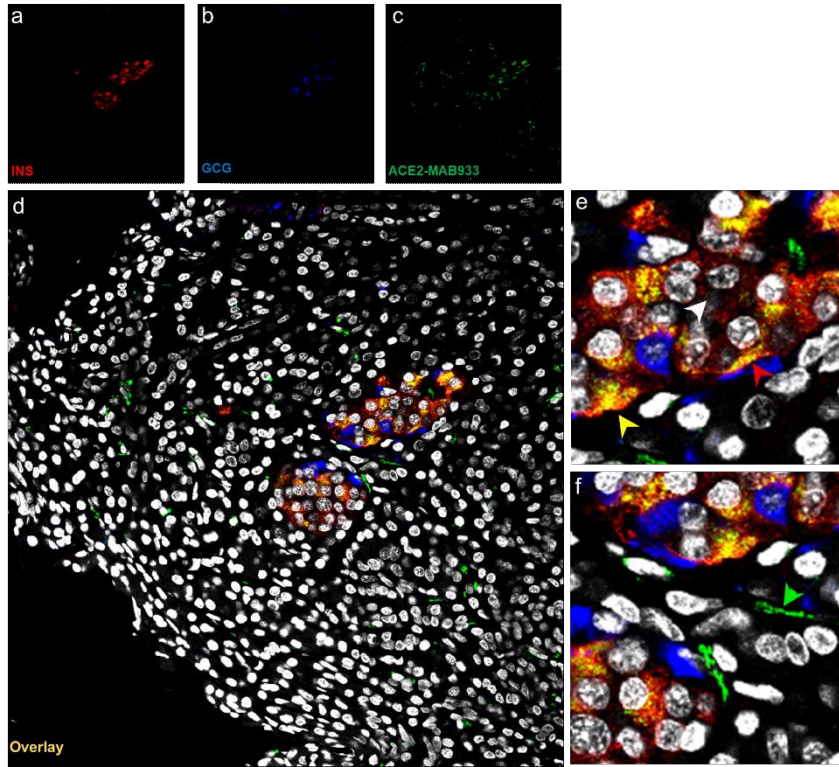
**Figure 28. ACE2 MAB933 immunofluorescence in FFPE pancreatic sections.** Representative images of all cases showing expression of insulin (red), glucagon (blue) and ACE2 (MAB933, green), in human pancreatic FFPE sections obtained from seven different adult non-diabetic multiorgan donors.

**Table 3.** ACE2-Insulin and ACE2-Glucagon colocalization rate (reported as percentage values) in human pancreatic islets of EUnPOD non-diabetic cases. Two different FFPE pancreas blocks per case were analysed; results for each block are reported separately in the table below.

<b>Case ID</b>	<b>Pancreas Block ID</b>	<b>ACE2-INS (Colocalization Rate- %)</b>	<b>ACE2-GCG (Colocalization Rate- %)</b>
110118	Body 01A	47.5%	8.3%
110118	Head 02A	59.3%	12.2%
110119	Body 01A	63.2%	3.1%
110119	Tail 01A	59.3%	2.3%
141117	Body 01B	83.6%	6.6%
141117	Tail 03B	55.0%	5.6%
161118	Body 01A	73.9%	6.8%
161118	Tail 01A	81.9%	12.6%
181117	Head 02B	53.6%	7.0%
181117	Tail 01A	62.2%	9.2%
210518	Body 01B	39.5%	7.5%
210518	Head 02A	35.6%	11.3%
300318	Body 01A	61.8%	4.1%
300318	Tail 01A	39.0%	1.5%



A



B

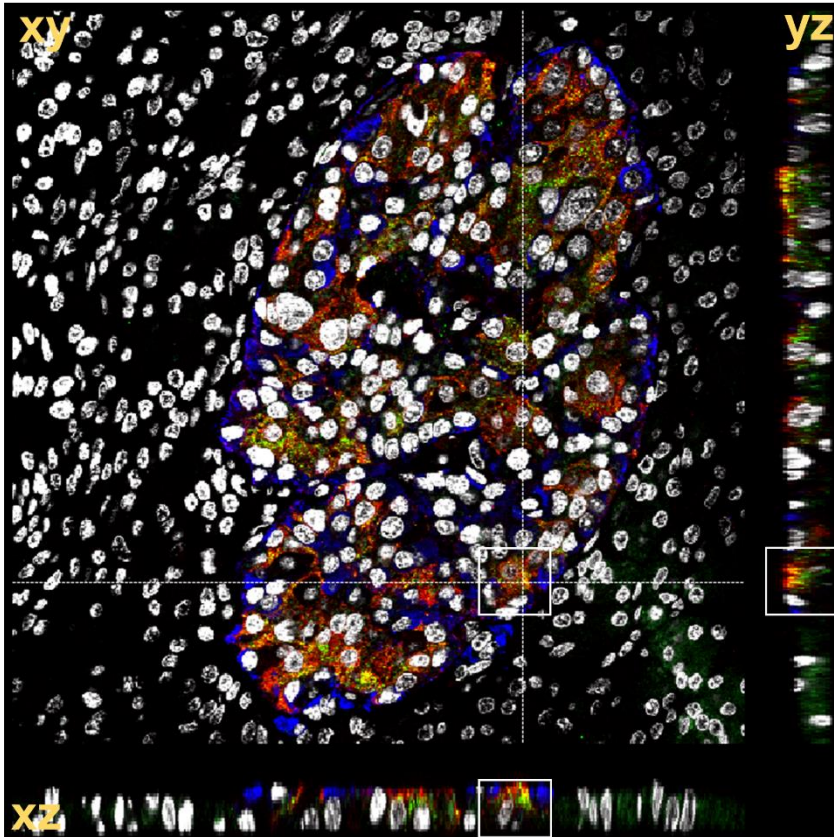
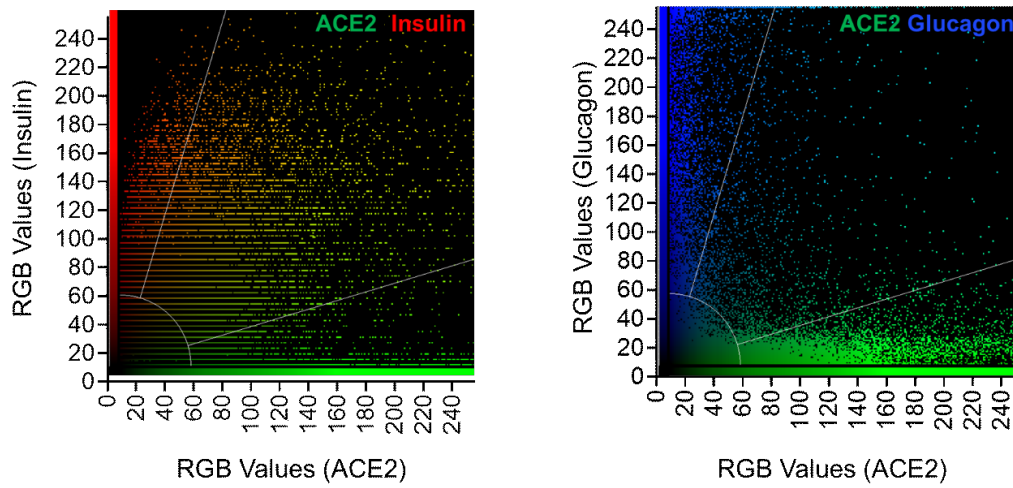


**Figure 29. (A)** Triple immunofluorescence staining and image analysis of FFPE human pancreatic section (case #210518) stained for insulin (red, panel-a), glucagon (blue, panel-b) and ACE2 MAB933 (green, panel-c), alongside with overlay (panel-d) and zoom overlays (panel-e and -f). White- Figure S5. (A) Triple immunofluorescence staining and image analysis of FFPE human pancreatic section (case #210518) stained for insulin (red, panel-a), glucagon (blue, panel-b) and ACE2-MAB933 (green, panel-c), alongside with overlay (panel-d) and zoom overlays (panel-e and -f). red-arrow: ACE2-positivity prevalently associated to plasma membrane in a  $\beta$ -cell; green-arrow: plasma membrane localization of ACE2 in microvasculature-associated pericyte. **(B)** Z-stack 3D analysis of a pancreatic islet stained for ACE2-MAB933, insulin and glucagon. Representative image of a human pancreatic islet of case 210518 analysed performing triple immunofluorescence staining for ACE2 (green), insulin (red), glucagon (blue) and DAPI (white). Acquisition of 40 different focal planes allowed a XYZ 3D reconstruction and z-sectioning (xz and yz). White rectangles highlight an example of the partial colocalization of ACE2 and insulin signals within  $\beta$ -cells, highlighting the different subcellular compartmentalization (cytoplasmic/granular and plasma membrane) of ACE2.

A



B

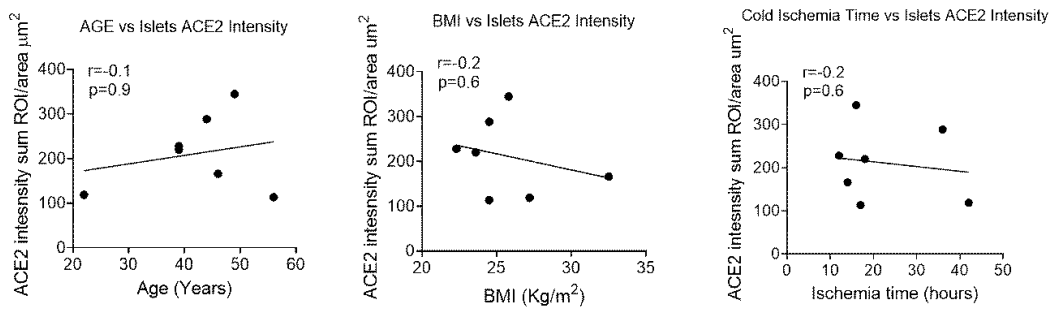


**Figure 30.** (A) Colocalization plots of ACE2-MAB933-insulin and ACE2-MAB933-glucagon in a human pancreatic islet of case 210518. (B) Correlation analysis among ACE2 pancreatic islets staining intensity of all cases analyzed (see Figure 27C) and Age (years), BMI (kg/m<sup>2</sup>) and cold ischemia time (hours). Statistics performed using Spearman R correlation test.



### 5.3 A short ACE2 isoform is prevalently expressed in the human $\beta$ -cell line EndoC- $\beta$ H1

Using Western Blot (WB) and immunofluorescence analysis, we explored the expression of ACE2 in the human  $\beta$ -cell line EndoC- $\beta$ H1, a model of functional  $\beta$ -cells for diabetes research (27, 44). To do so we used R&D MAB933, Abcam Ab15348 and Ab108252 antibodies, as previously done in the above-described pancreas immunohistochemistry experiments. In WB analysis, MAB933 revealed the presence of a prevalent 50 kDa band corresponding to the short-ACE2 isoform; use of this Ab showed the brightest signal in immunofluorescence staining among the three antibodies tested (**Figure 31A**). Abcam Ab15348 worked better in WB for the recognition of both ACE2 isoforms and indicated that the most prevalent ACE2 isoform present in human b-cells is the short-ACE2 (50 kDa, blue arrow) (**Figure 31B**). In contrast, Ab108252 recognized only the long-ACE2 isoform (>110 kDa- red arrow) (**Figure 31C**). Of note, the results obtained through WB analysis are in line with the immunofluorescence signal which revealed that Ab108252 only stained a minor fraction of EndoC- $\beta$ H1 and the obtained signal was mainly found on the plasma membrane (**Figures 31C, panel-B**). Conversely, Ab15348 and MAB933, which recognized both ACE2 isoforms, showed a higher signal and a different subcellular localization with respect to Ab108252 (**Figures 31A, B, panel-B**). MAB933 ACE2-insulin double immunofluorescence staining confirmed the main punctuate and likely granular cytoplasmic ACE2 signal which also partially overlapped with insulin-positive secretory granules (**Figures 31D, panel-A-H**). In addition, we also observed some spots putatively localized on the plasma membrane (**Figure 31D**). Of note, the specificity of ACE2-MAB933 signal observed in EndoC- $\beta$ H1 was orthogonally tested in comparison to HeLa cells which showed very low/absent ACE2 mRNA expression (**Figure 32A**) and resulted indeed negative for ACE2 in immunofluorescence (**Figure 32B**). An additional evidence of the presence of ACE2 in EndoC- $\beta$ H1 was provided by the shotgun proteomic analysis, aimed at detecting specific peptides derived from ACE2 protein independently of the use of specific antibodies. By this independent approach, we observed the presence of both N-terminal and C-terminal unique ACE2-derived peptides (**Figure S8**), which further confirmed the presence of the ACE-2 protein in human  $\beta$ -cells.

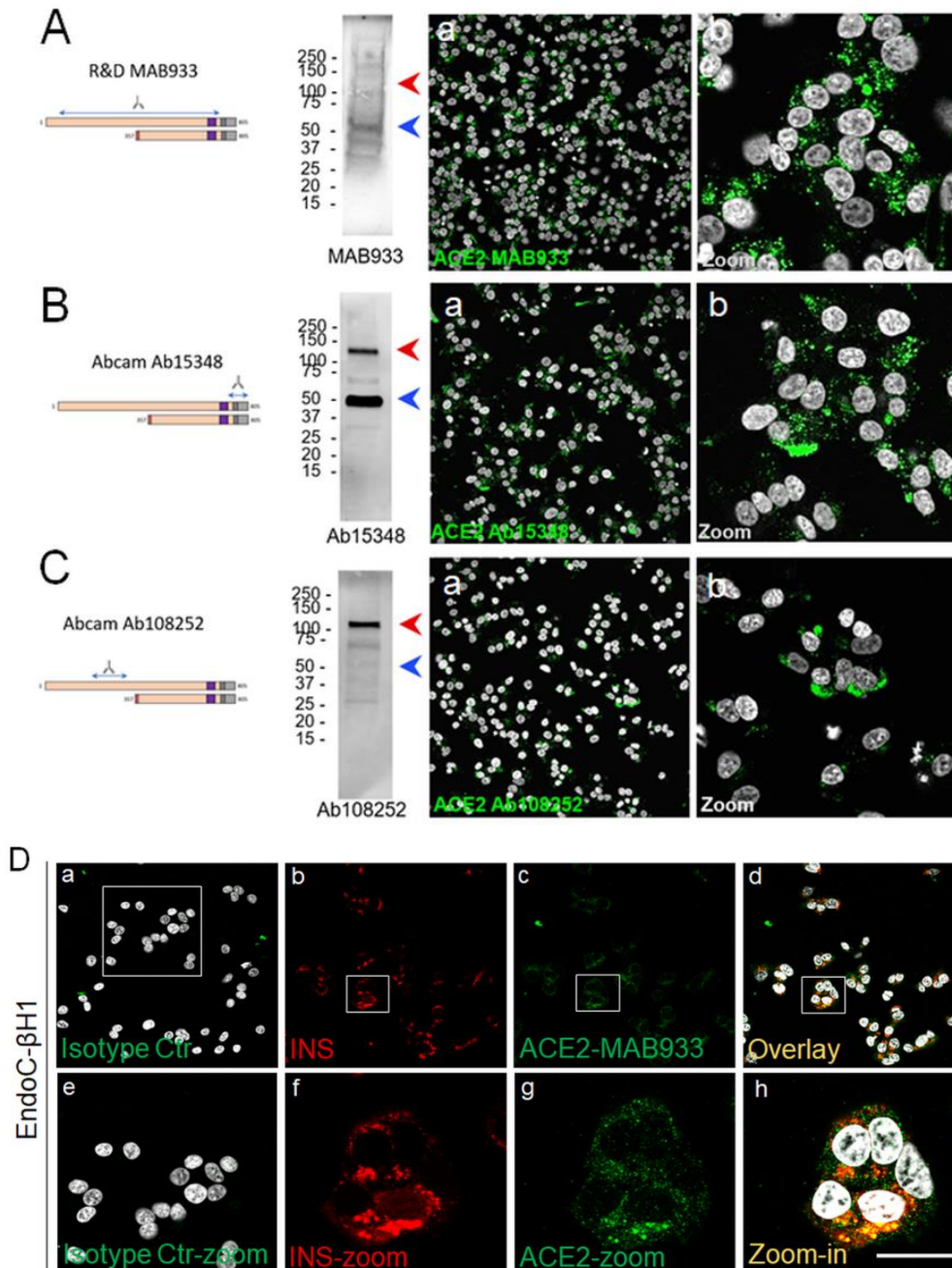


**Figure 31. A short-ACE2 isoform is prevalently expressed in human  $\beta$ -cell line EndoC- $\beta$ H1.**

Western Blot and Immunofluorescence analysis of EndoC- $\beta$ H1 using (A) R&D monoclonal MAB933, (B) Abcam polyclonal Ab15348 and (C) Abcam monoclonal Ab108252 anti-ACE2 antibody. For each antibody adopted, specific target sequence is reported within the aligned ACE2 isoforms. In western blot analysis, molecular weight markers (from 15 kDa to 250 kDa) are reported; red arrows indicate long-ACE2 isoform (expected band of  $\sim$ 110kDa), while blue arrows indicate short-ACE2 isoform ( $\sim$ 50kDa). (D) ACE2 (R&D MAB933) and insulin double

immunofluorescence analysis in EndoC- $\beta$ H1 cultured cells. Negative isotype primary antibody control (relative to ACE2 primary antibody) is shown in panel-a. Insulin (red) and ACE2 (green) are reported in panels-b and -c, while overlay is reported in panel-d. Digital zoom-in images are reported from panels-e to -h. Scale bar in panel-h = 15  $\mu$ m.

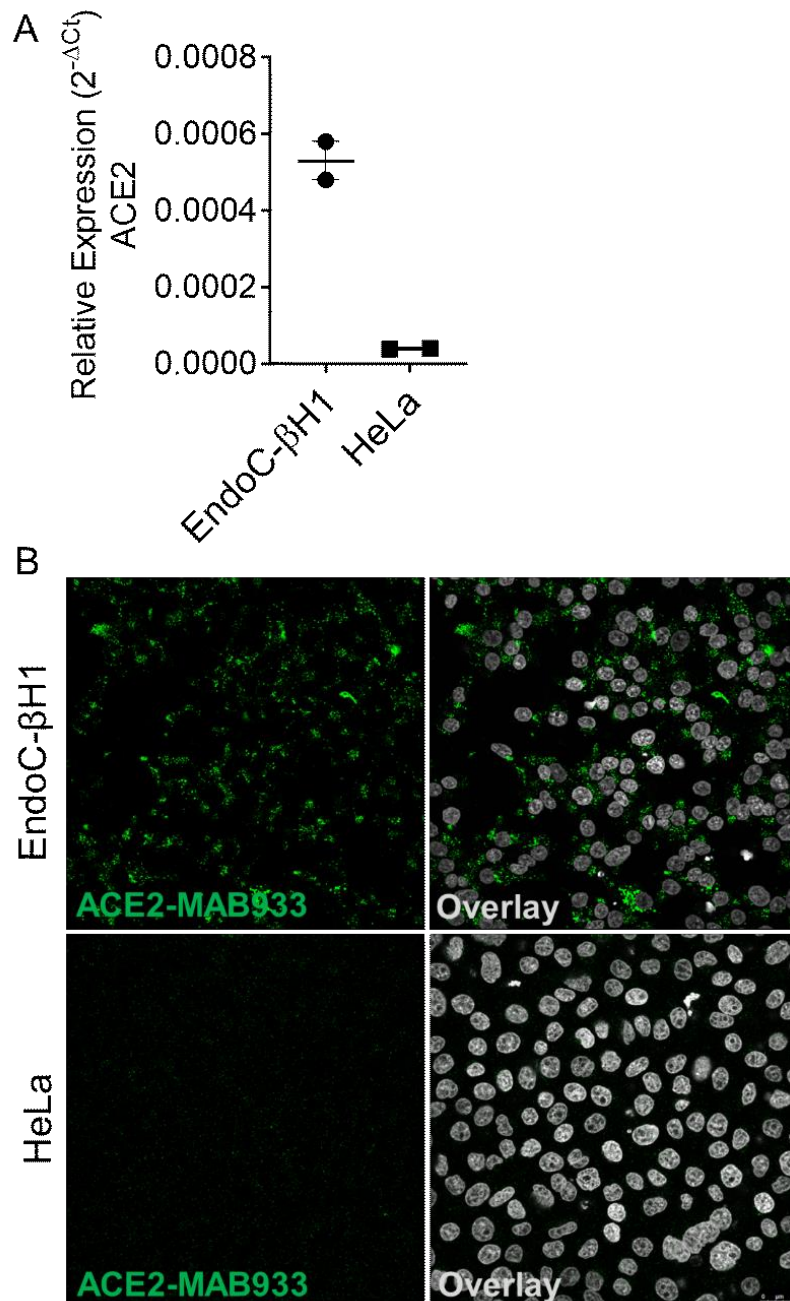
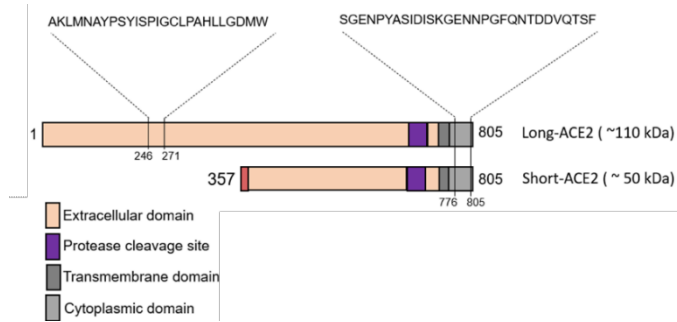


**Figure 32. Orthogonal validation of ACE2 R&D MAB933 antibody in cultured cell lines. (A)** ACE2 mRNA expression using qRT-PCR in EndoC- $\beta$ H1 and HeLa cells. Cycle Threshold values of ACE2 were normalized using  $\beta$ -Actin and GAPDH values. Final values are reported as normalized 2-dCt relative values. **(B)** Immunofluorescence analysis of ACE2 (R&D, MAB933) in EndoC- $\beta$ H1 and HeLa cells stained using the same protocol.



```

# Aligned sequences: 2
# 1: EMBOSS_001
# 2: EMBOSS_001
# Matrix: EBLOSUM62
# Gap penalty: 10.0
# Extend penalty: 0.5
#
# Length: 805
# Identity: 452/805 (56.1%)
# Similarity: 452/805 (56.1%)
# Gaps: 346/805 (43.0%)
# Score: 2387.0
#

```

```

EMBOSS_001 1 MSSSSWLLLSLVAVTAAQSTIEEQAKTFLDKFNHEAEDLFYQSSLASWNY 50
EMBOSS_001 1 ----- 0
EMBOSS_001 51 NTNITEENVQNNAGDKWSAFLKEQSTLAQMYPLEIQNLTVKILQAL 100
EMBOSS_001 1 ----- 0
EMBOSS_001 101 QQNGSSVLSEDKSKRLNTILMTMSTIYSTGKVCNPDNPQCLLLEPGLNE 150
EMBOSS_001 1 ----- 0
EMBOSS_001 151 IMANSLDYNERLWAWESWRSEVQKQLRPLYEEYVVLKNEMARANHYEDYG 200
EMBOSS_001 1 ----- 0
EMBOSS_001 201 DYNRGDYEVNNGVDGYDSRQQLIEDVEHTFEIKPLVEHLHAYVRAKIMN 250
EMBOSS_001 1 ----- 0
EMBOSS_001 251 AYPSPYISPIGCLPAHLGDMWGRFWTNLYSLTVFPQKPNIDVTDAMVDQ 300
EMBOSS_001 1 ----- 0
EMBOSS_001 301 ANDAQRIFKEAEKFFVSVGLFNNMTQGFWENSMITDPGNVQKAVCHPTAMD 350
EMBOSS_001 1 -----MRKNGWD .....II 7
EMBOSS_001 351 LQKGDFRILMCTKVTMDDFLTAHHEMGIQYIMAYAAQPFLLANGANEGF 400
EMBOSS_001 8 KGG---RIIMCTKVTMDDFLTAHHEMGIQYIMAYAAQPFLLANGANEGF 54
EMBOSS_001 401 HEAVGEIMLSAATPKHLKSIQLLSPDFQIDNTEINFLKQALTIWGTL 450
EMBOSS_001 55 HEAVGEIMLSAATPKHLKSIQLLSPDFQIDNTEINFLKQALTIWGTL 104
EMBOSS_001 451 PFTYMLEKRRKRVFKGEI PKDQMMKQNNMKREIVGVVEFVPHDETYCDP 500
EMBOSS_001 105 PFTYMLEKRRKRVFKGEI PKDQMMKQNNMKREIVGVVEFVPHDETYCDP 154
EMBOSS_001 501 ASLFHVSNDYSFIRYYTRTLVQFQFQALCQAARHEGFLHKCDISNSTEA 550
EMBOSS_001 155 ASLFHVSNDYSFIRYYTRTLVQFQFQALCQAARHEGFLHKCDISNSTEA 204
EMBOSS_001 551 GQKLFNMLRLGKSEPWTLALENVVGAQDDIVRPLLNYPFLFTWLKQNK 600
EMBOSS_001 205 GQKLFNMLRLGKSEPWTLALENVVGAQDDIVRPLLNYPFLFTWLKQNK 254
EMBOSS_001 601 NSFVGSWSDWSFYADQSIKVRISLKSALGDKAYEWNDEMFLFRSSVAYA 650
EMBOSS_001 255 NSFVGSWSDWSFYADQSIKVRISLKSALGDKAYEWNDEMFLFRSSVAYA 304
EMBOSS_001 651 MRQYFLKVNQMLFGEDDVRVANLKPRISFNFPVTAPOKNSDIIPRTEV 700
EMBOSS_001 305 MRQYFLKVNQMLFGEDDVRVANLKPRISFNFPVTAPOKNSDIIPRTEV 354
EMBOSS_001 701 EKAI RMSRSRINDAFLRNDNSLEFLGIQPTLGPFPVSIWLIIVGVVM 750
EMBOSS_001 355 EKAI RMSRSRINDAFLRNDNSLEFLGIQPTLGPFPVSIWLIIVGVVM 404
EMBOSS_001 751 GVIVVGIVLIFTGIRDRKKKQKARSGENPYASIDISKGENNPGFQNTDD 800
EMBOSS_001 405 GVIVVGIVLIFTGIRDRKKKQKARSGENPYASIDISKGENNPGFQNTDD 454
EMBOSS_001 801 YQTSF 805
EMBOSS_001 455 YQTSF 459

```

**Figure 33. ACE2 Targeted Mass Spectrometry-Shotgun Proteomic Analysis of EndoC-βH1.**

(A) Representative scheme of ACE2 isoforms (short-ACE2 and long-ACE2) and consistent peptides identified in EndoC-βH1 using shotgun proteomics in n=2 independent experiments. Below, alignment of ACE2 isoforms protein FASTA sequences performed using EMBOSS. Red sequence: short-ACE2; black sequence: long-ACE2; yellow highlighted sequences: shotgun proteomics identified peptides.

## 5.4 Total ACE2 mRNA is expressed in human pancreatic islets and in the human beta-cell line EndoC-βH1

To confirm the ACE2 expression in human islets, we also evaluated its transcriptional activity both in collagenase isolated and in Laser-Capture Microdissected (LCM) human pancreatic islets by measuring its mRNA expression using TaqMan RT-Real Time PCR. In order to avoid detection of genomic DNA, we used specific primers set generating an amplicon spanning the exons 17–18 junction of ACE2 gene, thus uniquely identifying its mRNA (**Figure 34A**). Of note, the selected amplicon is shared between short- and long-ACE2 isoforms thus identifying total ACE2 mRNA.

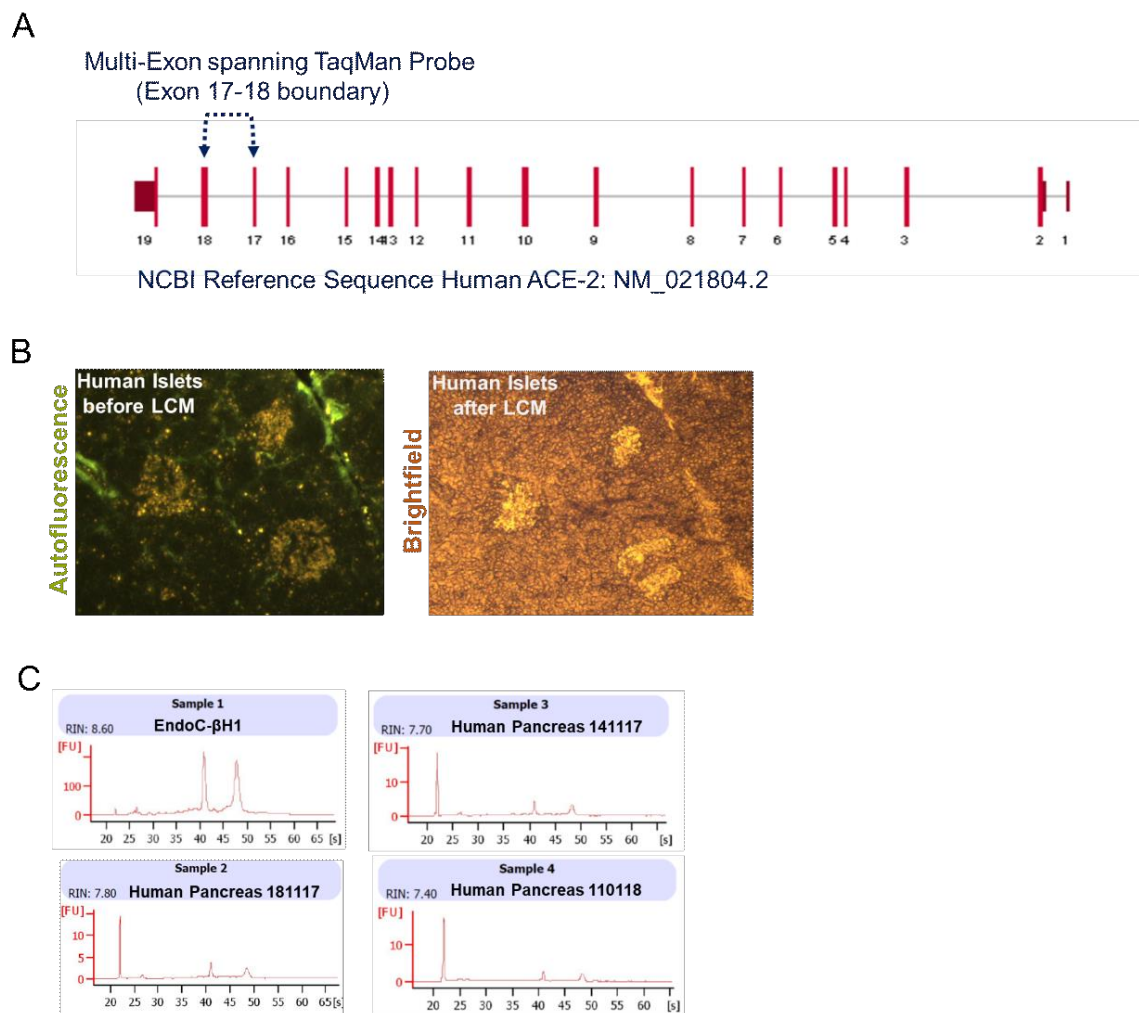


**Figure 34. ACE2 mRNA expression.** (A) ACE2 gene scheme reporting exons of full-length transcript (Ref Seq: NM\_021804.2) and showing the location of the TaqMan Assay (Hs01085333\_m1, assay location 2332nt, exon 17-18, amplicon length: 141nt) used to detect ACE2 mRNA expression. (B) Human pancreatic islets autofluorescence and brightfield images in a human

pancreatic frozen section, before and after laser capture microdissection procedure. (C) Electropherogram of total RNA extracted from EndoC- $\beta$ H1 cells and from LCM-islets from human pancreatic sections obtained from five non-diabetic multiorgan donors. Representative RNA Integrity Number (RIN) is reported for each RNA sample analyzed.

First, as a positive control we analyzed total ACE2 expression in RNA extracted from a lung parenchyma biopsy tissue (**Figures 35A, E**). Collagenase-isolated human pancreatic islets obtained from four different non-diabetic donors' pancreata (**Table 1**) showed ACE2 mRNA expression, as demonstrated by RT-Real-Time PCR raw cycle threshold (Ct) values, reporting a Ct range between 28 and 29 (**Figures 35B, F**). Since human pancreatic islet enzymatic isolation procedures may induce some changes in gene expression (45), we microdissected human islets from frozen pancreatic tissues obtained from five non-diabetic multiorgan donors recruited within INNODIA EUnPOD network (46) and evaluated ACE2 mRNA levels. The LCM procedure (**Figure 34B**) allowed us to extract high quality total RNA (**Figure 34C**) from human pancreatic islets directly obtained from their native microenvironment, thus maintaining transcriptional architecture. ACE2 mRNA expression in LCM-human pancreatic islets showed a consistent expression among cases, similar to isolated islets, as shown by ACE2 mRNA raw Ct and normalized values (**Figures 35C, G**). Finally, we analyzed total ACE2 mRNA expression in the human  $\beta$ -cell line EndoC- $\beta$ H1. Analysis of ACE2 mRNA expression in these cells demonstrated a similar expression level in comparison to human pancreatic islets (**Figures 35D, H**), with raw Ct values ranging from 28 to 30.



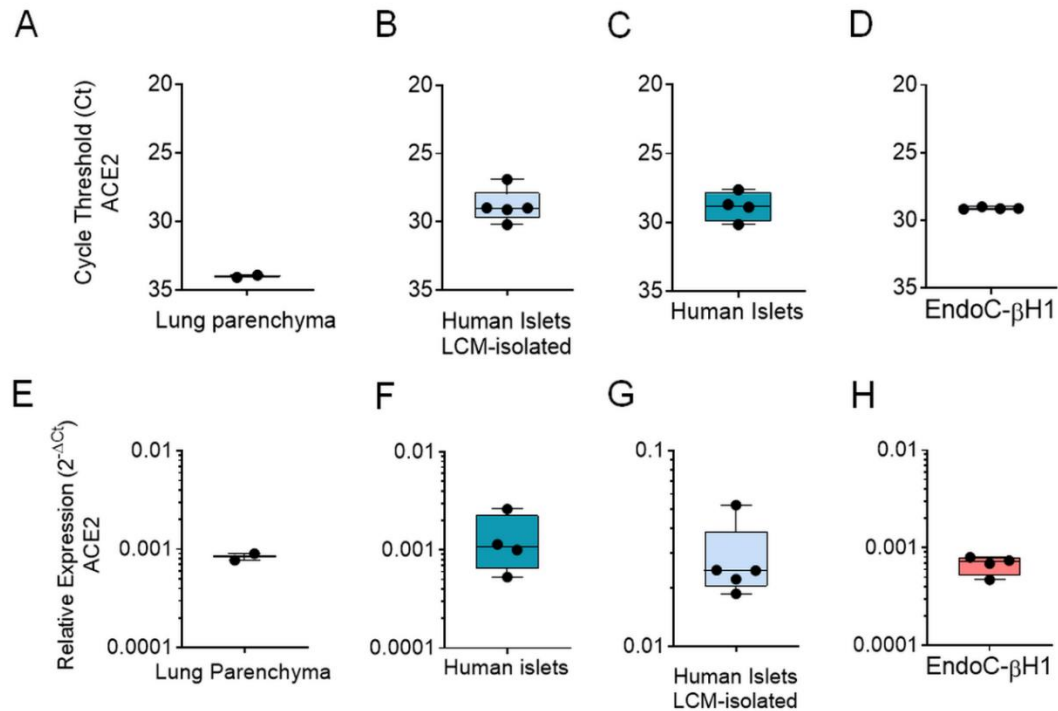


**Figure 35. qRT-Real Time PCR analysis of ACE2 mRNA.** (A–D) ACE2 raw Ct values results in lung tissue (n = 1, in duplicate), in enzymatic-isolated human pancreatic islets samples (n = 4), in LCM-microdissected islets (n = 5) and in EndoC-βH1 (n = 4). (E–H) ACE2 expression values normalized using GAPDH and β2- microglobulin of the samples analysed in A–D. Values are reported as 2<sup>-ΔCt</sup>. Mean ± S.D. values are shown.

### 5.5 ACE2 expression is increased in EndoC-βH1 cells and in human pancreatic islets by pro-inflammatory cytokines

In order to determine whether metabolic or inflammatory stress conditions modify pancreatic endocrine β-cell expression of ACE2, we exposed the human β-cell line EndoC-βH1 and isolated human pancreatic islets to metabolic or inflammatory stressors and subsequently evaluated ACE2 expression levels. Exposure to palmitate (2 mM palmitate for 24 h) did not significantly modulate ACE2 expression (**Figure 36A**). On the other hand, upon 24 h exposure to a proinflammatory cytokines mix (IL-1β – IFNγ and TNFα), EndoC-βH1 cells significantly upregulated ACE2 mRNA levels (fold change: 12.3 vs. not-treated control, p = 0.031) (**Figure 36B**). The same results were confirmed through immunofluorescence analysis aimed at measuring ACE2 protein levels and subcellular

localization in EndoC- $\beta$ H1 exposed or not to the same proinflammatory condition (**Figure 36C**). Indeed, we observed a significant increase in ACE2 mean intensity values upon cytokine treatment, confirming the upregulation of ACE2 protein as well (**Figure 36E**). These results were confirmed using an automated micro-confocal high content images screening system (31) which allowed us to measure ACE2 intensity in cytokine-treated vs not treated EndoC- $\beta$ H1 cells (**Figures 36D, F**). In support of the observed increase of ACE2 upon proinflammatory stress, RNA sequencing data analysis of EndoC- $\beta$ H1 cells exposed to IL-1 $\beta$  + IFN $\gamma$  (48 h) or to IFN $\alpha$  (18 h) further confirmed such increase (**Table 5**). Indeed, we observed a 24.5 and 55.2 fold-increase ( $p < 0.0001$ ) in total ACE2 mRNA [transcript (ENST00000252519.8)] (**Table 5 and Figure 37A**) expression in EndoC- $\beta$ H1 cells treated with IL-1 $\beta$  + IFN $\gamma$  or with IFN $\alpha$ , respectively. Importantly, the same expression pattern was observed also in human pancreatic islets exposed to the same cytokine mix, as demonstrated by a 2.4 and 5.1 fold-increase in ACE2 mRNA expression following IL-1 $\beta$  + IFN $\gamma$  or IFN $\alpha$  treatment respectively ( $p < 0.0001$ ) (**Table 5 and Figure 37B**).



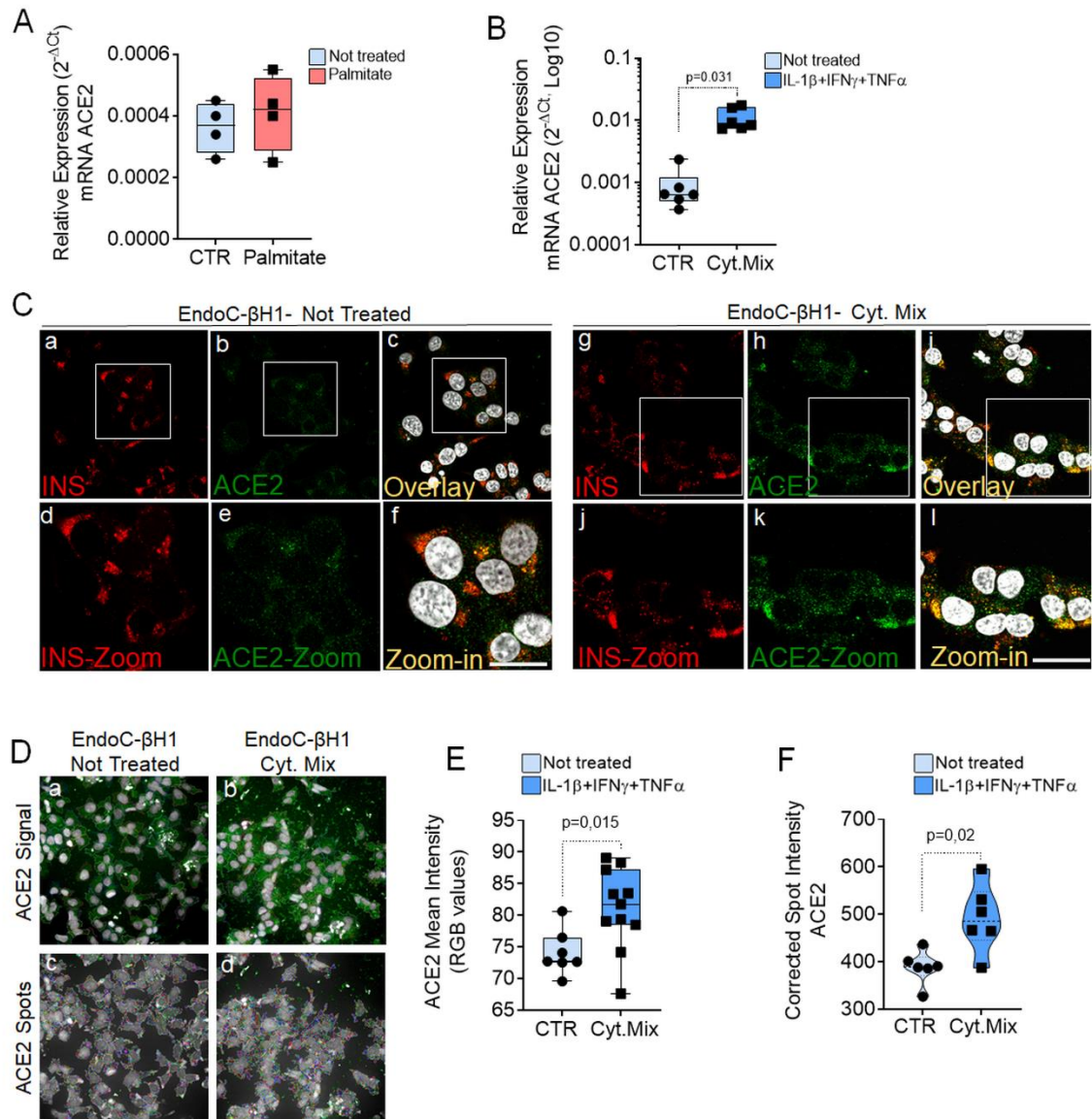


**Figure 36. ACE2 expression is increased by inflammatory stress.** ACE2 mRNA RT-Real-Time PCR analysis in EndoC- $\beta$ H1 treated or not (CTR) with Palmitate (2.0 mM) (A) or with cytokines (IL-1 $\beta$  + IFN $\gamma$  + TNF $\alpha$ ) (Cyt. Mix) (B) for 24 h. Results are reported as mean  $\pm$  S.D of  $2^{-\Delta C_T}$  normalized values. p-values were calculated using Wilcoxon matched-pairs signed rank test. (C) Immunofluorescence analysis of insulin (red, panels-a and -g) and ACE2 (green, panels-b and -h) in EndoC- $\beta$ H1 not-treated (panels-a to -f) or treated (panels-g to -l) with cytokines for 24 h. Digital zoom-in images are reported in panels-d to -f and in panels-j to -l. Scale bar in panel-f: 10  $\mu$ m. Scale bar in panel-l: 15  $\mu$ m. (D) Representative images of ACE2 staining (green) and analysis using micro-confocal High-content screening in EndoC- $\beta$ H1 treated or not with cytokines (IL-1 $\beta$  + IFN $\gamma$  + TNF $\alpha$ ). Panels-a and -b: ACE2 signal (green) and automated cell cytoplasm segmentation and identification. Panels-c and -d: identification of ACE2 granular spots within segmented cytoplasm

in panels-a and -b. Each ACE2 granular spot intensity was measured and analyzed. (E) Mean intensity imaging analysis related to data reported in (C) of EndoC- $\beta$ H1 treated or not with cytokines. Data are reported as individual values alongside with mean  $\pm$  S.D of RGB gray-intensity measures of 6–11 different experimental points related to two different independent experiments. Individual values alongside with mean  $\pm$  S.D are reported. P-value was calculated using Mann–Whitney U test. (F) High content screening analysis of Corrected Median Spot intensity of ACE2 signal in EndoC- $\beta$ H1 treated or not with cytokines. Median intensity values of six different experimental points are reported. P-value was calculated using Mann–Whitney U test ( $p < 0.05$ ).

<b>IL-1<math>\beta</math> + IFN<math>\gamma</math> (48h)</b>				
	Not treated	Treated (IL-1 $\beta$ + IFN $\gamma$ )	Log2 Fold Change (Cyt vs. nt)	pValue Adj
EndoC- $\beta$ H1	0.061	1.05	4.19	3.02E-35
Human Pancreatic islets	2.20	5.76	1.51	7.902E-17
<b>IFN<math>\alpha</math> (18h)</b>				
	Not treated	Treated (IFN $\alpha$ )	Log2 Fold Change (Cyt vs. nt)	pValue Adj
EndoC- $\beta$ H1	0.057	3.15	5.92	9.35E-42
Human Pancreatic islets	3.17	16.30	2.39	8.45E-26

**Table 5.** Expression of ACE2 mRNA (ENST00000252519.8) in RNA-seq dataset of five different samples of EndoC- $\beta$ H1, and five different Human Pancreatic islets preparations exposed or not to IL-1 $\beta$  + IFN $\gamma$  (48h), and five different samples of EndoC- $\beta$ H1 and six of Human Pancreatic islets exposed or not to IFN $\alpha$  (18h).

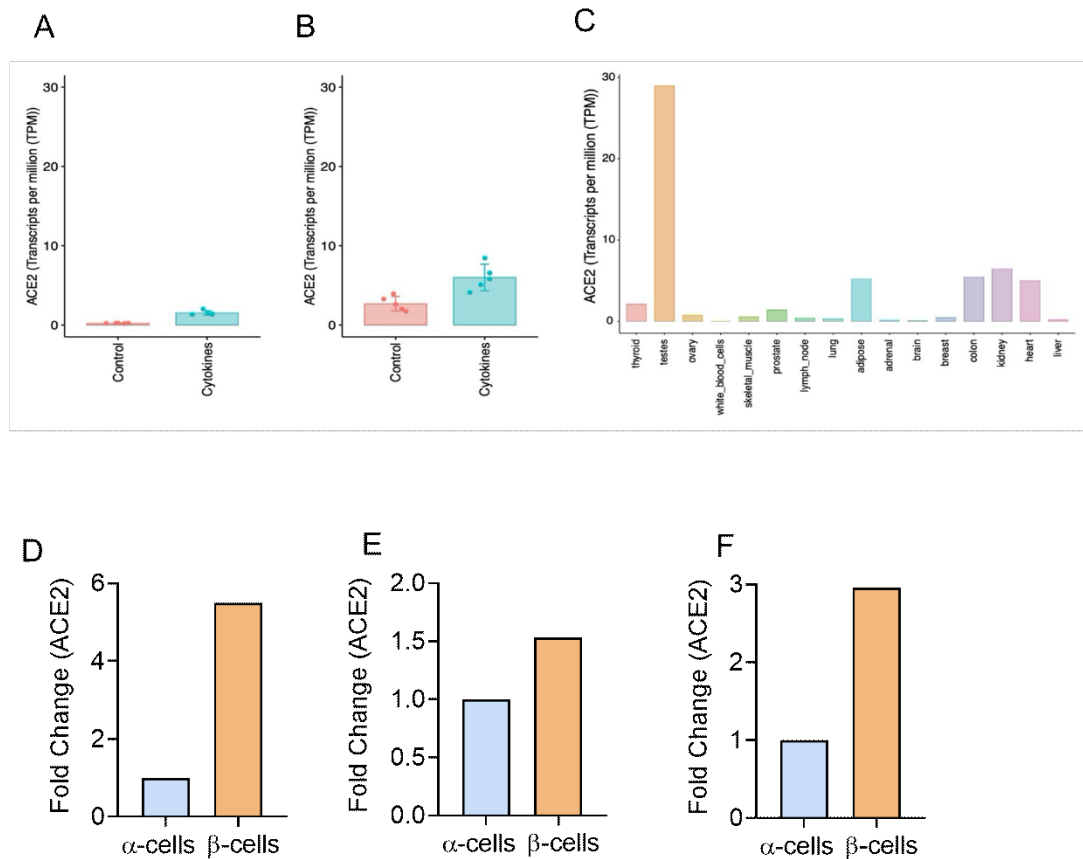


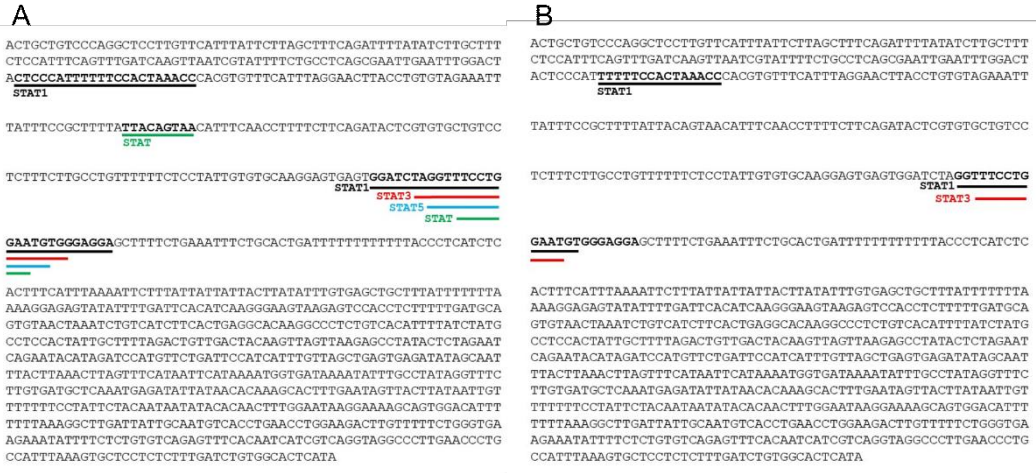
**Figure 37. Expression of ACE2 mRNA expression in different conditions and tissues.** The expression of ACE2 was evaluated in EndoC-βH1 cells (A) and pancreatic human islets (B) exposed or not to proinflammatory cytokines (IL1β + IFNγ) for 48h and in 16 different tissues from the Illumina Body Map 2.0 (GEO: GSE30554) (C) that were sequenced at a similar deep coverage (coverage > 150 x 10<sup>6</sup> reads / per sample). Values are represented as transcripts per million (TPM). All the samples were processed using the same RNA-seq pipeline as described in Methods. (D-E) ACE2 expression in β-cells and in α-cells, obtained from three different RNA-seq datasets. Data were extrapolated from supplementary files of normalized and analyzed datasets obtained from three different published studies which compared β- and α-cells transcriptomes. In (D) Dorrell et al 2011, in (E) Bramswig et al 2013, and in (F) Blodgett et al 2015 (Blodgett et al., 2015; Bramswig et al., 2013; Dorrell et al., 2011).

Additionally, in order to strengthen such observations, we focussed on the ACE2 gene promoter by analyzing its upstream sequence (−1000 bp) from ACE2 transcriptional start site (TSS). Using two different transcription factors (TF) binding motif databases, we found several binding sites for TFs related to cytokine signaling pathways such as STAT1 or STAT3 (**Figure 38**), thus reinforcing our results of an association between inflammation and ACE2 expression and confirming what was previously reported (49).

Moreover, in order to evaluate the pathway implicated in ACE2 regulation we evaluated ACE2 mRNA expression in human islets pre-treated for two hours with Baricitinib (n=3) or Nimbus (n=6), Janus kinase (Jak1/2) and Tyrosine kinase 2 (TYK2) inhibitors, respectively. Human islets then were exposed to proinflammatory cytokines, specifically IFN $\alpha$  and the combination IFN $\alpha$  + IL-1 $\beta$ , for 24 hours.

The analysis of ACE2 mRNA confirmed JAK1/2 and TYK2 inhibitors prevent cytokines induced ACE2 mRNA expression in human islets, demonstrating that ACE2 is regulated through the JAK-STAT pathway (**Figure 39**).

However, the analysis of ACE2 expression distribution in FFPE pancreas sections from a T1D longstanding donor (**see Table 1**) did not show remarkable changes in the levels or distribution of ACE2 in infiltrated islets (**Figure 40**). This is in line with RNAseq analysis of whole islets from two T1D patients and four controls, which indicated similar ACE2 expression (RPKM 1.2–1.7 in all cases) (50). Analysis of additional recent-onset T1D donors is needed to evaluate potential changes in ACE2 expression in  $\beta$ -cells of highly infiltrated pancreatic islets. Collectively these results demonstrate that ACE2 is upregulated upon *in vitro* exposure to early and acute inflammatory, but not metabolic, stressors both in EndoC- $\beta$ H1 and in human pancreatic islets.



**C**

Rank	P-value	Matrix ID	Matrix name
1	0,0009	M01478	V\$CPHX_01
2	0,0043	M00412	V\$AREB6_01
3	0,0063	M00250	V\$GF1B_01
4	0,0084	M01058	V\$GF1B_01
5	0,0100	M01232	V\$SATB1_01
6	0,0117	M00457	V\$STAT5A_01
7	0,0118	M01260	V\$STAT1_05
8	0,0119	M00119	V\$MAX_01
9	0,0124	M00459	V\$STAT5B_01
10	0,0129	M00347	V\$GATA1_06
11	0,0129	M01004	V\$HELIOSA_02
12	0,0157	M00711	V\$ZTA_02
13	0,0160	M00317	V\$LDSPOLYA_B
14	0,0180	M01446	V\$BARHL2_01
15	0,0190	M01022	V\$LEF1_02_01
16	0,0191	M01116	V\$CLOCKBMAL_Q6
17	0,0196	M00615	V\$MYC_MAX_03
18	0,0198	M01425	V\$SHF1B_01
19	0,0201	M01014	V\$SOX_Q6
20	0,0214	M00637	V\$GATA4_Q3
21	0,0216	M00318	V\$LDPOLYA_B
22	0,0217	M00802	V\$PI1_Q6
23	0,0231	M01665	V\$IRF8_Q6
24	0,0251	M00223	V\$STAT_01
25	0,0251	M01352	V\$NRX29_01
26	0,0311	M01124	V\$OCT4_Q2
27	0,0323	M00302	V\$NFAT_Q6
28	0,0335	M01185	V\$RCL6_Q2
29	0,0346	M00033	V\$P300_Q1
30	0,0367	M00799	V\$MYC_Q2
31	0,0376	M00055	V\$MYC_Q1
32	0,0384	M01009	V\$HES1_Q2
33	0,0391	M00451	V\$NRX3A_Q1
34	0,0399	M01383	V\$NRX3A_Q2
35	0,0405	M00671	V\$TCF4_Q5
36	0,0407	M00320	V\$MTA1A_B
37	0,0408	M00118	V\$MYC_MAX_Q1
38	0,0423	M01464	V\$HOKA10_Q1
39	0,0430	M00123	V\$MYC_MAX_Q2
40	0,0441	M00472	V\$FOXO4_Q1
41	0,0458	M01342	V\$CDP_Q3
42	0,0459	M00059	V\$YY1_Q1
43	0,0460	M01595	V\$STAT3_Q3
44	0,0469	M01457	V\$NRX23_Q1

**D**

Rank	P-value	Matrix ID	Matrix name
1	0,0090	MA0144.1	STAT3
2	0,0124	MA0058.1	MAX
3	0,0224	MA0137.2	STAT1
4	0,0278	MA0093.1	USF1
5	0,0317	MA0258.1	ESR2
6	0,0384	MA0004.1	Amt
7	0,0489	MA0150.1	NFE2L2

**Figure 38. ACE2 promoter Transcription factor binding motifs analysis.** TRAP analysis of transcription factors binding motifs in 1000 bp upstream sequence from ACE2 TSS (ACE2 proximal promoter). Analysis of TFs binding motifs using TRANSFAC database (A) and JASPAR database (B), alongside with related tables reporting ranking, p-values, TF matrix ID and TF binding motifs official name. STATs binding motifs are highlighted in different colours within ACE2 promoter sequences and reported in bold in the related table.

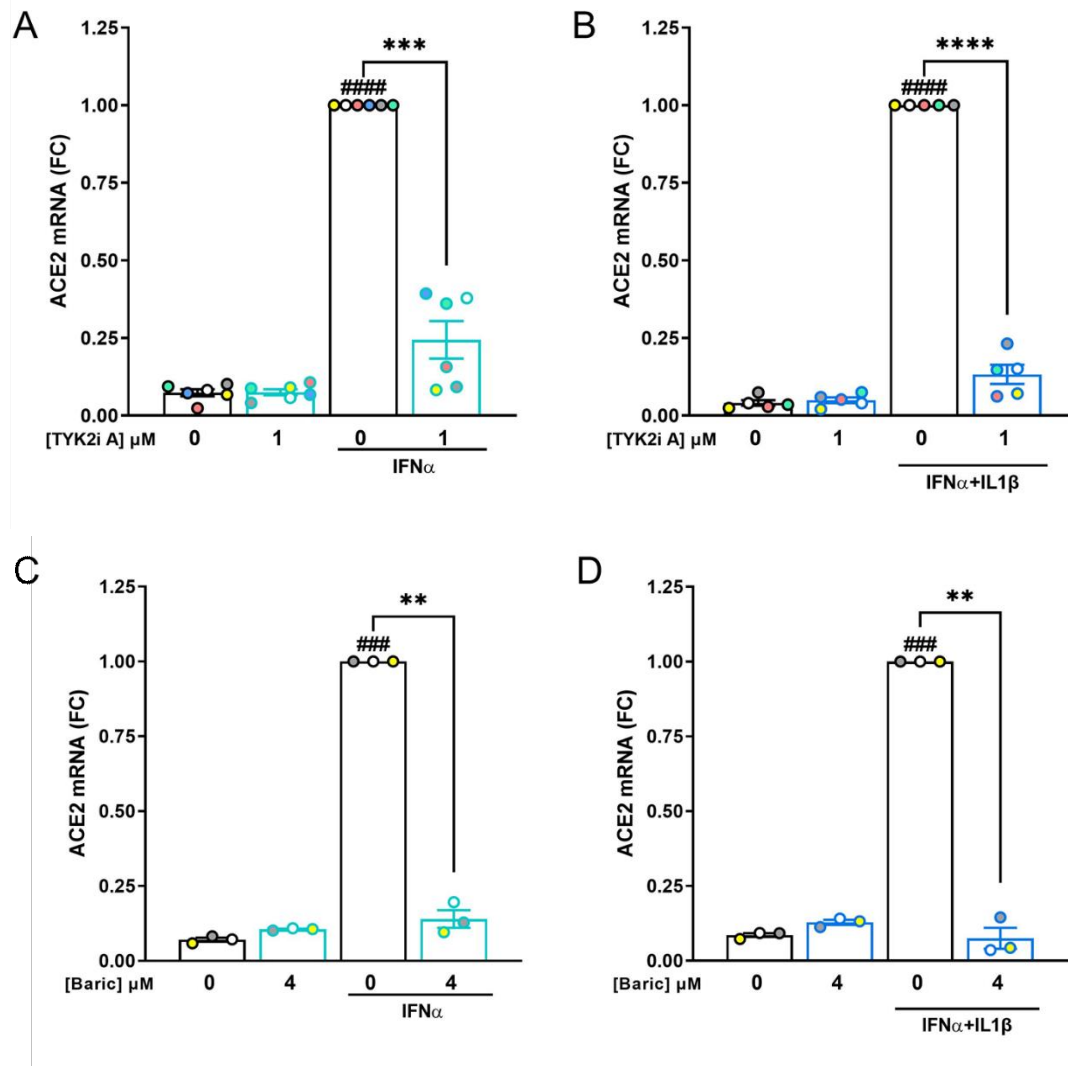


**Figure 39. Effect of IFN signal inhibitors on proinflammatory-induced ACE2 expression in human islets.** Dispersed human islets (6 independent preparations) were left untreated or pre-treated with the Tyk2 inhibitor A (TYK2iA) 1 $\mu$ M or DMSO (vehicle) for 2h and the exposed or not to IFN $\alpha$  (2000 U/ml) (**A**) or IFN $\alpha$  (2000U/ml) + IL-1 $\beta$  for 24h (**B**). Dispersed human islets (3 independent preparations) pre-treated with the Baracitinib 4 $\mu$ M or DMSO (vehicle) for 2h. Then and then exposed or not to IFN $\alpha$  (2000 U/ml) (**C**) or IFN $\alpha$  (2000U/ml) + IL-1 $\beta$  for 24h (**D**). The mRNA expression of ACE2 was analyzed by RT-qPCR. Values were normalized by Geometric mean of  $\beta$ -Actin and VAPA and, then by the control condition with IFN $\alpha$  or IFN $\alpha$ + IL-1 $\beta$  considered as 1. Results are mean  $\pm$  SEM of 3 independent experiments. ####p<0.001 vs control (no inhibitor and no IFN $\alpha$ + IL-1 $\beta$ ); \*\*p<0.01, as indicated by the bars; one-way ANOVA followed by Bonferroni correction.



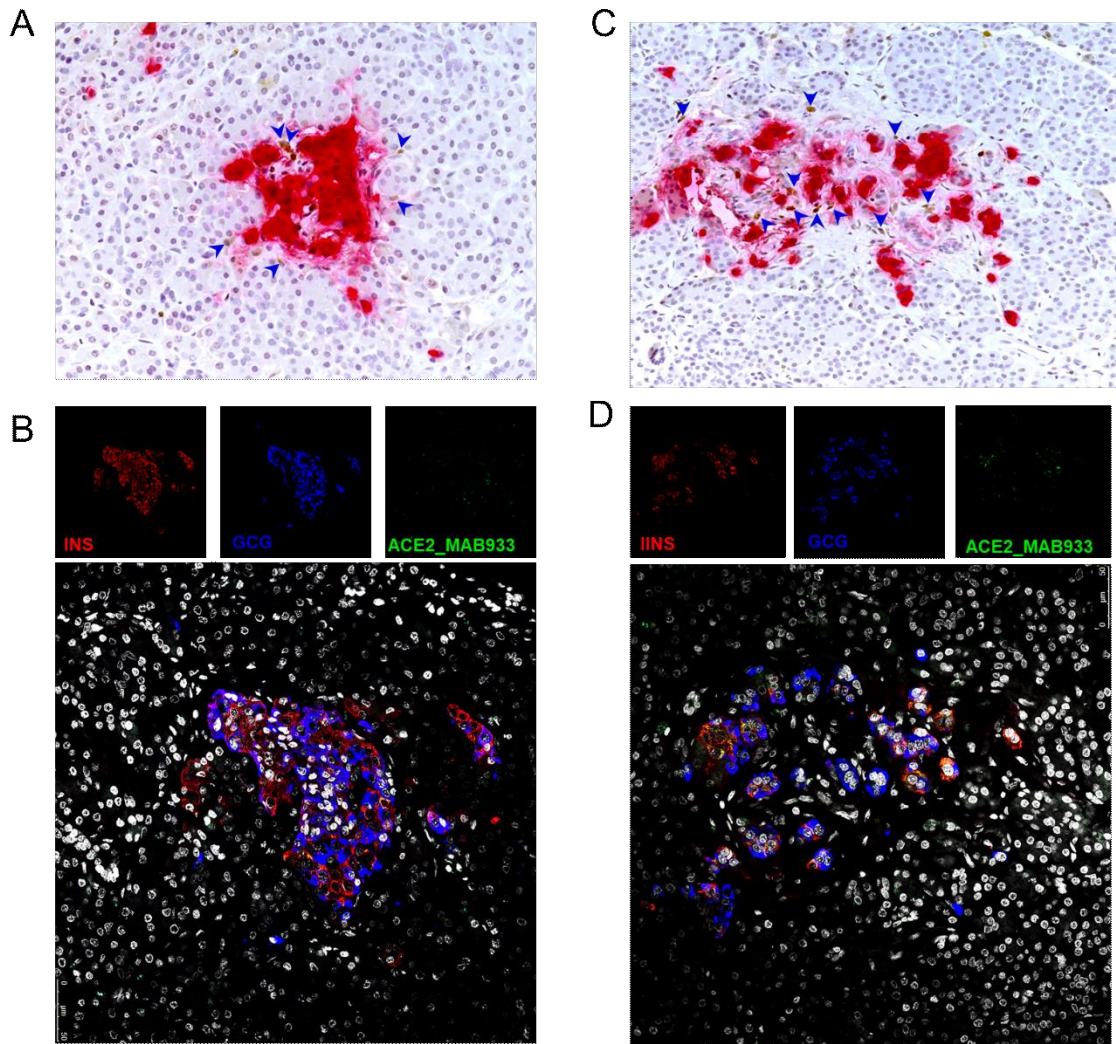


**Figure 40.** Triple immunofluorescence analysis of insulin (red), glucagon (blue) and ACE2-MAB933 (green) in a FFPE section of a longstanding T1D donor. Two infiltrated islets (A-B and C-D) were identified based on IHC insulin (red)-CD45 (brown) staining in a previous serial sections of the same T1D case.

## 5.6 Upregulation of ACE2 in T2D

As previously discussed, several studies demonstrated that COVID-19 has a more severe outcome in patients with diabetes; in addition, in normoglycemic patients, the infection can alter glycometabolic control increasing the risk to develop T2D or dysglycaemia. Thus, a bidirectional relationship between COVID-19 and diabetes can be hypothesized.

In order to detect pancreatic ACE2 protein expression and distribution, and to evaluate differences between non-diabetic (ND) and type 2 diabetic (T2D) donors, we performed a quadruple immunofluorescence on FFPE pancreatic sections obtained from n=20 ND and n=20 T2D multiorgan donors (**Table 2**). We used two different anti-ACE2 antibodies: (i) a monoclonal mouse IgG2a anti-human ACE2 (R&D, MAB933) and (ii) a rabbit polyclonal anti-ACE2 (Abcam, Ab15348).

In ND and T2D donor pancreata, both antibodies showed signals indicating that ACE2 is expressed in pancreatic islets where it is mostly colocalized with insulin signal, thus confirming that ACE2 is present in  $\beta$ -cells, as expected (**Figure 41A**).

In exocrine tissue, ACE2-positive cells showed a vasculature-like morphology and distribution, thus confirming our previous observations in line also with other reports (111,123) which demonstrate the localization of ACE2 also in pancreatic vascular cells (**Figure 41B**).

To evaluate putative ACE2 expression differences between ND and T2D pancreatic islets, we performed an analysis of the intensity of ACE2 signals including a total of n=1082 islets. Both antibodies revealed a higher intensity of ACE2 in T2D compared to ND pancreatic islets (**Figure 42A**). Analysis of ACE2 intensity confirmed the significantly increased expression of ACE2 in T2D pancreatic islets compared to ND donors as measured by R&D and Abcam antibodies (greyscale values of ACE2-MAB933 in T2D=52.5 $\pm$ 34.6 and in ND =37.1 $\pm$ 28.1,  $p < 0.001$ ; greyscale values of ACE2-ab15348 in T2D=53.2 $\pm$ 63.5 and in ND =27.3 $\pm$ 22.3,  $p < 0.001$ ) (**Figure 42C, D**).

To define whether the increased ACE2 expression occurred mainly in  $\beta$ -cells or in other islet cells we performed a colocalization rate analysis (reported as the percentage of the overlap of INS and ACE2 signals) of ACE2 MAB933/INS and ACE2 Ab15348/INS in T2D and ND pancreatic islets. We observed a significantly increased colocalization rate between ACE2 and INS in T2D compared to ND subjects (**Figure 42B**). The ACE2



colocalization rate analysis of n=1082 islets across all ND and T2D donors confirmed the increased colocalization rate between ACE2-MAB933/INS [T2D:  $12.5 \pm 7.6\%$  (mean  $\pm$  S.D.) vs ND  $9.23 \pm 7.0\%$  (mean  $\pm$  S.D.),  $p < 0.001$ ] and of ACE2-ab15348/INS [T2D:  $11.45 \pm 13.7\%$  (mean  $\pm$  S.D.) vs ND  $5.3\% \pm 5.3\%$ ;  $p < 0.001$ ] in T2D compared to ND (**Figure 2E,F**).

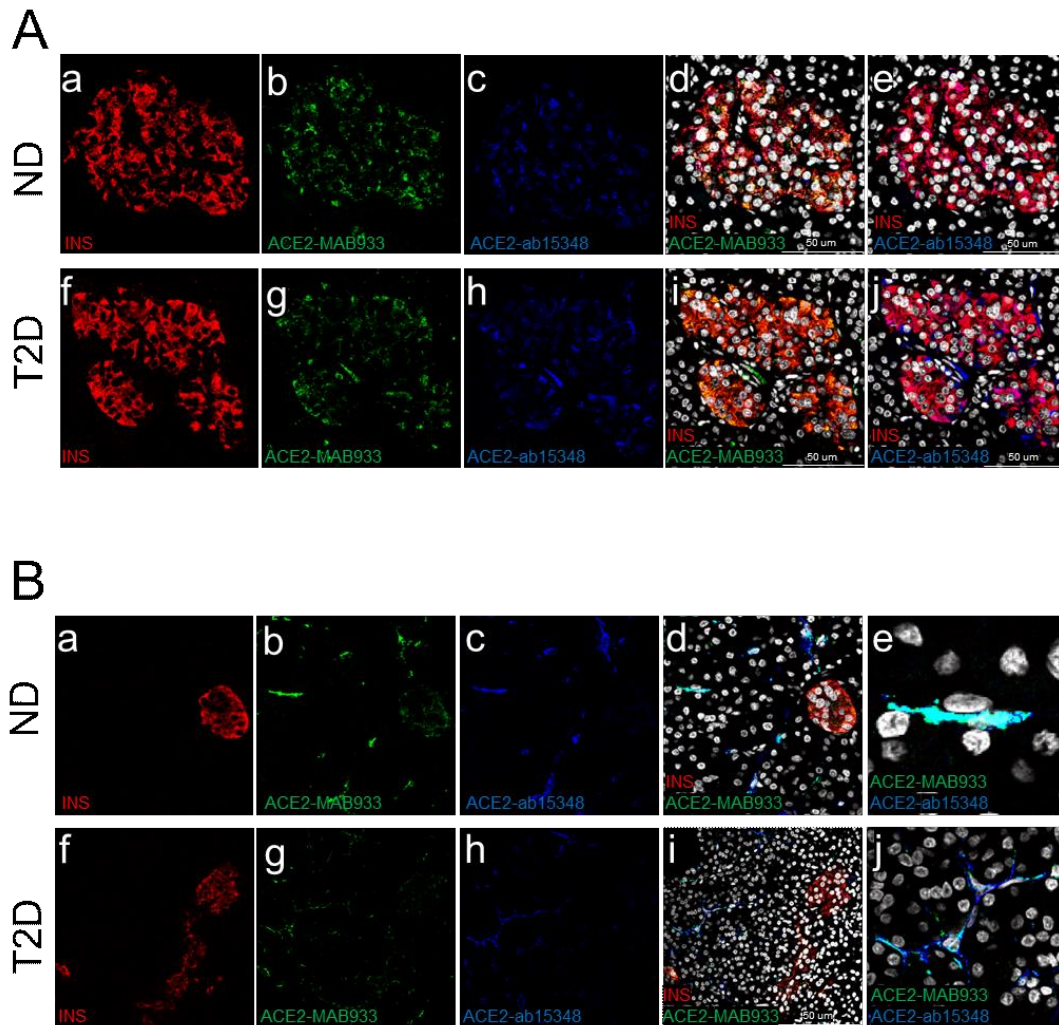


**Figure 41. Immunofluorescence detection of ACE2 expression in endocrine and exocrine pancreas using two different antibodies.** a) Representative confocal images of ACE2 staining in pancreatic islet in FFPE pancreatic sections derived from a non-diabetic case (ND) (panels a-e) and from a T2D case (panels f-j). Tissues were stained for DAPI (white), insulin (INS, red, panel A, F), ACE2-MAB933 (green, panels b, g) and ACE2-ab15348 (blue, panels c, h). Colocalization between insulin and ACE2-MAB933 is showed in yellow (panels d, i) and colocalization between insulin and ACE2-ab15348 is reported in magenta (panels E, J). Scale bars in panels d, e, i and j are 50  $\mu$ m. b) Representative confocal images of ACE2 in pancreas microvasculature in FFPE pancreatic

section derived from a non-diabetic case (ND) (panels a-e) and from a T2D case (panels f-j). Tissues were stained for DAPI (white), insulin (INS, red, panel a, f), ACE2-MAB933 (green, panels b, g) and ACE2-ab15348 (blue, panels c, h). Colocalization between ACE2-MAB933 and ACE2-ab15348 in cells of exocrine pancreatic tissue, showing a vasculature like-morphology (panel d, e, i, j). Zoom-in inset (panels e, j) shows details of ACE2 expression in microvasculature like cells in ND (panel e) and in T2D (panel j). Scale bars in panels d and i are 50  $\mu\text{m}$ .

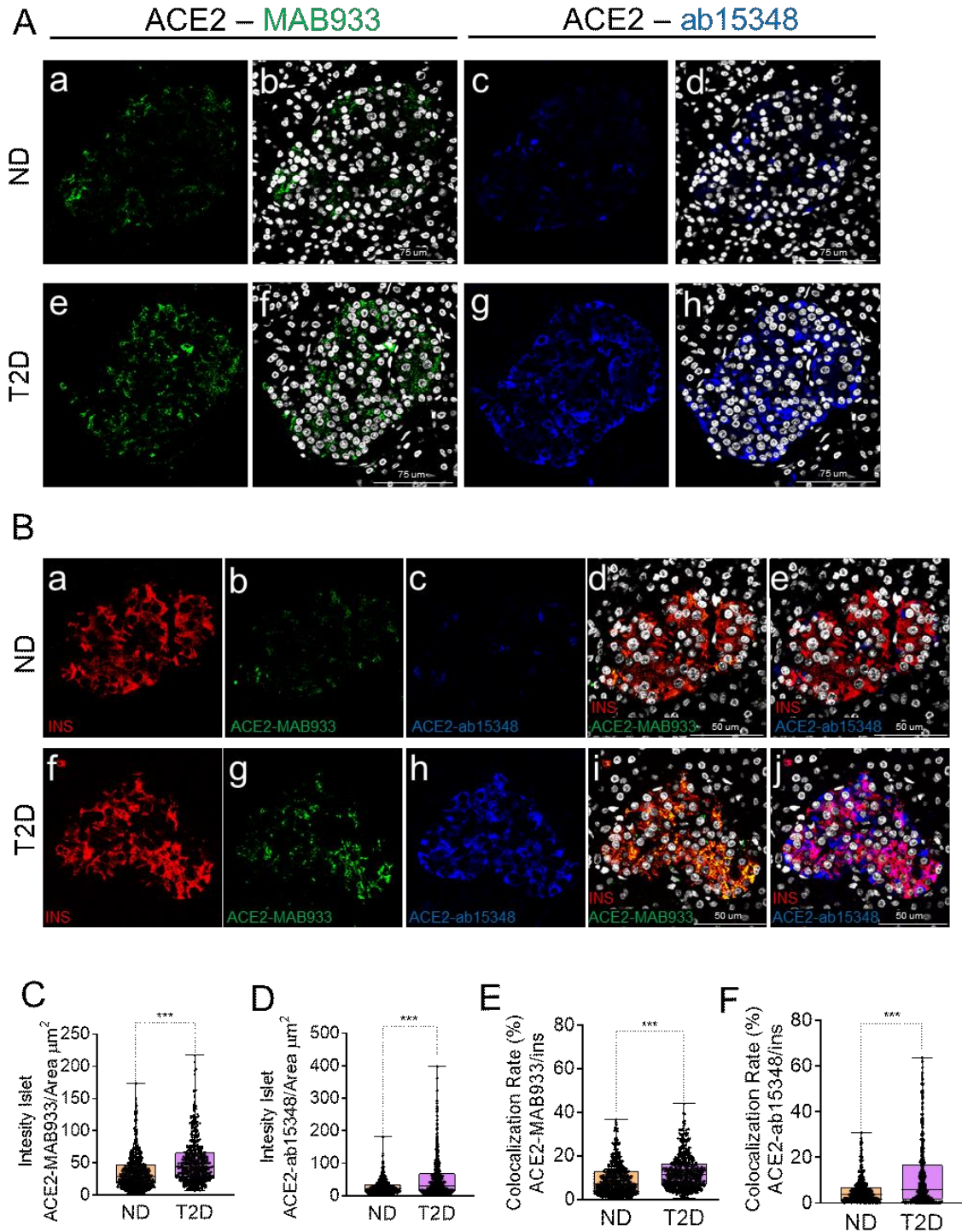


**Figure 42. Upregulation of ACE2 in pancreatic islets of T2D donors.** (A) Representative confocal images of FFPE pancreatic section from nondiabetic (ND) (case #13) and T2D donor (case #38). Pancreatic sections were stained with anti-ACE2 Ab MAB933 (green, panels a and e) and the merge with DAPI (white, nuclei) (panels b and f) showing the expression of ACE2-MAB933 in a pancreatic islet; pancreatic sections were stained with anti-ACE2 Ab ab15348 (blue, panels c and g) and the merge with DAPI (white, nuclei) (panel d and h) showed the expression of ACE2-

ab15348 in a pancreatic islet. (B) Representative confocal images of FFPE pancreatic section derived from a nondiabetic (ND) (case #2) and a T2D donor (case #32). Pancreatic sections were stained for insulin (INS, red, panels a and f), ACE2-MAB933 (green, panels b and g) and ACE2-ab15348 (blue, panels c and h). Colocalization between ACE2-MAB933 and insulin is showed in yellow (panels d and f), while colocalization between ACE2-ab15348 and insulin is reported in magenta (panels e and j). Signal intensity analysis measured with (c) anti-ACE2-MAB933 and with (d) anti-ACE2-ab15348 antibody in nondiabetic and T2D pancreatic sections; values are shown as fluorescence intensity of each islet detected (ND=556 islets; T2D=526 islets) reported as the sum of gray-scale values for each pixel normalized for the islets area (ROI, mm<sup>2</sup>). \*p < 0.05, \*\*p < 0.01, \*\*\*p < 0.001, non-parametric Mann-Whitney U test, performed after checking normality with the Kolmogorov-Smirnov normality test. Colocalization rate analysis between (e) ACE2-MAB933-Insulin and (f) ACE2-ab15348-insulin is higher. Values are shown the colocalization rate (ROI, mm<sup>2</sup>). \*p < 0.05, \*\*p < 0.01, \*\*\*p < 0.001, non-parametric Mann-Whitney U test, performed after checking normality with the Kolmogorov-Smirnov normality test.

In the multiple linear regression analysis (**Figure 43**), ACE2 expression (reported as staining intensity) was not associated with age, BMI, gender, ICU stay or duration of cold ischaemia, thus excluding the influence of these putative confounding variables on ACE2 levels. Of note, ACE2 expression was not associated with gender or blood glucose levels (**Figure 43**).

**a) Multiple least square linear regression analysis predicting dependency to pancreatic islets ACE2 expression measured using Ab MAB933 antibody**

Variable	Estimate	Standard error	95% CI (asymptotic)	P value
Age (years)	0,09676	0,6393	-1,220 to 1,414	0,8809
Gender (M/F)[M]	13,46	10,03	-7,204 to 34,12	0,1918
BMI (Kg/m <sup>2</sup> )	1,824	1,831	-1,947 to 5,596	0,3287
Abdominal circumference (cm)	-0,4605	0,405	-1,295 to 0,3736	0,2663
ICU stay (days)	0,05898	1,209	-2,432 to 2,550	0,9615
Cold Ischemia Time (hours)	-1,09	0,6228	-2,373 to 0,1922	0,0922
Mean glycemia (mg/dl)	-0,0366	0,07049	-0,1818 to 0,1086	0,6083

**b) Multiple least square linear regression predicting dependency to pancreatic islets ACE2 expression measured using Ab15348 antibody**

Variable	Estimate	Standard error	95% CI	P value
Age (years)	1,112	1,184	-1,326 to 3,550	0,3566
Gender (M/F)[M]	-15,02	18,58	-53,28 to 23,24	0,4265
BMI (Kg/m <sup>2</sup> )	2,871	3,391	-4,113 to 9,855	0,4052
Abdominal circumference (cm)	-0,9164	0,75	-2,461 to 0,6283	0,2332
ICU stay (days)	1,441	2,239	-3,172 to 6,053	0,5259
Cold Ischemia Time (hours)	-1,067	1,153	-3,443 to 1,308	0,3636
Mean glycemia (mg/dl)	0,09076	0,1305	-0,1781 to 0,3596	0,4933

**Figure 43.** Multiple least square regression analysis to identify putative correlations between ACE2 expression in pancreatic islets and clinical characteristics available in ND and T2D donors. "Age (years)", "BMI (Kg/m<sup>2</sup>)", "Abdominal circumference (cm)", "ICU stay (days)", "Cold Ischemia Time (hours)", "Mean glycemia (mg/dl)" and "Gender (M/F)[M]" were included as independent variable while ACE2 expression measured using MAB933 (a) and Ab15348 (b) as independent variables in two separate models. *Estimate* values reports the increase (positive values) or decrease (negative values) of ACE2 expression for each unit of the dependent variables.

We next sought to determine a possible link between ACE2 expression and innate immune inflammation in the pancreas of T2D donors. Islet inflammation has long been proposed to contribute to  $\beta$  cell impairment in T2D. To investigate a possible link between ACE2 expression and inflammation triggered by innate immune cells, we analysed CD68+ macrophages in pancreatic tissue. In the whole pancreatic section, CD68+ macrophages showed an abundance of about 6.2 cells per mm<sup>2</sup> in T2D and 5.1 cells per mm<sup>2</sup> in ND. Interestingly, CD68+ macrophages in the peri-islets showed increased abundance in T2D compared to ND donors (0.22 vs. 0.15 CD68+ cells/islet), which is consistent with the increased ACE2 expression observed in the pancreatic islets of previous serial sections.

Overall, these data show an increased expression of ACE2 in pancreatic beta cells in T2D compared to ND donors. Although such increase is independent of available clinical variables related to glycometabolic outcomes, we observed an increase in peri-islets CD68+-macrophages thus putatively associating ACE2 expression increase to inflammatory insults.



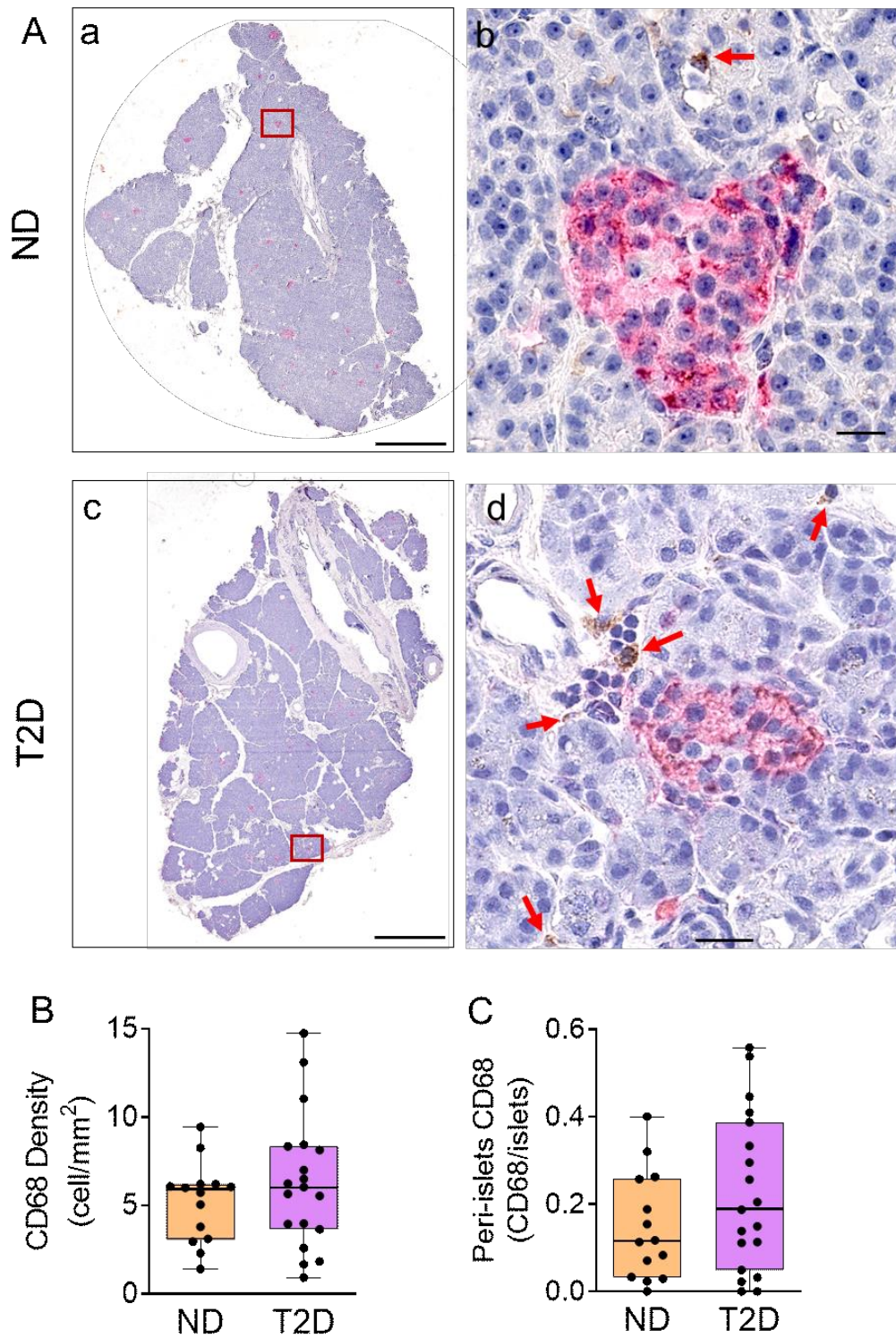


**Figure 44. Immunohistochemical staining of CD68+ macrophages.** a) Representative whole-slide images of FFPE pancreatic section from ND (case #7) (panels a) and T2D donor (case #39) (panels c). Tissues were stained for insulin (red) and CD68 (brown). Zoom-in inset reported peri-islets CD68 in ND case (panel b) and T2D case (panel d). CD68 density (b) is reported as cell/mm<sup>2</sup>. Peri-islets CD68 (d) is considered <250  $\mu$ m from islets.

## **5.7 Presence of SARS-CoV-2 nucleocapsid in pancreatic $\beta$ -cells of COVID-19 donors**

SARS-CoV-2 has been previously shown to infect in-vitro human pancreatic islets and human pancreatic  $\beta$ -cell lines which expressed ACE2 receptor (124,125). To determine whether SARS-CoV-2 infection naturally occurs in pancreatic tissues, we analysed SARS-CoV-2 nucleocapsid (NP) protein expression pattern in autaptic human pancreatic tissue sections obtained from n=13 donors without COVID-19 and n=16 with reported COVID-19 medical history, collected at Université Libre de Bruxelles (ULB) (**Table 3**).

First, we performed a haematoxylin/eosin staining to check the morphological quality of the autaptic tissues and then proceeded with a triple immunofluorescence analysis to detect NP protein and insulin on good quality FFPE pancreatic sections.

Among these FFPE pancreatic sections only n=3 control subjects (case #1, case #2 and case #11) and n=3 COVID-19+ patients (case #15, case #21 and case #29) were analyzed due to the morphological conditions of the sections. Indeed, some pancreatic tissue sections showed massive pancreatic autolysis probably caused by the late autopsy which was necessarily performed 72 hours after the death of the patients.

In control patients no signal for SARS-CoV-2 NP was found in exocrine or endocrine pancreas of the analyzed cases (**Figure 45**). Notably, in COVID-19+ donors, SARS-CoV-2 NP was found in  $\beta$ -cells (**Figure 46, panels d, m and zoom in inset in panels h, n**), in some insulin- and glucagon-negative cells within pancreatic islets (**Figure 46A, panels d and zoom in inset in panel l**) and in exocrine cells (**Figure 46B, C**).

Collectively, these results indicate the ability of SARS-CoV-2 to infect exocrine cells and endocrine pancreatic islets.

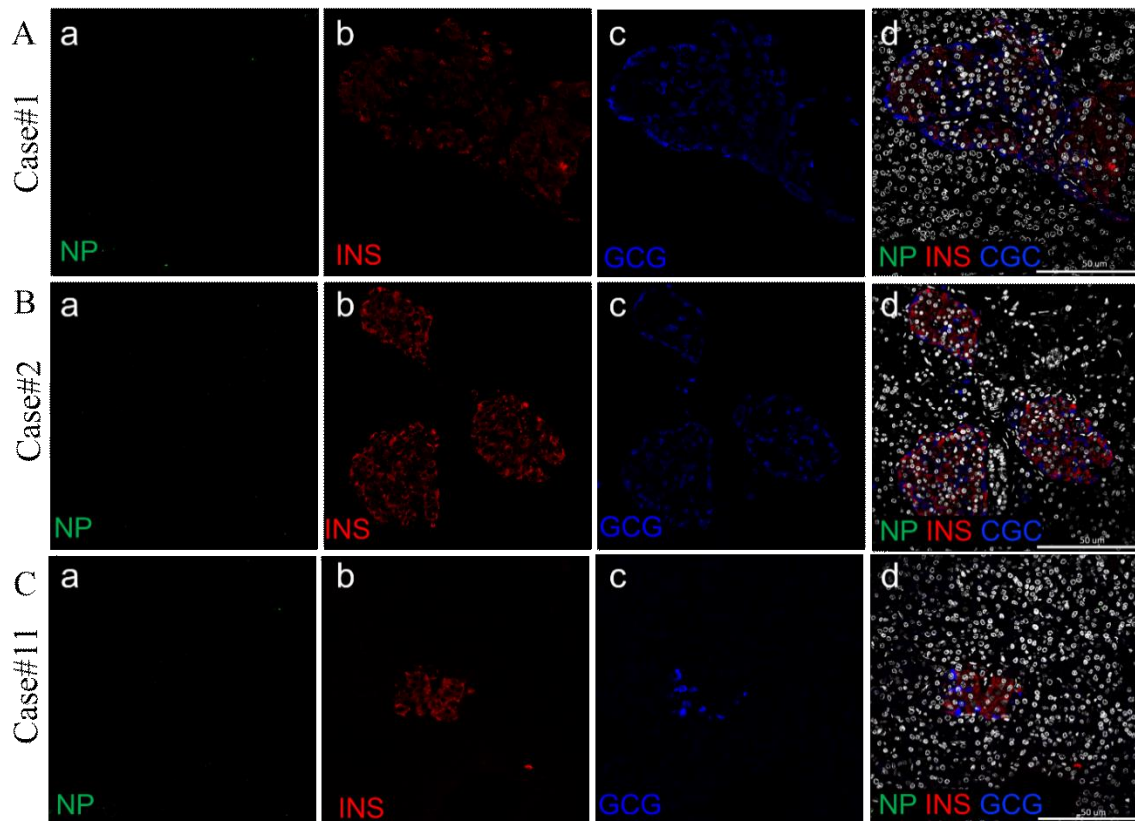


**Figure 45. Immunofluorescence detection of nucleocapsid in pancreatic tissues of control cases.** A) Representative confocal images of FFPE pancreatic section derived from case #1. Tissue was stained for nucleocapsid (NP, green, panel a), insulin (INS, red, panel b) and glucagon (GCG, blue, panel c). Channels merge evidence no NP signal in a huge pancreatic islet (panel d). B) Representative confocal images of FFPE pancreatic section derived from case #2. Tissue was stained for nucleocapsid (NP, green, panel a), insulin (INS, red, panel b) and glucagon (GCG, blue, panel c). Channels merge evidence no NP signal in a multiple pancreatic islets (panel d). C) Representative confocal images of FFPE pancreatic section derived from case #11. Tissue was stained for nucleocapsid (NP, green, panel a), insulin (INS, red, panel b) and glucagon (GCG, blue, panel c). Channels merge evidence no NP signal in exocrine and endocrine pancreas (panel d). Scale bars in panel d is 50  $\mu\text{m}$ .





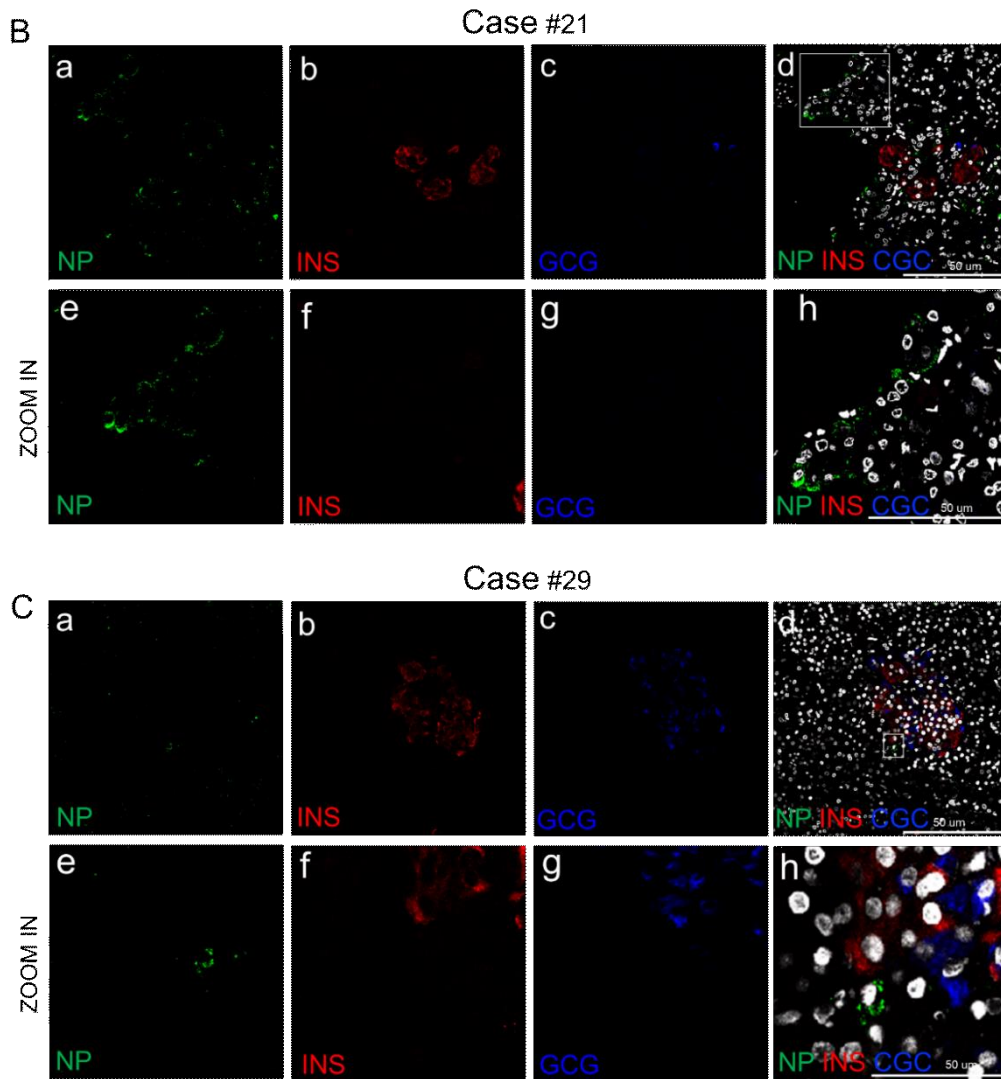


**Figure 46: immunofluorescence detection of nucleocapsid in pancreatic tissues of COVID-19+ patients.** A) Representative confocal and NanoZoomer images of FFPE pancreatic section derived from case #15. Tissue was stained for NP (green, panels a, e, i), INS (red, panels b, f, j) and GCG (blue, panels c, g, k). Channels merge evidence NP signal in pancreatic islet (panels d, m), in some INS- and GCG-negative cells within pancreatic islet (panel d) and in exocrine pancreas (panel o). Zoom-in inset report details of NP in pancreatic islets (panels from e to h and panels m, n), in INS- and GCG-negative cells within pancreatic islet (panels from i to l) and in exocrine pancreas (panels o, p). B) Representative confocal images of FFPE pancreatic section derived from case #21. Tissue was stained for NP (green, panel a, e), INS (red, panel b, f) and GCG (blue, panel c, g). Channels merge evidence NP signal in exocrine pancreas (panel d). Zoom in inset report details of NP detection in exocrine pancreas (panels from e to h). C) Representative confocal images of FFPE pancreatic section derived from case #29. Tissue was stained for NP (green, panel a, e), INS (red, panel b, f) and GCG (blue, panel c, g). Channels merge evidence peri islet localization of NP (panel d). Zoom in inset report details of NP detection cell with peri islet localization (panels from e to h). Scale bars are 50  $\mu\text{m}$ .

## 6. Discussion and conclusions

Since the beginning of the pandemic caused by SARS-CoV-2 the relationship between the virus and diabetes mellitus has been studied due to several data that showed a more severe outcome in patients with diabetes (128) and new onset diabetes in patients that are infected by SARS-CoV-2 (149).

Diabetic patients showed a poor prognosis for SARS-CoV-2 infection due to different factors such as age, sex, comorbidities, obesity and pro-inflammatory state (131). Indeed, several studies demonstrated a more severe outcome in diabetic patients, including a higher probability of ICU admission (135) and an higher mortality rate in people with T2D (137,150,151).

Furthermore, several studies have demonstrated that SARS-CoV-2 infection may be related with new onset T1D and T2D cases. Regarding T1D, several studies investigated the relationship between pandemic and new onset T1D and diabetic ketoacidosis (DKA) with controversial results. Denina and colleagues showed that the incidence of new onset T1D and DKA was increased compared to the incidence of T1D and DKA before pandemic; in addition, they showed an higher rate of new onset T1D children which were positive for SARS-CoV-2 (23%) respect to the rate of positivity in a reference age-matched general population (4.1%) (152); moreover, a Czech study showed an increased incidence of T1D in pediatric patients (0-15 years) during the COVID-19 pandemic years 2020 (incidence of 27.2/100.000/year) and 2021 (incidence of 28.4/100.000/year) compared to the trends over 2010-2019 (incidence rate ratio, IRR=1.16, 95%CI 1.06-1.28, p= 0.0022) (35982508) and a systemic review and meta-analysis performed on 24 studies with more than 120.000 children showed that the risk of DKA was significantly increased during the pandemic in new onset T1D subjects population with a statistically significant increased risk of a severe form of DKA (153). A pre-printed manuscript published in 2022 confirms these data comparing the characteristics of children between 6 months and 16 years with new onset T1D or pre-existing diabetes with DKA during COVID-19 pandemic (2020-2021) and the preceding years (2019-2020); there was a 17% increase in new onset diabetes, a 43% increase in children presenting DKA, a 79% increase in severe DKA and an 89% increase in admissions to intensive care unit (154,155). In contrast, other studies highlighted no correlation between COVID-19 infection and new onset T1D. Particularly, Rewers and colleagues considered more than 50.000 children and adolescents from Colorado, USA and

Bavaria-Germany, that were screened for islet autoantibodies and SARS-CoV-2 antibodies and no association was found between SARS-CoV-2 infection and autoimmunity related to the development of T1D (156).

Evidence of hyperglycaemia after SARS-CoV-2 infection were demonstrated in different studies, such as a retrospective cohort study conducted on more than 2 million of veterans that showed how, following the SARS-CoV-2 infection, 0.5 % of veterans developed diabetes in the following 120 days and 0,6% of them in 193 days from the infection. Moreover, among hospitalized individuals, the rate of diabetes development were 2,8% and 3,2% in 120 days and 193 days post-infections, respectively (142).

Even if the role of diabetes mellitus in SARS-CoV-2 infection is not clear, diabetes molecular mechanisms, complications and comorbidities seem to play an important role in SARS-CoV-2 infection; these also include the typical alterations of the immune system response. Of note, it has been observed that in COVID-19 the innate and adaptive immunity cooperate to contrast viral replication and facilitate viral clearance. In people with diabetes some immune cells are affected by hyperglycaemia and their level decrease or become dysfunctional. For example, natural killer (NK) cells showed reduced functionality in case of hyperglycaemia (157), while macrophages and neutrophils activation and phagocytosis are decreased in patient with poor glycaemic control (158). As a consequence, patients with chronic hyperglycaemia have an impaired innate immune response. Regarding the adaptive immune response, hyperglycaemia affects the T-cells function, particularly impairing CD4 lymphocytes differentiation towards T helper 2 (Th2) phenotype, thus inducing an imbalance between pro-inflammatory and anti-inflammatory activity (159). Collectively, diabetic subjects are more prone to the alterations of the immune system during SARS-CoV-2 infection, thus exacerbating COVID-19 related symptoms and disease severity.

It has been demonstrated that SARS-CoV-2 can infect human host cells through the binding to the N-terminal domain of the ACE2 receptor, which is expressed in different tissues and organs such as ileum, colon, kidney, lung and pancreas. Different studies demonstrated the expression of ACE2 in multiple cell lines, primary cells and tissues (101,124), thus defining them as potentially susceptible to the infection by SARS-CoV-2.

Therefore, we adopted multiple technologies and reagents to thoroughly analyze the presence of ACE2, both at mRNA and protein level, in order to evaluate its expression and localization in pancreatic tissue samples obtained from adult non-diabetic multiorgan

donors from the INNODIA EUnPOD biobank collection, in enzymatic- and LCM-isolated primary adult human pancreatic islets and in human  $\beta$ -cell line EndoC- $\beta$ H1. Then, we evaluated potential differential expression of ACE2 in type 2 diabetic donors respect to non-diabetic donors.

In human adult pancreas, we primarily observed ACE2 expression in microvasculature component (endothelial cell associated pericytes, both in endocrine and exocrine compartments). The expression of ACE2 in the pancreatic microvasculature compartment was associated, but not superimposed, with the endothelial cells specific marker CD31 (or PECAM-1). Such staining pattern strongly suggests the presence of ACE2 in pancreatic vascular pericytes which are tightly associated with endothelial cells. Of interest, although the exocrine pancreas and the pancreatic islets are highly vascularized (160), only a subset of pancreatic pericyte cells markedly express ACE2. Additionally, ACE2 expression in microvascular compartment is surprisingly lobular, resembling the heterogeneous staining pattern of several inflammatory markers. Additional observations on multiple pancreatic lobules are required to confirm such heterogeneous lobular patterning observed. The presence of ACE2 in pancreatic pericytes is of sure interest. As a matter of fact, the vascular leakage and endothelial it was reported as a typical sign of SARS-CoV-2 infection in various organs, driving early local inflammation and the subsequent exacerbation of immune responses (161,162). Of note, multiple studies addressed the importance of an intact islet microvasculature in order to render pancreatic islets fully functional (30,163). Therefore, a pancreatic islet local vascular damage and inflammation due to SARS-CoV-2 direct infection of ACE2<sup>+</sup> pancreatic pericyte cells is a potential contributory factor for islet dysfunction.

Moreover, our results indicate that ACE2 is expressed also in the pancreatic islets, and this expression is mostly located in  $\beta$ -cells as compared to  $\alpha$ -cells. Initially, these results were in contrast with other manuscripts (111,123) which failed to observe ACE2 expression in pancreatic islet endocrine cells. Such discrepancies may be explained by a resulting sum of differences in primary antibodies sensitivity, different epitopes targeted, tissue sections preparation and pre-treatment, as well as immunodetection methodology sensitivity (immunohistochemistry vs. immunofluorescence). Such variables may be of critical importance when detecting a low-expressed protein and may generate different results. Furthermore, it should be taken into consideration that ACE2 expression may vary greatly among individuals due to genetic or environmental factors (107). Such intrinsic ACE2

variability has been previously observed also in other cellular contexts, with some authors reporting high ACE2 levels and others low or absent (164).

Subsequent studies further confirmed the presence of ACE2 in pancreatic islets and in  $\beta$ -cells, even though it was low expressed but necessary for the productive infection of SARS-CoV-2. In fact, ACE2 has been demonstrated to be primarily used by the SARS-CoV-2 to directly infect pancreatic cells (125–127), inducing a direct damage to  $\beta$ -cells, thus suggesting a mechanism to explain the hyperglycaemia and new onset diabetes cases related to COVID-19 infection (142,143,149). It has been observed that human pancreatic islets isolated from four human donors and exposed to SARS-CoV-2 can be infected by the virus which induces, in endocrine pancreatic cells, a dilatation and a vacuolization of the endoplasmic reticulum (ER)-Golgi apparatus complex and also critical transcriptional changes (127). As a matter of fact, human coronavirus infection has been suggested to trigger necroptosis, that explain the necrosis aspect of pancreatic islet exposed to SARS-CoV-2. To confirm the presence of necroptosis, a staining for the detection of phosphorylation-site in the pseudokinase mixed lineage kinase domain like (pMLKL) protein was performed and all COVID-19 patient samples presented positivity for the pMLKL protein. The death of SARS-CoV-2 infected  $\beta$ -cells was also showed by other research group that quantified the insulin content and glucose stimulated insulin secretion (GSIS) in SARS-CoV-2 infected human islets, showing a decrease in insulin content and GSIS, that might be caused by  $\beta$ -cells apoptosis (124). An additional mechanism that might explain the hyperglycaemia and new onset diabetes cases after SARS-CoV-2 infection could be the  $\beta$ -cell transdifferentiation that was examined by using single cell RNA-seq data analysis of the expression level of INS in  $\beta$ -cells mock versus SARS-CoV-2 infected human islets. The level of insulin was lower in  $\beta$ -cells infected by SARS-CoV-2 than in mock islets (125).

In our study, localization of ACE2 in pancreatic islet endocrine cells was observed using two out of three different antibodies tested. Surprisingly, we were not able to observe ACE2 pancreatic islets positive signal using Abcam monoclonal antibody Ab108252, while signal was clearly evident in microvasculature and scattered ductal cells. On the contrary, by using two different antibodies (MAB933 and Ab15348)—which can recognize the C-terminal domain portion of ACE2, we obtained clear and concordant results, with identification of ACE2 in pancreatic islet endocrine cells in addition to the microvasculature. As a negative positive controls for the antibodies quality and our IHC procedure, MAB933 and Ab15348

were subjected to antibodies specificity immunofluorescence test (AbII-only, peptide competition assay and orthogonal validation in negative/positive cell lines), and tested in FFPE lung tissue sections, showing positive staining in AT2 pneumocytes, overlapping with results obtained in other published studies (165,166).

Considering the importance of the ACE2 receptor in SARS-CoV-2 infection, several studies have focused on the evaluation of its structure and function. Two studies, identified a novel ACE2 isoform, called short ACE2 (s-ACE2), composed by 11 exons, starting with a new unannotated first exon, called exon 9a and exons 10-19 of the long ACE2 transcript (112,113). The short transcript of ACE2 is an IFN-regulated gene; indeed, the expression of the short ACE2 isoform is under the control of its own promoter elements that are activated in the presence of IFN and/or viral infections, known to be potent inducer of the IFN response. Therefore, this short ACE2 isoform lacks of the N-terminal domain which is used by the SARS-CoV-2 to bind and enter host cells. However, the role of this newly identified isoform in the pathogenesis of the COVID-19 needs further investigations, even though several hypotheses have been formulated especially regarding its structural supportive role to the ACE2 complex (167). Overall, these results suggest that the short-ACE2 isoform may be the prevalent one expressed in  $\beta$ -cells. Indeed, ACE2 western blot analyses of the human  $\beta$ -cell line EndoC- $\beta$ H1 support this hypothesis by confirming that short-ACE2 is prevalent over long-ACE2, the latter being present but low expressed in  $\beta$ -cells. Based on these results we suggest that in human  $\beta$ -cells both ACE2 isoforms are present, with a predominance of the short-ACE2. Although the presence of the short-ACE2 isoform, alongside with long-ACE2, is clearly evident in human  $\beta$ -cells, its functional role remains to be established. A previous study suggested the ability of the short-ACE2 isoform to form homodimers or heterodimers with the long-ACE2 isoform, thus potentially being able to modulate both the activity and structural protein domain conformation of the long-ACE2 (167). Significantly, short-ACE2 is missing the aminoacidic residues reported as fundamental for virus binding; however, due to the lack of detailed data regarding its function we cannot exclude that the short-ACE2 may modulate SARS-CoV-2 susceptibility by interacting with long-ACE2 or additional membrane proteins which may mediate the binding to SARS-CoV-2 spike protein [e.g. ITGA5, as previously observed (168)].

As described above, we report that in human pancreatic islets, ACE2 is enriched in insulin-producing  $\beta$ -cells. This in-situ ACE2 expression pattern data are in line with three different bulk RNAseq datasets analysing human  $\beta$ - and  $\alpha$ -cells' transcriptome, reporting higher

expression of ACE2 mRNA in  $\beta$ -cells as compared to  $\alpha$ -cells (169–171). Of note, such datasets rely on b- or a-cells bulk RNA-seq and do not suffer from common limitations present in single-cell RNA-seq (172), which usually detects only 1,000–3,000 genes/cell, thus representing a minor fraction (25–30%) of the total number of genes identified by bulk cells RNA sequencing (>20,000 genes).

Another recent study analyzed SARS-CoV-2 host receptors expression using two different methods (microarray and bulk RNA-seq) and further confirmed that ACE2 is indeed expressed in human pancreatic islets and also demonstrated that ACE2 expression was higher in sorted pancreatic  $\beta$ -cells relative to other endocrine cells (173). Additional evidence of ACE2 expression in endocrine pancreas and in  $\beta$ -cells derive also from mouse studies, which demonstrated ACE2 expression in insulin-producing cells as well as its critical role in the regulation of  $\beta$ -cell phenotype and function (119,174,175).

Collectively, our in-situ expression data alongside with multiple published datasets and reports both in human and mouse show that ACE2 is expressed in pancreatic islets, albeit at relatively low levels. ACE2 expression in human  $\beta$ -cells render these cells sensitive to SARS-CoV-2 entry. Indeed, multiple evidence (62,176,177) showed that enteroviruses are capable to competently infect  $\beta$ -cells but less so  $\alpha$ -cells (178,179); these viruses are thus being considered as one of the potential triggering causes of type 1 diabetes (T1D) (180). Of note, it has been previously demonstrated that human b-cells exclusively express virus receptor isoform Coxsackie and adenovirus receptor-SIV (CAR-SIV), making them prone to infection by certain viruses (181). Therefore, it would not be surprising that, under particular conditions, human  $\beta$ -cells could be directly infected by SARS-CoV-2.

Our data also indicate that in  $\beta$ -cells, total ACE2 mRNA expression is upregulated upon different pro-inflammatory conditions. Importantly, these observations were obtained both in the human  $\beta$ -cell line EndoC- $\beta$ H1 and in human primary pancreatic islet cells, as shown by qRT-PCR, RNA-seq datasets and immunofluorescence. As a matter of fact, ACE2 has been previously indicated as an interferon-stimulated gene (ISG) in a variety of cells (107). Of interest, a previous report suggested that the short-ACE2 may represent the prevalent ACE2 isoform upregulated upon inflammatory stress (113). Our analysis of JAK1/2 and TYK2 inhibition prevent cytokines-induced ACE2 mRNA expression in human islets, demonstrating that ACE2 is regulated through the JAK-STAT pathway.



Despite the bidirectional relationship between SARS-CoV-2 infection and diabetes mellitus has been hypothesised since the beginning of the pandemic, an accurate evaluation of ACE2 expression in the pancreas of ND and T2D donors is still lacking.

Therefore, we analysed an extended cohort of T2D multiorgan donors (n=20 donors) in comparison to age- and sex-matched nondiabetic cohort (n=20 donors) to evaluate ACE2 expression and distribution using two different antibodies (MAB933 and Ab15348), with which we have previously obtained clear and concordant results. ACE2 has been detected in pancreatic islets and in particular in insulin-secreting cells, in exocrine pancreas and in particular within acini, but also in cells with a vasculature like-morphology, confirming previous results that showed ACE2 in vascular pancreatic cells.

We demonstrated that ACE2 is increased in pancreatic islets of T2D donors and showed a higher colocalization rate in beta cells. Notably, we considered a total of n=1082 pancreatic islets across all ND and T2D donors; these analyses confirmed the increased expression of ACE2 in pancreatic islets of T2D in comparison with ND donors.

Overall, our data support an increased expression of the SARS-CoV2 receptor in  $\beta$ -cells of T2D donors and are in-line with other reports demonstrating the upregulation of ACE2 in other organs exposed to a diabetic milieu such as lung, kidney and heart (165,182,183). Indeed, ACE2 expression was found increased in bronchial epithelium and alveolar tissue of T2D donors and a linear relationship was detected between blood glucose levels and ACE2 expression in alveolar tissue 33024003. In the heart tissue, ACE2 expression was significantly increased in cardiomyocytes of T2D patients with poor glycaemic control respect to ND patients and T2D patients with good glycaemic control (182). In kidney organoids ACE2 was expressed in tubular-like cells and an oscillatory glucose regimen induced the expression of ACE2 (183). Collectively, we can hypothesise that ACE2 expression is increased upon exposure to inflammation and/or high glucose or other stressors and that such chronic stress stimuli also exert their deleterious effect on beta cells favouring the upregulation of ACE2. Unlike other reports, we cannot find a significant correlation between ACE2 expression and blood glucose levels. Therefore, we investigated the potential contribution of inflammation by analysing pancreatic tissue resident CD68+ macrophages. We observed an increase in CD68+ macrophages in the peri-islets, although not significant. However, this increase is also supported by other observations that showed an increase in CD68+ macrophages in the peri-islets of T2D pancreata compared to ND

donors (184). Thus, additional analyses should be considered to further explore the inflammatory mechanisms leading to ACE2 upregulation in  $\beta$ -cells, such as the infiltration of other innate immune cells (i.e. neutrophils, dendritic cells) or the contribution of adaptive immune cells (i.e. CD8 T cells) recently suggested to be particularly enriched in peri-islet area in T2D pancreata.

It has been suggested that the increased expression of ACE2 may explain the increased infectivity or severity of COVID-19 in patients with diabetes. In this context, we can argue that increased expression of ACE2 in  $\beta$ -cells may lead to increased susceptibility of beta cells to SARS-CoV-2 infection, making beta cells more prone to virus tropism in patients already infected with SARS-CoV-2.

In addition in our study we also have detected SARS-CoV-2 NP in exocrine and endocrine pancreas, in details we detect NP in  $\beta$ -cells, in some insulin- and glucagon-negative cells within the pancreatic islets, demonstrating that SARS-CoV-2 can infect pancreas and in particular  $\beta$ -cells probably, using the ACE2 receptor. Our findings are in accordance with Wu and colleagues who demonstrated that SARS-CoV-2 can infect isolated human islets and that SARS-CoV-2 NP was in pancreatic autoptic samples from 9 donors who had COVID-19 infection; moreover, they demonstrated that infected human islets decreased insulin content and glucose-stimulated insulin secretion (GSIS), while increased  $\beta$ -cell death (124). Another study showed that SARS-CoV-2 NP is present in pancreatic endocrine and non-endocrine cells derived from autoptic sample of COVID-19 donors, suggesting that the infection can cause an higher chemokine and cytokine expression, cell stress signal and  $\beta$ -cells transdifferentiation (125). Finally, in a pre-print manuscript published in 2021, the authors demonstrated that rhesus macaques inoculated with the virus showed the presence of SARS-CoV-2 NP in pancreatic islets, in particular in  $\beta$ -cells. Of note, SARS-CoV-2 infection drove a massive decrease of  $\beta$ -cells area caused by  $\beta$ -cell stress and atrophy (185).

Overall, our and other authors' data confirmed the SARS-CoV-2 ability to infect pancreatic  $\beta$ -cells using ACE2 receptor which is specifically expressed in pancreatic islets.

In conclusion our data demonstrated the expression of ACE2 in pancreatic  $\beta$ -cells. Moreover, we observed the upregulation of ACE2 in pancreatic islet  $\beta$ -cells of T2D donors, and putatively driven by inflammatory-mediated mechanisms. Higher ACE2 expression in T2D islets might increase their susceptibility to SARS-CoV-2 infection during COVID-19

disease in T2D patients, thus exacerbating glycometabolic outcomes and worsening the severity of the disease. Indeed, we have confirmed the ability of the virus to infect the exocrine and endocrine human pancreas. This mechanism could occur together with other peripheral inflammatory changes that increase insulin resistance and thus exacerbate pancreatic  $\beta$ -cell dysfunction

In conclusion, these data might help to explain the severe outcome of T2D patients and the hyperglycaemic cases and/or new onset diabetes cases following SARS-CoV-2 infection.

## 7. Bibliography

1. Aamodt KI, Powers AC. Signals in the pancreatic islet microenvironment influence  $\beta$ -cell proliferation. *Diabetes Obes Metab.* 2017;19 Suppl 1:124–136.
2. Dolenšek J, Rupnik MS, Stožer A. Structural similarities and differences between the human and the mouse pancreas. *Islets.* 2015;7(1):e1024405.
3. Brissova M, Fowler MJ, Nicholson WE, Chu A, Hirshberg B, Harlan DM, et al. Assessment of human pancreatic islet architecture and composition by laser scanning confocal microscopy. *J Histochem Cytochem.* 2005 Sep;53(9):1087–1097.
4. Kim A, Miller K, Jo J, Kilimnik G, Wojcik P, Hara M. Islet architecture: A comparative study. *Islets.* 2009 Oct;1(2):129–136.
5. Ionescu-Tirgoviste C, Gagniuic PA, Gubceac E, Mardare L, Popescu I, Dima S, et al. A 3D map of the islet routes throughout the healthy human pancreas. *Sci Rep.* 2015 Sep 29;5:14634.
6. Cabrera O, Berman DM, Kenyon NS, Ricordi C, Berggren P-O, Caicedo A. The unique cytoarchitecture of human pancreatic islets has implications for islet cell function. *Proc Natl Acad Sci USA.* 2006 Feb 14;103(7):2334–2339.
7. Brereton MF, Iberl M, Shimomura K, Zhang Q, Adriaenssens AE, Proks P, et al. Reversible changes in pancreatic islet structure and function produced by elevated blood glucose. *Nat Commun.* 2014 Aug 22;5:4639.
8. Noguchi GM, Huising MO. Integrating the inputs that shape pancreatic islet hormone release. *Nat Metab.* 2019 Dec 13;1(12):1189–1201.
9. Unger RH, Orci L. The essential role of glucagon in the pathogenesis of diabetes mellitus. *Lancet.* 1975 Jan 4;1(7897):14–16.
10. Cryer PE. Minireview: Glucagon in the pathogenesis of hypoglycemia and hyperglycemia in diabetes. *Endocrinology.* 2012 Mar;153(3):1039–1048.
11. de Heer J, Rasmussen C, Coy DH, Holst JJ. Glucagon-like peptide-1, but not glucose-dependent insulintropic peptide, inhibits glucagon secretion via

- somatostatin (receptor subtype 2) in the perfused rat pancreas. *Diabetologia*. 2008 Dec;51(12):2263–2270.
12. Ben-Othman N, Vieira A, Courtney M, Record F, Gjernes E, Avolio F, et al. Long-Term GABA Administration Induces Alpha Cell-Mediated Beta-like Cell Neogenesis. *Cell*. 2017 Jan 12;168(1-2):73–85.e11.
  13. Egea PF, Stroud RM, Walter P. Targeting proteins to membranes: structure of the signal recognition particle. *Curr Opin Struct Biol*. 2005 Apr;15(2):213–220.
  14. Patzelt C, Labrecque AD, Duguid JR, Carroll RJ, Keim PS, Henrikson RL, et al. Detection and kinetic behavior of proinsulin in pancreatic islets. *Proc Natl Acad Sci USA*. 1978 Mar;75(3):1260–1264.
  15. Huang XF, Arvan P. Intracellular transport of proinsulin in pancreatic  $\beta$ -cells: structural maturation probed by disulfide accessibility. *J Bio Chem*. 1995;
  16. Ramzy A, Asadi A, Kieffer TJ. Revisiting Proinsulin Processing: Evidence That Human  $\beta$ -Cells Process Proinsulin With Prohormone Convertase (PC) 1/3 but Not PC2. *Diabetes*. 2020 Apr 14;69(7):1451–1462.
  17. Marchetti P, Lupi R, Bugliani M, Kirkpatrick CL, Sebastiani G, Grieco FA, et al. A local glucagon-like peptide 1 (GLP-1) system in human pancreatic islets. *Diabetologia*. 2012 Dec;55(12):3262–3272.
  18. Fu Z, Gilbert ER, Liu D. Regulation of insulin synthesis and secretion and pancreatic Beta-cell dysfunction in diabetes. *Curr Diabetes Rev*. 2013;
  19. Vasiljević J, Torkko JM, Knoch K-P, Solimena M. The making of insulin in health and disease. *Diabetologia*. 2020 Oct;63(10):1981–1989.
  20. Dorrell C, Schug J, Canaday PS, Russ HA, Tarlow BD, Grompe MT, et al. Human islets contain four distinct subtypes of  $\beta$  cells. *Nat Commun*. 2016 Jul 11;7:11756.
  21. Kailey B, van de Bunt M, Cheley S, Johnson PR, MacDonald PE, Gloyn AL, et al. SSTR2 is the functionally dominant somatostatin receptor in human pancreatic  $\beta$ - and  $\alpha$ -cells. *Am J Physiol Endocrinol Metab*. 2012 Nov 1;303(9):E1107–16.

22. Chera S, Baronnier D, Ghila L, Cigliola V, Jensen JN, Gu G, et al. Diabetes recovery by age-dependent conversion of pancreatic  $\delta$ -cells into insulin producers. *Nature*. 2014 Oct 23;514(7523):503–507.
23. Zhang J, McKenna LB, Bogue CW, Kaestner KH. The diabetes gene Hhex maintains  $\delta$ -cell differentiation and islet function. *Genes Dev*. 2014 Apr 15;28(8):829–834.
24. Rahier J, Wallon J, Loozen S, Lefevre A, Gepts W, Haot J. The pancreatic polypeptide cells in the human pancreas: the effects of age and diabetes. *J Clin Endocrinol Metab*. 1983 Mar;56(3):441–444.
25. Aragón F, Karaca M, Novials A, Maldonado R. Pancreatic polypeptide regulates glucagon release through PPYR1 receptors expressed in mouse and human alpha-cells. ... *et Biophysica Acta (BBA)* .... 2015;
26. Mattsson G. The endothelial cells in islets of langerhans. *Ups J Med Sci*. 2005;
27. Muratore M, Santos C, Rorsman P. The vascular architecture of the pancreatic islets: A homage to August Krogh. *Comp Biochem Physiol Part A, Mol Integr Physiol*. 2021 Feb;252:110846.
28. Sordi V, Piemonti L. Mesenchymal stem cells as feeder cells for pancreatic islet transplants. *Rev Diabet Stud*. 2010 Aug 10;7(2):132–143.
29. Garcia PE, Scales MK, Allen BL, Pasca di Magliano M. Pancreatic fibroblast heterogeneity: from development to cancer. *Cells*. 2020 Nov 12;9(11).
30. Almaça J, Weitz J, Rodriguez-Diaz R, Pereira E, Caicedo A. The pericyte of the pancreatic islet regulates capillary diameter and local blood flow. *Cell Metab*. 2018 Mar 6;27(3):630–644.e4.
31. Veld PI, Marichal M. Microscopic anatomy of the human islet of Langerhans. *The islets of Langerhans*. 2010;
32. Faber CL, Deem JD, Campos CA, Taborsky GJ, Morton GJ. CNS control of the endocrine pancreas. *Diabetologia*. 2020 Oct;63(10):2086–2094.
33. American Diabetes Association. Diagnosis and classification of diabetes mellitus. *Diabetes Care*. 2004 Jan;27 Suppl 1:S5–S10.

34. American Diabetes Association. 2. Classification and Diagnosis of Diabetes: Standards of Medical Care in Diabetes-2019. *Diabetes Care*. 2019 Jan;42(Suppl 1):S13–S28.
35. Shaw JE, Sicree RA, Zimmet PZ. Global estimates of the prevalence of diabetes for 2010 and 2030. *Diabetes Res Clin Pract*. 2010 Jan;87(1):4–14.
36. IDF DIABETES ATLAS. 10th ed. Brussels: International Diabetes Federation; 2021.
37. Cerf ME. Beta cell dysfunction and insulin resistance. *Front Endocrinol (Lausanne)*. 2013 Mar 27;4:37.
38. Atkinson MA, Eisenbarth GS. Type 1 diabetes: new perspectives on disease pathogenesis and treatment. *Lancet*. 2001 Jul 21;358(9277):221–229.
39. Herold KC, Vignali DAA, Cooke A, Bluestone JA. Type 1 diabetes: translating mechanistic observations into effective clinical outcomes. *Nat Rev Immunol*. 2013 Apr 1;13(4):243–256.
40. American Diabetes Association. Diagnosis and classification of diabetes mellitus. *Diabetes Care*. 2011 Jan;34 Suppl 1:S62–9.
41. Fuchsberger C, Flannick J, Teslovich TM, Mahajan A, Agarwala V, Gaulton KJ, et al. The genetic architecture of type 2 diabetes. *Nature*. 2016 Aug 4;536(7614):41–47.
42. Atkinson MA, Eisenbarth GS, Michels AW. Type 1 diabetes. *Lancet*. 2014 Jan 4;383(9911):69–82.
43. Insel RA, Dunne JL, Atkinson MA, Chiang JL, Dabelea D, Gottlieb PA, et al. Staging presymptomatic type 1 diabetes: a scientific statement of JDRF, the Endocrine Society, and the American Diabetes Association. *Diabetes Care*. 2015 Oct;38(10):1964–1974.
44. Mathieu C, Lahesmaa R, Bonifacio E, Achenbach P, Tree T. Immunological biomarkers for the development and progression of type 1 diabetes. *Diabetologia*. 2018 Nov;61(11):2252–2258.

45. Yi L, Swensen AC, Qian W-J. Serum biomarkers for diagnosis and prediction of type 1 diabetes. *Transl Res*. 2018 Aug 1;201:13–25.
46. Pihoker C, Gilliam LK, Hampe CS, Lernmark A. Autoantibodies in diabetes. *Diabetes*. 2005 Dec;54 Suppl 2:S52–61.
47. Noble JA, Valdes AM. Genetics of the HLA region in the prediction of type 1 diabetes. *Curr Diab Rep*. 2011 Dec;11(6):533–542.
48. Wieczorek M, Abualrous ET, Sticht J, Álvaro-Benito M, Stolzenberg S, Noé F, et al. Major histocompatibility complex (MHC) class I and MHC class II proteins: conformational plasticity in antigen presentation. *Front Immunol*. 2017 Mar 17;8:292.
49. Wong FS, Wen L. B cells in autoimmune diabetes. *Rev Diabet Stud*. 2005 Nov 10;2(3):121–135.
50. Morran MP, Vonberg A, Khadra A, Pietropaolo M. Immunogenetics of type 1 diabetes mellitus. *Mol Aspects Med*. 2015 Apr;42:42–60.
51. Colli ML, Szymczak F, Eizirik DL. Molecular footprints of the immune assault on pancreatic beta cells in type 1 diabetes. *Front Endocrinol (Lausanne)*. 2020 Sep 15;11:568446.
52. Mauvais F-X, Diana J, van Endert P. Beta cell antigens in type 1 diabetes: triggers in pathogenesis and therapeutic targets. [version 1; peer review: 3 approved]. *F1000Res*. 2016 Apr 22;5.
53. Steck AK, Rewers MJ. Genetics of type 1 diabetes. *Clin Chem*. 2011 Feb;57(2):176–185.
54. Permutt MA, Wasson J, Cox N. Genetic epidemiology of diabetes. *J Clin Invest*. 2005 Jun;115(6):1431–1439.
55. Nyaga DM, Vickers MH, Jefferies C, Perry JK, O’Sullivan JM. The genetic architecture of type 1 diabetes mellitus. *Mol Cell Endocrinol*. 2018 Dec 5;477:70–80.



56. Sharp RC, Abdulrahim M, Naser ES, Naser SA. Genetic variations of PTPN2 and PTPN22: role in the pathogenesis of type 1 diabetes and crohn's disease. *Front Cell Infect Microbiol.* 2015 Dec 24;5:95.
57. Burn GL, Svensson L, Sanchez-Blanco C, Saini M, Cope AP. Why is PTPN22 a good candidate susceptibility gene for autoimmune disease? *FEBS Lett.* 2011 Dec 1;585(23):3689–3698.
58. Kasela S, Kisand K, Tserel L, Kaleviste E, Remm A, Fischer K, et al. Pathogenic implications for autoimmune mechanisms derived by comparative eQTL analysis of CD4+ versus CD8+ T cells. *PLoS Genet.* 2017 Mar 1;13(3):e1006643.
59. Pociot F, Lernmark Å. Genetic risk factors for type 1 diabetes. *Lancet.* 2016 Jun 4;387(10035):2331–2339.
60. Knip M, Simell O. Environmental triggers of type 1 diabetes. *Cold Spring Harb Perspect Med.* 2012 Jul;2(7):a007690.
61. Jäidane H, Hober D. Role of coxsackievirus B4 in the pathogenesis of type 1 diabetes. *Diabetes Metab.* 2008 Dec;34(6 Pt 1):537–548.
62. Dotta F, Censini S, van Halteren AGS, Marselli L, Masini M, Dionisi S, et al. Coxsackie B4 virus infection of beta cells and natural killer cell insulinitis in recent-onset type 1 diabetic patients. *Proc Natl Acad Sci USA.* 2007 Mar 20;104(12):5115–5120.
63. Bernard H, Teijeiro A, Chaves-Pérez A, Perna C, Satish B, Novials A, et al. Coxsackievirus B Type 4 Infection in  $\beta$  Cells Downregulates the Chaperone Prefoldin URI to Induce a MODY4-like Diabetes via Pdx1 Silencing. *Cell Reports Medicine.* 2020 Oct;1(7):100125.
64. Nekoua MP, Bertin A, Sane F, Gimeno J-P, Fournier I, Salzet M, et al. Persistence of coxsackievirus B4 in pancreatic  $\beta$  cells disturbs insulin maturation, pattern of cellular proteins, and DNA methylation. *Microorganisms.* 2021 May 22;9(6).
65. Sioofy-Khojine A-B, Lehtonen J, Nurminen N, Laitinen OH, Oikarinen S, Huhtala H, et al. Coxsackievirus B1 infections are associated with the initiation of insulin-driven autoimmunity that progresses to type 1 diabetes. *Diabetologia.* 2018 May;61(5):1193–1202.

66. Varela-Calvino R, Calviño-Sampedro C, Gómez-Touriño I, Cordero OJ. Apportioning blame: autoreactive CD4<sup>+</sup> and CD8<sup>+</sup> T cells in type 1 diabetes. *Arch Immunol Ther Exp (Warsz)*. 2017 Aug;65(4):275–284.
67. Tsai S, Shameli A, Santamaria P. Chapter 4 CD8<sup>+</sup> T Cells in Type 1 Diabetes. *Immunopathogenesis of Type 1 Diabetes Mellitus*. Elsevier; 2008. p. 79–124.
68. Di Lorenzo TP, Peakman M, Roep BO. Translational mini-review series on type 1 diabetes: Systematic analysis of T cell epitopes in autoimmune diabetes. *Clin Exp Immunol*. 2007 Apr;148(1):1–16.
69. Gojanovich GS, Murray SL, Buntzman AS, Young EF, Vincent BG, Hess PR. The use of peptide-major-histocompatibility-complex multimers in type 1 diabetes mellitus. *J Diabetes Sci Technol*. 2012 May 1;6(3):515–524.
70. Ilonen J, Lempainen J, Veijola R. The heterogeneous pathogenesis of type 1 diabetes mellitus. *Nat Rev Endocrinol*. 2019 Sep 18;15(11):635–650.
71. Chatterjee S, Khunti K, Davies MJ. Type 2 diabetes. *Lancet*. 2017 Jun 3;389(10085):2239–2251.
72. Hu A, Zou H, Chen B, Zhong J. Posttranslational modifications in diabetes: Mechanisms and functions. *Rev Endocr Metab Disord*. 2022 Jun 13;
73. Cersosimo E, Triplitt C, Mandarino LJ, DeFronzo RA. Pathogenesis of type 2 diabetes mellitus. In: De Groot LJ, Chrousos G, Dungan K, Feingold KR, Grossman A, Hershman JM, et al., editors. *Endotext*. South Dartmouth (MA): MDText.com, Inc.; 2000.
74. Donath MY, Shoelson SE. Type 2 diabetes as an inflammatory disease. *Nat Rev Immunol*. 2011 Feb;11(2):98–107.
75. Nigi L, Grieco GE, Ventriglia G, Brusco N, Mancarella F, Formichi C, et al. Micrnas as regulators of insulin signaling: research updates and potential therapeutic perspectives in type 2 diabetes. *Int J Mol Sci*. 2018 Nov 22;19(12).
76. Kitamura YI, Kitamura T, Kruse J-P, Raum JC, Stein R, Gu W, et al. FoxO1 protects against pancreatic beta cell failure through NeuroD and MafA induction. *Cell Metab*. 2005 Sep;2(3):153–163.

77. Linnemann AK, Blumer J, Marasco MR, Battiola TJ, Umhoefer HM, Han JY, et al. Interleukin 6 protects pancreatic  $\beta$  cells from apoptosis by stimulation of autophagy. *FASEB J*. 2017 Sep;31(9):4140–4152.
78. Guo S, Dai C, Guo M, Taylor B, Harmon JS, Sander M, et al. Inactivation of specific  $\beta$  cell transcription factors in type 2 diabetes. *J Clin Invest*. 2013 Aug;123(8):3305–3316.
79. Langenberg C, Lotta LA. Genomic insights into the causes of type 2 diabetes. *Lancet*. 2018 Jun 16;391(10138):2463–2474.
80. Poulsen P, Grunnet LG, Pilgaard K, Storgaard H, Alibegovic A, Sonne MP, et al. Increased risk of type 2 diabetes in elderly twins. *Diabetes*. 2009 Jun;58(6):1350–1355.
81. Brunetti A, Chiefari E, Foti D. Recent advances in the molecular genetics of type 2 diabetes mellitus. *World J Diabetes*. 2014 Apr 15;5(2):128–140.
82. Hani EH, Boutin P, Durand E, Inoue H, Permutt MA, Velho G, et al. Missense mutations in the pancreatic islet beta cell inwardly rectifying K<sup>+</sup> channel gene (KIR6.2/BIR): a meta-analysis suggests a role in the polygenic basis of Type II diabetes mellitus in Caucasians. *Diabetologia*. 1998 Dec;41(12):1511–1515.
83. Lyssenko V, Lupi R, Marchetti P, Del Guerra S, Orho-Melander M, Almgren P, et al. Mechanisms by which common variants in the TCF7L2 gene increase risk of type 2 diabetes. *J Clin Invest*. 2007 Aug;117(8):2155–2163.
84. Mambiya M, Shang M, Wang Y, Li Q, Liu S, Yang L, et al. The Play of Genes and Non-genetic Factors on Type 2 Diabetes. *Front Public Health*. 2019 Nov 19;7:349.
85. Marseglia L, Manti S, D'Angelo G, Nicotera A, Parisi E, Di Rosa G, et al. Oxidative stress in obesity: a critical component in human diseases. *Int J Mol Sci*. 2014 Dec 26;16(1):378–400.
86. Spruijt-Metz D, O'Reilly GA, Cook L, Page KA, Quinn C. Behavioral contributions to the pathogenesis of type 2 diabetes. *Curr Diab Rep*. 2014 Apr;14(4):475.
87. Lean ME, Leslie WS, Barnes AC, Brosnahan N, Thom G, McCombie L, et al. Primary care-led weight management for remission of type 2 diabetes (DiRECT): an open-label, cluster-randomised trial. *Lancet*. 2018 Feb 10;391(10120):541–551.

88. Quansah DY, Ha K, Jun S, Kim S-A, Shin S, Wie G-A, et al. Associations of Dietary Antioxidants and Risk of Type 2 Diabetes: Data from the 2007-2012 Korea National Health and Nutrition Examination Survey. *Molecules*. 2017 Oct 5;22(10).
89. Larsen N, Vogensen FK, van den Berg FWJ, Nielsen DS, Andreasen AS, Pedersen BK, et al. Gut microbiota in human adults with type 2 diabetes differs from non-diabetic adults. *PLoS One*. 2010 Feb 5;5(2):e9085.
90. Ding M, Bhupathiraju SN, Chen M, van Dam RM, Hu FB. Caffeinated and decaffeinated coffee consumption and risk of type 2 diabetes: a systematic review and a dose-response meta-analysis. *Diabetes Care*. 2014 Feb;37(2):569–586.
91. Yang Y, Peng N, Chen G, Wan Q, Yan L, Wang G, et al. Interaction between smoking and diabetes in relation to subsequent risk of cardiovascular events. *Cardiovasc Diabetol*. 2022 Dec;21(1):14.
92. Hasan SS, Mamun AA, Clavarino AM, Kairuz T. Incidence and risk of depression associated with diabetes in adults: evidence from longitudinal studies. *Community Ment Health J*. 2015 Feb;51(2):204–210.
93. Zhou H, Ji J, Chen X, Bi Y, Li J, Wang Q, et al. Identification of novel bat coronaviruses sheds light on the evolutionary origins of SARS-CoV-2 and related viruses. *Cell*. 2021 Aug;184(17):4380–4391.e14.
94. Taka E, Yilmaz SZ, Golcuk M, Kilinc C, Aktas U, Yildiz A, et al. Critical Interactions Between the SARS-CoV-2 Spike Glycoprotein and the Human ACE2 Receptor. *J Phys Chem B*. 2021 May 12;
95. Shang J, Ye G, Shi K, Wan Y, Luo C, Aihara H, et al. Structural basis of receptor recognition by SARS-CoV-2. *Nature*. 2020 May;581(7807):221–224.
96. Song P, Li W, Xie J, Hou Y, You C. Cytokine storm induced by SARS-CoV-2. *Clin Chim Acta*. 2020 Oct;509:280–287.
97. Thepmankorn P, Bach J, Lasfar A, Zhao X, Souayah S, Chong ZZ, et al. Cytokine storm induced by SARS-CoV-2 infection: The spectrum of its neurological manifestations. *Cytokine*. 2021 Feb;138:155404.
98. Wang J, Jiang M, Chen X, Montaner LJ. Cytokine storm and leukocyte changes in mild versus severe SARS-CoV-2 infection: Review of 3939 COVID-19 patients in

- China and emerging pathogenesis and therapy concepts. *J Leukoc Biol.* 2020 Jul;108(1):17–41.
99. Rehman SU, Tabish M. Alternative splicing of ACE2 possibly generates variants that may limit the entry of SARS-CoV-2: a potential therapeutic approach using SSOs. *Clin Sci.* 2020 May 29;134(10):1143–1150.
  100. Niu M-J, Yang J-K, Lin S-S, Ji X-J, Guo L-M. Loss of angiotensin-converting enzyme 2 leads to impaired glucose homeostasis in mice. *Endocrine.* 2008 Oct 28;34(1-3):56–61.
  101. Hikmet F, Méar L, Edvinsson Å, Micke P, Uhlén M, Lindskog C. The protein expression profile of ACE2 in human tissues. *Mol Syst Biol.* 2020 Jul;16(7):e9610.
  102. Wu C, Zheng S, Chen Y, Zheng M. Single-cell RNA expression profiling of ACE2, the putative receptor of Wuhan 2019-nCoV, in the nasal tissue. *medRxiv.* 2020 Feb 13;
  103. Hamming I, Timens W, Bulthuis MLC, Lely AT, Navis GJ, van Goor H. Tissue distribution of ACE2 protein, the functional receptor for SARS coronavirus. A first step in understanding SARS pathogenesis. *J Pathol.* 2004 Jun;203(2):631–637.
  104. Ren X, Glende J, Al-Falah M, de Vries V, Schwegmann-Wessels C, Qu X, et al. Analysis of ACE2 in polarized epithelial cells: surface expression and function as receptor for severe acute respiratory syndrome-associated coronavirus. *J Gen Virol.* 2006 Jun;87(Pt 6):1691–1695.
  105. Chua RL, Lukassen S, Trump S, Hennig BP, Wendisch D, Pott F, et al. COVID-19 severity correlates with airway epithelium-immune cell interactions identified by single-cell analysis. *Nat Biotechnol.* 2020 Aug;38(8):970–979.
  106. Lukassen S, Chua RL, Trefzer T, Kahn NC, Schneider MA, Muley T, et al. SARS-CoV-2 receptor ACE2 and TMPRSS2 are primarily expressed in bronchial transient secretory cells. *EMBO J.* 2020 May 18;39(10):e105114.
  107. Ziegler CGK, Allon SJ, Nyquist SK, Mbanjo IM, Miao VN, Tzouanas CN, et al. SARS-CoV-2 Receptor ACE2 Is an Interferon-Stimulated Gene in Human Airway Epithelial Cells and Is Detected in Specific Cell Subsets across Tissues. *Cell.* 2020 May 28;181(5):1016–1035.e19.

108. McCracken IR, Saginc G, He L, Huseynov A, Daniels A, Fletcher S, et al. Lack of Evidence of Angiotensin-Converting Enzyme 2 Expression and Replicative Infection by SARS-CoV-2 in Human Endothelial Cells. *Circulation*. 2021 Feb 23;143(8):865–868.
109. Muhl L, He L, Sun Y, Andaloussi Mäe M, Pietilä R, Liu J, et al. The SARS-CoV-2 receptor ACE2 is expressed in mouse pericytes but not endothelial cells: Implications for COVID-19 vascular research. *Stem Cell Rep*. 2022 May 10;17(5):1089–1104.
110. He L, Mäe MA, Muhl L, Sun Y, Pietilä R, Nahar K. Pericyte-specific vascular expression of SARS-CoV-2 receptor ACE2—implications for microvascular inflammation and hypercoagulopathy in COVID-19. *BioRxiv*. 2020;
111. Coate KC, Cha J, Shrestha S, Wang W, Gonçalves LM, Almaça J, et al. SARS-CoV-2 Cell Entry Factors ACE2 and TMPRSS2 Are Expressed in the Microvasculature and Ducts of Human Pancreas but Are Not Enriched in  $\beta$  Cells. *Cell Metab*. 2020 Dec 1;32(6):1028–1040.e4.
112. Blume C, Jackson CL, Spalluto CM, Legebeke J, Nazlamova L, Conforti F, et al. A novel ACE2 isoform is expressed in human respiratory epithelia and is upregulated in response to interferons and RNA respiratory virus infection. *Nat Genet*. 2021 Feb;53(2):205–214.
113. Onabajo OO, Banday AR, Stanifer ML, Yan W, Obajemu A, Santer DM, et al. Interferons and viruses induce a novel truncated ACE2 isoform and not the full-length SARS-CoV-2 receptor. *Nat Genet*. 2020 Dec;52(12):1283–1293.
114. Gwathmey TM, Pendergrass KD, Reid SD, Rose JC, Diz DI, Chappell MC. Angiotensin-(1-7)-angiotensin-converting enzyme 2 attenuates reactive oxygen species formation to angiotensin II within the cell nucleus. *Hypertension*. 2010 Jan;55(1):166–171.
115. Memon B, Abdelalim EM. ACE2 function in the pancreatic islet: Implications for relationship between SARS-CoV-2 and diabetes. *Acta Physiol (Oxf)*. 2021 Dec;233(4):e13733.

116. Ma X, Gao F, Chen Q, Xuan X, Wang Y, Deng H, et al. ACE2 modulates glucose homeostasis through GABA signaling during metabolic stress. *J Endocrinol*. 2020 Sep;246(3):223–236.
117. Shi T-T, Yang F-Y, Liu C, Cao X, Lu J, Zhang X-L, et al. Angiotensin-converting enzyme 2 regulates mitochondrial function in pancreatic  $\beta$ -cells. *Biochem Biophys Res Commun*. 2018 Jan 1;495(1):860–866.
118. Zhang F, Liu C, Wang L, Cao X, Wang YY, Yang JK. Antioxidant effect of angiotensin (1-7) in the protection of pancreatic  $\beta$  cell function. *Mol Med Rep*. 2016 Sep;14(3):1963–1969.
119. Shoemaker R, Yiannikouris F, Thatcher S, Cassis L. ACE2 deficiency reduces  $\beta$ -cell mass and impairs  $\beta$ -cell proliferation in obese C57BL/6 mice. *Am J Physiol Endocrinol Metab*. 2015 Oct 1;309(7):E621–31.
120. Hörnich BF, Großkopf AK, Schlagowski S, Tenbusch M, Kleine-Weber H, Neipel F, et al. SARS-CoV-2 and SARS-CoV Spike-Mediated Cell-Cell Fusion Differ in Their Requirements for Receptor Expression and Proteolytic Activation. *J Virol*. 2021 Apr 12;95(9).
121. Daniloski Z, Jordan TX, Wessels H-H, Hoagland DA, Kasela S, Legut M, et al. Identification of Required Host Factors for SARS-CoV-2 Infection in Human Cells. *Cell*. 2021 Jan 7;184(1):92–105.e16.
122. Zamorano Cuervo N, Grandvaux N. ACE2: Evidence of role as entry receptor for SARS-CoV-2 and implications in comorbidities. *Elife*. 2020 Nov 9;9.
123. Kusmartseva I, Wu W, Syed F, Van Der Heide V, Jorgensen M, Joseph P, et al. Expression of SARS-CoV-2 Entry Factors in the Pancreas of Normal Organ Donors and Individuals with COVID-19. *Cell Metab*. 2020 Dec 1;32(6):1041–1051.e6.
124. Wu C-T, Lidsky PV, Xiao Y, Lee IT, Cheng R, Nakayama T, et al. SARS-CoV-2 infects human pancreatic  $\beta$  cells and elicits  $\beta$  cell impairment. *Cell Metab*. 2021 Aug 3;33(8):1565–1576.e5.
125. Tang X, Uhl S, Zhang T, Xue D, Li B, Vandana JJ, et al. SARS-CoV-2 infection induces beta cell transdifferentiation. *Cell Metab*. 2021 Aug 3;33(8):1577–1591.e7.

126. Steenblock C, Richter S, Berger I, Barovic M, Schmid J, Schubert U, et al. Viral infiltration of pancreatic islets in patients with COVID-19. *Nat Commun.* 2021 Jun 10;12(1):3534.
127. Müller JA, Groß R, Conzelmann C, Krüger J, Merle U, Steinhart J, et al. SARS-CoV-2 infects and replicates in cells of the human endocrine and exocrine pancreas. *Nat Metab.* 2021 Feb 3;3(2):149–165.
128. Zhu L, She Z-G, Cheng X, Qin J-J, Zhang X-J, Cai J, et al. Association of Blood Glucose Control and Outcomes in Patients with COVID-19 and Pre-existing Type 2 Diabetes. *Cell Metab.* 2020 Jun 2;31(6):1068–1077.e3.
129. Rubino F, Amiel SA, Zimmet P, Alberti G, Bornstein S, Eckel RH, et al. New-Onset Diabetes in Covid-19. *N Engl J Med.* 2020 Aug 20;383(8):789–790.
130. Bornstein SR, Rubino F, Khunti K, Mingrone G, Hopkins D, Birkenfeld AL, et al. Practical recommendations for the management of diabetes in patients with COVID-19. *Lancet Diabetes Endocrinol.* 2020 Jun;8(6):546–550.
131. Apicella M, Campopiano MC, Mantuano M, Mazoni L, Coppelli A, Del Prato S. COVID-19 in people with diabetes: understanding the reasons for worse outcomes. *Lancet Diabetes Endocrinol.* 2020 Sep;8(9):782–792.
132. Guo W, Li M, Dong Y, Zhou H, Zhang Z, Tian C, et al. Diabetes is a risk factor for the progression and prognosis of COVID-19. *Diabetes Metab Res Rev.* 2020 Mar 31;36(7):e3319.
133. Bhatraju PK, Ghassemieh BJ, Nichols M, Kim R, Jerome KR, Nalla AK, et al. Covid-19 in Critically Ill Patients in the Seattle Region - Case Series. *N Engl J Med.* 2020 May 21;382(21):2012–2022.
134. Zhang Y, Cui Y, Shen M, Zhang J, Liu B, Dai M, et al. Association of diabetes mellitus with disease severity and prognosis in COVID-19: A retrospective cohort study. *Diabetes Res Clin Pract.* 2020 Jul;165:108227.
135. Roncon L, Zuin M, Rigatelli G, Zuliani G. Diabetic patients with COVID-19 infection are at higher risk of ICU admission and poor short-term outcome. *J Clin Virol.* 2020 Jun;127:104354.



136. Fadini GP, Morieri ML, Boscari F, Fioretto P, Maran A, Busetto L, et al. Newly-diagnosed diabetes and admission hyperglycemia predict COVID-19 severity by aggravating respiratory deterioration. *Diabetes Res Clin Pract.* 2020 Oct;168:108374.
137. Kumar A, Arora A, Sharma P, Anikhindi SA, Bansal N, Singla V, et al. Is diabetes mellitus associated with mortality and severity of COVID-19? A meta-analysis. *Diabetes Metab Syndr.* 2020 May 6;14(4):535–545.
138. Wu J, Zhang J, Sun X, Wang L, Xu Y, Zhang Y, et al. Influence of diabetes mellitus on the severity and fatality of SARS-CoV-2 (COVID-19) infection. *Diabetes Obes Metab.* 2020 Jul 7;22(10):1907–1914.
139. Zhou Y, Chi J, Lv W, Wang Y. Obesity and diabetes as high-risk factors for severe coronavirus disease 2019 (Covid-19). *Diabetes Metab Res Rev.* 2021 Feb;37(2):e3377.
140. Yang J, Zheng Y, Gou X, Pu K, Chen Z, Guo Q. Prevalence of comorbidities in the novel Wuhan coronavirus (COVID-19) infection: a systematic review and meta-analysis. *Int J Infect ....* 2020;
141. Lecube A, Hernández C, Genescà J, Esteban JI, Jardí R, Simó R. High prevalence of glucose abnormalities in patients with hepatitis C virus infection: a multivariate analysis considering the liver injury. *Diabetes Care.* 2004 May;27(5):1171–1175.
142. Wander PL, Lowy E, Beste LA, Tulloch-Palomino L, Korpak A, Peterson AC, et al. The Incidence of Diabetes Among 2,777,768 Veterans With and Without Recent SARS-CoV-2 Infection. *Diabetes Care.* 2022 Apr 1;45(4):782–788.
143. Montefusco L, Ben Nasr M, D’Addio F, Loretelli C, Rossi A, Pastore I, et al. Acute and long-term disruption of glycometabolic control after SARS-CoV-2 infection. *Nat Metab.* 2021 Jun;3(6):774–785.
144. Nasr MB, D’Addio F, Montefusco L, Usuelli V, Loretelli C, Rossi A, et al. Indirect and Direct Effects of SARS-CoV-2 on Human Pancreatic Islets. *Diabetes.* 2022 May 2;

145. Baggio LL, Varin EM, Koehler JA, Cao X, Likhnygina Y, Stevens SR, et al. Plasma levels of DPP4 activity and sDPP4 are dissociated from inflammation in mice and humans. *Nat Commun.* 2020 Jul 28;11(1):3766.
146. Birabaharan M, Kaelber DC, Pettus JH, Smith DM. Risk of new-onset type 2 diabetes in 600 055 people after COVID-19: A cohort study. *Diabetes Obes Metab.* 2022 Jun;24(6):1176–1179.
147. Yang L, Han Y, Nilsson-Payant BE, Gupta V, Wang P, Duan X, et al. A Human Pluripotent Stem Cell-based Platform to Study SARS-CoV-2 Tropism and Model Virus Infection in Human Cells and Organoids. *Cell Stem Cell.* 2020 Jul 2;27(1):125–136.e7.
148. van der Heide V, Jangra S, Cohen P, Rathnasinghe R, Aslam S, Aydillo T, et al. Limited extent and consequences of pancreatic SARS-CoV-2 infection. *Cell Rep.* 2022 Mar 15;38(11):110508.
149. Bornstein SR, Dalan R, Hopkins D, Mingrone G, Boehm BO. Endocrine and metabolic link to coronavirus infection. *Nat Rev Endocrinol.* 2020 Jun;16(6):297–298.
150. Fadini GP, Morieri ML, Longato E, Avogaro A. Prevalence and impact of diabetes among people infected with SARS-CoV-2. *J Endocrinol Invest.* 2020 Jun;43(6):867–869.
151. Zhou F, Yu T, Du R, Fan G, Liu Y, Liu Z, et al. Clinical course and risk factors for mortality of adult inpatients with COVID-19 in Wuhan, China: a retrospective cohort study. *Lancet.* 2020 Mar 28;395(10229):1054–1062.
152. Denina M, Trada M, Tinti D, Funicello E, Novara C, Moretto M, et al. Increase in newly diagnosed type 1 diabetes and serological evidence of recent SARS-CoV-2 infection: Is there a connection? *Front Med (Lausanne).* 2022 Jul 28;9:927099.
153. Elgenidy A, Awad AK, Saad K, Atef M, El-Leithy HH, Obiedallah AA, et al. Incidence of diabetic ketoacidosis during COVID-19 pandemic: a meta-analysis of 124,597 children with diabetes. *Pediatr Res.* 2022 Aug 11;

154. Ponmani C, Nijman R, Roland D, Barrett M. Children Presenting with Diabetes and Diabetic Ketoacidosis to Emergency Departments During the COVID-19 Pandemic in the UK and Ireland: An International .... Available at SSRN ....
155. Kendall EK, Olaker VR, Kaelber DC, Xu R, Davis PB. Association of SARS-CoV-2 Infection With New-Onset Type 1 Diabetes Among Pediatric Patients From 2020 to 2021. *JAMA Netw Open*. 2022 Sep 1;5(9):e2233014.
156. Rewers M, Bonifacio E, Ewald D, Geno Rasmussen C, Jia X, Pyle L, et al. SARS-CoV-2 Infections and Presymptomatic Type 1 Diabetes Autoimmunity in Children and Adolescents From Colorado, USA, and Bavaria, Germany. *JAMA*. 2022 Aug 5;
157. Kim JH, Park K, Lee SB, Kang S, Park JS, Ahn CW, et al. Relationship between natural killer cell activity and glucose control in patients with type 2 diabetes and prediabetes. *J Diabetes Investig*. 2019 Sep;10(5):1223–1228.
158. Lecube A, Pachón G, Petriz J, Hernández C, Simó R. Phagocytic activity is impaired in type 2 diabetes mellitus and increases after metabolic improvement. *PLoS One*. 2011 Aug 18;6(8):e23366.
159. Kartika R, Purnamasari D, Pradipta S, Larasati RA, Wibowo H. Impact of Low Interferon- $\gamma$  and IL-10 Levels on TNF- $\alpha$  and IL-6 Production by PHA-Induced PBMCs in Type 2 Diabetes Mellitus. *J Inflamm Res*. 2020 Apr 22;13:187–193.
160. El-Gohary Y, Tulachan S, Branca M, Sims-Lucas S, Guo P, Prasad K, et al. Whole-mount imaging demonstrates hypervascularity of the pancreatic ducts and other pancreatic structures. *Anat Rec (Hoboken)*. 2012 Mar;295(3):465–473.
161. Teuwen L-A, Geldhof V, Pasut A, Carmeliet P. COVID-19: the vasculature unleashed. *Nat Rev Immunol*. 2020 Jul;20(7):389–391.
162. Varga Z, Flammer AJ, Steiger P, Haberecker M, Andermatt R, Zinkernagel AS, et al. Endothelial cell infection and endotheliitis in COVID-19. *Lancet*. 2020 May 2;395(10234):1417–1418.
163. Richards OC, Raines SM, Attie AD. The role of blood vessels, endothelial cells, and vascular pericytes in insulin secretion and peripheral insulin action. *Endocr Rev*. 2010 Jun;31(3):343–363.

164. Singh M, Bansal V, Feschotte C. A Single-Cell RNA Expression Map of Human Coronavirus Entry Factors. *Cell Rep.* 2020 Sep 22;32(12):108175.
165. Wijnant SRA, Jacobs M, Van Eeckhoutte HP, Lapauw B, Joos GF, Bracke KR, et al. Expression of ACE2, the SARS-CoV-2 Receptor, in Lung Tissue of Patients With Type 2 Diabetes. *Diabetes.* 2020 Dec;69(12):2691–2699.
166. Lee IT, Nakayama T, Wu C-T, Goltsev Y, Jiang S, Gall PA, et al. ACE2 localizes to the respiratory cilia and is not increased by ACE inhibitors or ARBs. *Nat Commun.* 2020 Oct 28;11(1):5453.
167. Chee YJ, Ng SJH, Yeoh E. Diabetic ketoacidosis precipitated by Covid-19 in a patient with newly diagnosed diabetes mellitus. *Diabetes Res Clin Pract.* 2020 Jun;164:108166.
168. Bristow MR, Zisman LS, Altman NL, Gilbert EM, Lowes BD, Minobe WA, et al. Dynamic Regulation of SARS-Cov-2 Binding and Cell Entry Mechanisms in Remodeled Human Ventricular Myocardium. *JACC Basic Transl Sci.* 2020 Sep;5(9):871–883.
169. Dorrell C, Schug J, Lin CF, Canaday PS, Fox AJ, Smirnova O, et al. Transcriptomes of the major human pancreatic cell types. *Diabetologia.* 2011 Nov;54(11):2832–2844.
170. Bramswig NC, Everett LJ, Schug J, Dorrell C, Liu C, Luo Y, et al. Epigenomic plasticity enables human pancreatic  $\alpha$  to  $\beta$  cell reprogramming. *J Clin Invest.* 2013 Mar;123(3):1275–1284.
171. Blodgett DM, Nowosielska A, Afik S, Pechhold S, Cura AJ, Kennedy NJ, et al. Novel Observations From Next-Generation RNA Sequencing of Highly Purified Human Adult and Fetal Islet Cell Subsets. *Diabetes.* 2015 Sep;64(9):3172–3181.
172. Luecken MD, Theis FJ. Current best practices in single-cell RNA-seq analysis: a tutorial. *Mol Syst Biol.* 2019 Jun 19;15(6):e8746.
173. Taneera J, El-Huneidi W, Hamad M, Mohammed AK, Elaraby E, Hachim MY. Expression Profile of SARS-CoV-2 Host Receptors in Human Pancreatic Islets Revealed Upregulation of ACE2 in Diabetic Donors. *Biology (Basel).* 2020 Aug 7;9(8).

174. Roca-Ho H, Palau V, Gimeno J, Pascual J, Soler MJ, Riera M. Angiotensin-converting enzyme 2 influences pancreatic and renal function in diabetic mice. *Lab Invest.* 2020 Sep;100(9):1169–1183.
175. Xuan X, Gao F, Ma X, Huang C, Wang Y, Deng H, et al. Activation of ACE2/angiotensin (1-7) attenuates pancreatic  $\beta$  cell dedifferentiation in a high-fat-diet mouse model. *Metab Clin Exp.* 2018;81:83–96.
176. Krogvold L, Edwin B, Buanes T, Frisk G, Skog O, Anagandula M, et al. Detection of a low-grade enteroviral infection in the islets of langerhans of living patients newly diagnosed with type 1 diabetes. *Diabetes.* 2015 May;64(5):1682–1687.
177. Richardson SJ, Leete P, Bone AJ, Foulis AK, Morgan NG. Expression of the enteroviral capsid protein VP1 in the islet cells of patients with type 1 diabetes is associated with induction of protein kinase R and downregulation of Mcl-1. *Diabetologia.* 2013 Jan;56(1):185–193.
178. Op de Beeck A, Eizirik DL. Viral infections in type 1 diabetes mellitus--why the  $\beta$  cells? *Nat Rev Endocrinol.* 2016 May;12(5):263–273.
179. Spagnuolo I, Patti A, Sebastiani G, Nigi L, Dotta F. The case for virus-induced type 1 diabetes. *Curr Opin Endocrinol Diabetes Obes.* 2013 Aug;20(4):292–298.
180. Vehik K, Lynch KF, Wong MC, Tian X, Ross MC, Gibbs RA, et al. Prospective virome analyses in young children at increased genetic risk for type 1 diabetes. *Nat Med.* 2019 Dec 2;25(12):1865–1872.
181. Ifie E, Russell MA, Dhayal S, Leete P, Sebastiani G, Nigi L, et al. Unexpected subcellular distribution of a specific isoform of the Coxsackie and adenovirus receptor, CAR-SIV, in human pancreatic beta cells. *Diabetologia.* 2018 Nov;61(11):2344–2355.
182. Marfella R, D'Onofrio N, Mansueto G, Grimaldi V, Trotta MC, Sardu C, et al. Glycated ACE2 reduces anti-remodeling effects of renin-angiotensin system inhibition in human diabetic hearts. *Cardiovasc Diabetol.* 2022 Aug 5;21(1):146.
183. Garreta E, Prado P, Stanifer ML, Monteil V, Marco A, Ullate-Agote A, et al. A diabetic milieu increases ACE2 expression and cellular susceptibility to SARS-

CoV-2 infections in human kidney organoids and patient cells. *Cell Metab.* 2022 Jun 7;34(6):857–873.e9.

184. Wu M, Lee MYY, Bahl V, Traum D, Schug J, Kusmartseva I, et al. Single-cell analysis of the human pancreas in type 2 diabetes using multi-spectral imaging mass cytometry. *Cell Rep.* 2021 Nov 2;37(5):109919.
185. Millette K, Cuala J, Wang P, Marks C, Woo V, Hayun M, et al. SARS-CoV2 infects pancreatic beta cells in vivo and induces cellular and subcellular disruptions that reflect beta cell dysfunction. *Res Sq.* 2021 Jul 20;

# *Curriculum Vitae*

## **Personal Information:**

Name: Daniela

Surname: Fignani

Address: Strada di Pieve al Bozzone 38, 53100 Siena (Italy)

Telephone: 3316190085

Mail: [dfignani@gmail.com](mailto:dfignani@gmail.com)

## **Professional Experience:**

- From 01/10/2019 to present, **PhD student** in Biotecnologie Mediche (XXXV Ciclo) at Università degli Studi di Siena. Main research in analysis of molecular mechanisms related to type-1 and type-2 diabetes.

- From 16/07/2020 to present, **scholarship holder** at U.O.C Diabetologia dell'Azienda ospedaliero-universitaria Senese aimed at evaluation of circulating microRNAs as markers predictors of efficacy and tolerability of GLP1-RA therapy.

- From 01/01/2017 to 01/01/2018, **research laboratory technician** at Centro di Emofilia e Trombosi, Fondazione IRCCS Cà Granda Ospedale Maggiore Policlinico di Milano, Milan (Italy). Main responsibilities in clinical research on Basic and clinical research activity in the field of thrombotic microangiopathies.

## **Education:**

- From 01/10/2017 to 23/10/2019, Master's Degree in MEDICAL BIOTECHNOLOGIES (LM-9 D.M 270/2004) at Università degli Studi di Siena with grade of 110/110 cum Laude. Dissertation in "*Evaluation of circulating non-coding small RNAs in plasma of T1D patients: application of Next Generation Sequencing approach for High-Throughput biomarker discovery*".

- From 01/10/2013 to 24/11/2016, Bachelor's Degree in BIOMEDICAL LABORATORY TECHNIQUES (L/SNT3 D.M 270/2004) at Università degli Studi di Siena with grade of 110/110 cum Laude. Dissertation in "*Role of MECP2 in neurons-derived iPSCs from Rett syndrom patients*"



### **Projects involvement:**

- National Research Project **PRIN 2018** aimed at “Metabolic therapy of immuno-inflammation: in search for the best strategy to counteract type 2 diabetes and its complications”.
- European Research Project **INNODIA** (Translational approaches to disease modifying therapy of type 1 diabetes: an innovative approach towards understanding and arresting type 1 diabetes) aimed at identifying and validating novel biomarkers of type 1 diabetes.
- European Research Project: **HEDIMED** (Human Exposomic Determinants of Immune Mediated Diseases) aims to identify the disease mechanisms and environmental factors of type 1 diabetes, celiac disease, asthma and allergies, with the specific aim to evaluate small RNAs content in extracellular vesicles.
- Curiosity-driven (F-CUR) Project: characterization of AGO2-bound and Extracellular Vesicles-enclosed circulating Small RNAs in plasma of Type 1 Diabetic patients and non-diabetic control subjects (**AGOEV-T1D**).

### **Membership Associations:**

- Italian Society of Diabetology (SID), from 2018
- YoSID (Young of SID), from 2018
- International Society of Extracellular Vesicles (ISEV), from 2021
- Società Italiana per le Vescicole Extracellulari (EVIta), from 2021

### **Abstract presented at National and International level:**

- **D. Fignani**, G.E. Grieco, N. Brusco, G. Licata, L. Nigi, C. Formichi, G. Sebastiani, F. Dotta. *A novel method to isolate plasma circulating exosomes from INNODIA samples.* INNODIA and INNODIA HARVEST Annual Plenum Meeting, 21-23 Ottobre 2020. (Oral Presentation).
- **D. Fignani**, G.E. Grieco, N. Brusco, G. Licata, L. Nigi, C. Formichi, G. Sebastiani, F. Dotta. *A combined method to isolate blood plasma extracellular vesicles to support Small RNAs sequencing for biomarkers discovery.* ISEV2021, 10<sup>th</sup> annual meeting of the International Society for Extracellular Vesicles, 18 -21 Maggio 2021. (Poster Presentation)
- **D. Fignani**, G.E. Grieco, N. Brusco, G. Licata, C. Formichi, L. Nigi, A. Castela, D.L. Eizirik, G. Sebastiani and F. Dotta. *Long and short isoforms of SARS CoV 2 receptor Angiotensin I-Converting Enzyme type 2 (ACE2) are upregulated in response to*

*proinflammatory cytokines in human beta cells*. SIE 2021, Congresso Nazionale Società Italiana di Endocrinologia, 14-17 Luglio 2021, Roma, Italia. (Poster Presentation)

- **D. Fignani**, G. Licata, N. Brusco, E. Aiello, G.E. Grieco, C. Formichi, L. Nigi, L. Marselli, P. Marchetti, G. Sebastiani and F. Dotta, *Long and short isoforms of SARS-CoV-2 receptor Angiotensin I-Converting Enzyme type 2 (ACE2) are increased in pancreatic islets of type 2 diabetic patients*. nPOD Scientific Meeting, 22-24 Febbraio 2022. (Poster Presentation)

- **D. Fignani**, G. Licata, N. Brusco, E. Aiello, G.E. Grieco, C. Formichi, L. Nigi, L. Marselli, P. Marchetti, G. Sebastiani and F. Dotta, *Long and short isoforms of SARS-CoV-2 receptor Angiotensin I-Converting Enzyme type 2 (ACE2) are increased in pancreatic islets of type 2 diabetic patients*. EASD 2022, European Association for the Study of Diabetes. 19-23 Settembre 2022. (Short Oral Presentation)

- **D. Fignani**, G. Licata, E. Aiello, G.E. Grieco, C. Formichi, L. Nigi, L. Marselli, P. Marchetti, G. Sebastiani and F. Dotta, *Aumentata espressione del recettore del SARS-CoV-2 in isole pancreatiche di donatori con DM2*. SID 2022, Congresso Nazionale Società Italiana di Diabetologia. 26-29 Ottobre 2022. (Oral Presentation)

- **D. Fignani**, M. Bruttini, G.E. Grieco, S. Auddino, E. Aiello, A. Mori, G. Licata, L. Nigi, C. Formichi, G. Sebastiani, F. Dotta, *MicroRNAs are minor component of EVs content*. ISEV Workshop "QuantitatEVs: Multiscale analyses, from bulk to single vesicle". Trento, Italy - January 31st to February 2nd, 2023. (Short Oral Presentation)

### **Scientific articles published in Peer-Reviewed journals**

- **D.Fignani**, G. Licata, N. Brusco, L. Nigi, G.E. Grieco, L. Marselli, L. Overbergh, C. Gysemans, M.L. Colli, P. Marchetti, C. Mathieu, D.L. Eizirik, G. Sebastiani and Francesco Dotta. *SARS-CoV-2 Receptor Angiotensin I-Converting Enzyme Type 2 (ACE2) Is Expressed in Human Pancreatic  $\beta$ -Cells and in the Human Pancreas Microvasculature*. Frontiers in Endocrinology. 2020 (doi: 10.3389/fendo.2020.596898)

- G.E. Grieco, N. Brusco, G. Licata, **D. Fignani**, C. Formichi, L. Nigi, G. Sebastiani, F. Dotta. *The landscape of micrnas in  $\beta$ cell: Between phenotype maintenance and protection*. International journal of molecular sciences. 2021 (doi: 10.3390/ijms22020803)

- G.E. Grieco, **D. Fignani**, C. Formichi, L. Nigi, G. Licata, C. Maccora, N. Brusco, G. Sebastiani, F. Dotta. *Extracellular Vesicles in Immune System Regulation and Type 1 Diabetes: Cell-to-Cell Communication Mediators, Disease Biomarkers, and Promising Therapeutic Tools*. Frontiera in Immunology. 2021 (doi: 10.3389/fimmu.2021.682948)

- C. Formichi, L. Nigi, G.E. Grieco, C. Maccora, **D. Fignani**, N. Brusco, G. Licata, G. Sebastiani and Francesco Dotta. *Non-Coding RNAs: Novel Players in Insulin Resistance and Related Diseases*. International journal of molecular sciences. 2021 (doi: 10.3390/ijms22147716)
- G.E. Grieco, G. Sebastiani, **D. Fignani**, N. Brusco, L. Nigi, C. Formichi, G. Licata, M. Bruttini, R. D'Aurizio, C. Mathieu, C. Gysemans, F. Dotta. *Protocol to analyze circulating small non-coding RNAs by high-throughput RNA sequencing from human plasma samples*. STAR Protocol. 2021 (doi: 10.1016/j.xpro.2021.100606)
- C. Formichi, **D. Fignani**, L. Nigi, G.E. Grieco, N. Brusco, G. Licata, C. Sabato, E. Ferretti, G. Sebastiani, F. Dotta. *Circulating microRNAs Signature for Predicting Response to GLP1-RA Therapy in Type 2 Diabetic Patients: A Pilot Study*. International journal of molecular sciences. 2021 (doi: 10.3390/ijms22179454)
- P. Faucher, F. Beuvon, **D. Fignani**, G. Sebastiani, G. Afonso, Z. Zhou, B. Dousset, C. Boitard, F. Dotta, R. Mallone, E. Larger. *Immunoregulated insulinitis and slow-progressing type 1 diabetes after duodenopancreatectomy*. Diabetologia. 2021 (10.1007/s00125-021-05563-8)
- G.E. Grieco, N. Brusco, **D. Fignani**, L. Nigi, C. Formichi, G. Licata, L. Marselli, P. Marchetti, L. Salvini, L. Tinti, A. Po, E. Ferretti, G. Sebastiani, F. Dotta. *Reduced miR-184-3p expression protects pancreatic  $\beta$ -cells from lipotoxic and proinflammatory apoptosis in type 2 diabetes via CRTCI upregulation*. Cell death discovery. 2022 (10.1038/s41420-022-01142-x)
- G.E. Grieco, Z.M. Besharat, G. Licata, **D. Fignani**, N. Brusco, L. Nigi, C. Formichi, A. Po, C. Sabato, A. Dardano, A. Natali, F. Dotta, G. Sebastiani, E. Ferretti. *Circulating microRNAs as clinically useful biomarkers for Type 2 Diabetes Mellitus: miRNomics from bench to bedside*. Translational research. 2022 (10.1016/j.trsl.2022.03.008)
- E. Shaba, L. Vantaggiato, L. Governini, A. Haxhiu, G. Sebastiani, **D. Fignani**, G.E. Grieco, L. Bergantini, L. Bini, C. Landi. *Multi-Omics Integrative Approach of Extracellular Vesicles: A Future Challenging Milestone*. Proteomes. 2022 (10.3390/proteomes10020012)
- L. Nigi, N. Brusco, G.E. Grieco, **D. Fignani**, G. Licata, C. Formichi, E. Aiello, L. Marselli, P. Marchetti, L. Krogvold, K.D. Jorgensen, G. Sebastiani, F. Dotta. *Increased Expression of Viral Sensor MDA5 in Pancreatic Islets and in Hormone-Negative Endocrine Cells in Recent Onset Type 1 Diabetic Donors*. Frontiers in Immunology. 2022 (10.3389/fimmu.2022.833141)

- N. Brusco, G. Sebastiani, G. Di Giuseppe, G. Licata, G.E. Grieco, **D. Fignani**, L. Nigi, C. Formichi, E. Aiello, S. Auddino, G. Quero, C.M.A. Cefalo, F. Cinti, A. Mari, P.M. Ferraro, A. Pontecorvi, S. Alfieri, A. Giaccari, F. Dotta, T. Mezza. *Intra-islet insulin synthesis defects are associated with endoplasmic reticulum stress and loss of beta cell identity in human diabetes*. Diabetologia. 2022 (10.1007/s00125-022-05814-2)

### **Workshops and Schools Participation:**

- ISEV Workshop "*QuantitatEVs: Multiscale analyses, from bulk to single vesicle*". Trento, Italy - January 31st to February 2nd, 2023.

### **Scientific Awards:**

- SID Award "Umberto Di Mario" 2021, for best scientific work for "*SARS-CoV-2 Receptor Angiotensin I-Converting Enzyme Type 2 (ACE2) Is Expressed in Human Pancreatic  $\beta$ -Cells and in the Human Pancreas Microvasculature*".

- 41<sup>st</sup> National Congress of the Italian Society of Endocrinology (SIE) best poster for "*Long and short isoforms of SARS CoV 2 receptor Angiotensin I-Converting Enzyme type 2 (ACE2) are upregulated in response to proinflammatory cytokines in human beta cells*". 14-17 Luglio 2021.

### **Research unique identifier(s):**

- Scopus Author ID: 57220069245.

- Google Scholar:

<https://scholar.google.it/citations?user=TKbYozoAAAAJ&hl=it&oi=ao>

### **Bibliometric Indicators:**

12 peer-reviewed articles (Scopus);

H-Index: 4 (Source: Scopus); 5 (Source: Google Scholar).

Total Citations: 126 (Source: Scopus)